

Beyond Pulse Position Modulation: a Feasibility Study

- An Experimental and Simulation Based Feasibility Study of
the Beyond Pulse Position Modulation (BPPM) Error Correction
Protocol Using Classical Light Pulses

*En experimentell och simulationsbaserad
genomförbarhetsstudie av felkorrigeringskod ämnad för
enkelfotoner*

Danielle Gustafsson

Supervisors :

Joakim Argillander, Information Coding, Linköping University
Jonas Almlöf, Quantum Technologies, Ericsson AB
Gemma Vall-llosera, Quantum Technologies, Ericsson AB
Hanna Brännström, Quantum Technologies, Ericsson AB

Examiner :

Guilherme B. Xavier, Information Coding, Linköping University



Linköpings universitet
SE-581 83 Linköping
+46 13 28 10 00 , www.liu.se

Abstract

During the thesis work, a feasibility study of the BPPM error correction protocol is performed. The beyond pulse position modulation (BPPM) protocol was invented at Ericsson AB and describes a modulation encoding using vertically and horizontally polarized single photons for transmission and error correction. The thesis work is a mixture of both experimental laboratory work and theoretical software simulations which are intended to mimic actual optical fiber transmission. One aspect of the project work involves designing the optical communication system which is used to evaluate the probabilities of transmission errors in the form of false detections and losses of light. During the project work, the BPPM protocol is implemented and used for simulated error generation and correction. With the available laboratory setup used as the point of reference, error correction using the BPPM protocol is studied using pulses of light containing more than one photon. The results show that the BPPM protocol can be used to recover some of the information that is lost during optical fiber transmission. Factors such as the size of the codewords, the number of photons/pulse and detection efficiency of the utilized single photon detector (SPD) has a significant impact on the success of the transmission.

Acknowledgements

I would first like to thank my supervisor Joakim Argillander and examiner Guilherme B. Xavier at Linköping University for all the help during my battles with the lab equipment and also for continuously nudging me in the right direction. Furthermore, I want to extend a big thank you to the team at Ericsson, Jonas Almlöf, Gemma Vall-llosera and Hanna Bränström, for letting me work on this thesis project for you and also for all the helpful input and support throughout our weekly update meetings. Finally, thank you to Shek Lun Leung for the interesting weekly updates regarding your project and to Richard Schatz for valuable input during the update meetings. Working on this project has been a lot of fun and I have learnt a lot along the way. Once again, thank you all!

Danielle Gustafsson

Abbreviations

PBS: Polarizing Beam Splitter
BS: Beam Splitter
ATT: Attenuator
PPM: Pulse Position Modulation
BPPM: Beyond Pulse Position Modulation
PC: Polarization Controller
FPGA: Field Programmable Gate Array
SPD: Single Photon Detector
TIR: Total Internal Reflection
VHDL: Very high-speed integrated circuit hardware description language
FEC: Forward Error Correction
RS: Reed-Solomon
DFB: Distributed-feedback
CW: Continuous wave
LAN: Local Area Network
BSC: Binary Symmetric Channel
MPC: Manual Polarization Controller
EPC: Electronic Polarization Controller
OOK: On-off Keying
EC: Error Correction
BER: Bit Error Rate
SNSPD: Superconducting Nanowire Single-photon Detector
ICCD: Intensified Charge Coupled Device
QWP: Quarter-Wave Plate
HWP: Half-Wave Plate
RZ: Return to Zero
NRZ: Non-Return to Zero

Contents

Abstract	ii
Acknowledgments	iii
Abbreviations	iv
Contents	v
List of Figures	vii
List of Tables	xiv
1 Introduction	1
1.1 Motivation	1
1.2 The Project Goal	2
1.3 Related work	2
1.4 Research questions	3
2 Background and Theory	4
2.1 Electromagnetic Waves	4
2.2 Signal Modulation	10
2.3 Light Propagation in Single-mode Fiber	13
2.4 Transmission Errors in Optical Communication	14
2.5 False Detections and Detector Losses	16
2.6 Bit-flips	17
2.7 Photon Statistics	20
2.8 Error-correction	23
2.9 The BPPM Error Correction Protocol Description	25
3 Method	34
3.1 Project Process	34
3.2 Delimitations	34
3.3 System Design	35
3.4 Control System and Transmission Process	38
3.5 Software	41
3.6 Experimental Process	45
4 Results and Discussion	51
4.1 Results of Software Simulated Transmissions of Super-blocks: Arbitrary Values for p_{loss} and p_{add}	51
4.2 Experiments	65
4.3 Results of Software Simulated Transmissions of Super-blocks: Experimentally Derived Values for p_{loss} and p_{add}	70

4.4	Simulated Image Transmission	86
4.5	Results and Discussion Summary	99
4.6	Future Work	101
5	Conclusion	102
A	System Design for Single Photons	103
A.1	System Design for Single Photons	103
Bibliography		106

List of Figures

2.1	Illustration of elliptical-, circular- and linear polarization in the cartesian coordinate system (\hat{x} , \hat{y} , \hat{z}), with electric field vectors \hat{E}_1 and \hat{E}_2 .	6
2.2	Illustration of the Poincaré sphere, where the linear polarizations: horizontal (H), vertical (V), diagonal (D), anti-diagonal (A) are illustrated as different spatial point on the sphere surface. At the top and bottom of the figure, right (R) and left (L) rotation are included.	6
2.3	Illustration of the relation between the electric field \hat{E} (direction \hat{x}), magnetic field \hat{H} (direction \hat{y}), and wave propagation direction \hat{K} (direction \hat{z}) of a linearly polarized electromagnetic wave.	7
2.4	Illustration of unpolarized light passing through a vertical linear polarizer followed by a horizontal linear polarizer. At the first polarizer, only the vertically polarized portion of the light will pass through to the other side. After the second polarizer, none of the remaining light will have passed though. Because the vertical and horizontal polarizations are orthogonal, their respective polarizer will cancel out the light of the other.	8
2.5	Signal illustrations of pulse position modulation using 8 time-slots (PPM-8) and on-off keying using 3 time-slots (OOK).	11
2.6	Signal illustrations of the pulse modulation techniques: pulse position modulation (PPM), pulse width modulation (PWM), pulse amplitude modulation (PAM).	12
2.7	Signal illustrations of the pulse amplitude modulation techniques: PAM-2 and PAM-4.	12
2.8	Illustration of light propagation in single-mode fiber. In this figure, n_1 and n_2 are the refractive indices of the core and cladding respectively. The angles θ_i and θ_r are the incident and reflected angles of light and θ_c is the critical angle.	14
2.9	Illustration of loss of light in fiber due to angle of incidence (θ_i) being smaller than the critical angle θ_c . In this figure, θ_t is the angle of the transmitted light and n_1 , n_2 are the refractive indices of the core and cladding respectively.	15
2.10	Illustrations of bit-flips in the BSC and z-channel, where p is the bit-flip probability.	18
2.11	Poisson distribution: Event registering probability (P_{poisson}) over photon number (k) for an average number of photons per pulse $u = 1, 2, 3, 4, 5, 6, 7, 8, 9, 10$.	20
2.12	Super-Poissonian distribution: Event registering probability ($P_{\text{super_poisson}}$) over photon number (k) for an average number of photons per pulse $u = 1, 2, 3, 4, 5, 6, 7, 8, 9, 10$.	21
2.13	Sub-Poissonian distribution: Event registering probability ($P_{\text{sub_poisson}}$) over photon number (k) for an average number of photons per pulse $u = 1, 2, 3, 4, 5, 6, 7, 8, 9, 10$.	22
2.14	Illustration of the dependence between polarization and order of sub-block lengths within super-blocks of size $n=2$, i.e. for permutations (1,2) and (2,1). In the figure, H=horizontal polarization and V=vertical polarization.	26
2.15	Illustration of super-block permutation (1,2,4,7), displaying signal power over time. In the figure, H=horizontal polarization and V=vertical polarization.	27

2.16	Illustration of the erroneous super-block (1,6,7), displaying signal power over time. In the figure, H=horizontal polarization and V=vertical polarization.	28
2.17	Illustration of the erroneous super-block (3,11), displaying signal power over time. In the figure, H=horizontal polarization and V=vertical polarization.	29
2.18	Illustration of the erroneous super-block (1,2,1,3,7), displaying signal power over time. In the figure, H=horizontal polarization, V=vertical polarization and X is either H- or V-polarization.	30
2.19	Illustration of the erroneous super-block (7,7), displaying signal power over time. In the figure, H=horizontal polarization and V=vertical polarization.	32
3.1	Scheme describing the experimental setup.	35
3.2	Photo of the experimental setup from the laboratory.	36
3.3	Illustration of the communication scheme between the control system, consisting of the software and the field programmable gate array (FPGA) with memory (row/data), and the experimental setup.	39
3.4	Detailed illustration of the hardware communication scheme between transmitter and receiver. The arrows in the figure illustrate the direction of the signals.	40
3.5	Table showing the binary, decimal and bit index values for most significant bit (MSB) and least significant bit (LSB), which are used to construct sub-block values in hardware representation.	41
3.6	Table showing the different data representations of super-block (size n=3) information. In this figure, H=horizontal polarization and V=vertical polarization.	42
3.7	Flow chart of the error correction process in software. In this figure, m is the actual number of sub-blocks in the received super-blocks and n is the expected number of sub-blocks in the super-block.	44
4.1	Error corrected simulated transmission with $p_{\text{add}} = 0\%$ and $p_{\text{loss}} = 10\%$. The plot shows the average number of successfully received (green) vs transmitted (pink) vs successfully received and error-corrected (blue) information bits per sub-block for each super-block of size n . The number of transmitted super-blocks per super-block size of n is 10 000 and all super-blocks are constructed with lengths in rising order: 1,2,4,7,...	52
4.2	The table shows the size n of the transmitted super-blocks and the respective percentage of super-blocks that were not distorted during the transmission, vs the percentage of super-blocks that were successfully corrected, vs the percentage of super-blocks that could not be corrected using EC.	52
4.3	The table shows the size n of the transmitted super-blocks and the respective average number of transmitted information bits per pulse, vs the average number of bits per pulse that were correctly received with and without EC, vs the ratio between the two.	53
4.4	Error-corrected simulated transmission with $p_{\text{add}} = 0\%$ and $p_{\text{loss}} = 10\%$. The plot shows the average number of successfully received (green) vs transmitted (pink) vs successfully received and error-corrected (blue) information bits per pulse for each super-block of size n . The number of transmitted super-blocks per super-block size of n is 10 000, out of which there are about as many of each super-block permutation.	53
4.5	The table shows the size n of the transmitted super-blocks and the respective percentage of super-blocks that were not distorted during the transmission, vs the percentage of super-blocks that were successfully corrected, vs the percentage of super-blocks that could not be corrected using EC.	54

4.6	The table shows the size n of the transmitted super-blocks and the respective average number of transmitted information bits per pulse, vs the average number of bits per pulse that were correctly received with and without EC, vs the ratio between the two.	54
4.7	Error-corrected simulated transmission with $p_{\text{add}} = 0\%$ and $p_{\text{loss}} = 10\%$. The plot shows the average number of successfully received (green) vs transmitted (pink) vs successfully received and error-corrected (blue) information bits per pulse for each super-block of size n . The number of transmitted super-blocks per super-block size of n is 10 000. All super-blocks are constructed with lengths in declining order: 7,4,2,1,...	55
4.8	The table shows the size n of the transmitted super-blocks and the respective percentage of super-blocks that are not distorted during the transmission, vs the percentage of super-blocks that are successfully corrected, vs the percentage of super-blocks that can not be corrected using EC.	55
4.9	The table shows the size n of the transmitted super-blocks and the respective average number of transmitted information bits per pulse, vs the average number of bits per pulse that are correctly received with and without EC, vs the ratio between the two.	56
4.10	Error-corrected simulated transmission with $p_{\text{add}} = 10\%$ and $p_{\text{loss}} = 0\%$. The plot shows the average number of successfully received (green) vs transmitted (pink) vs successfully received and error-corrected (orange) information bits per pulse for each super-block of size n . The number of transmitted super-blocks per super-block size of n is 10 000. All super-blocks are constructed with lengths in rising order: 1,2,4,7,...	57
4.11	The table shows the size n of the transmitted super-blocks and the respective percentage of super-blocks that are not distorted during the transmission, vs the percentage of super-blocks that were successfully corrected, vs the percentage of super-blocks that can not be corrected using EC.	58
4.12	The table shows the size n of the transmitted super-blocks and the respective average number of transmitted information bits per pulse, vs the average number of bits per pulse that are correctly received with and without EC, vs the ratio between the two.	58
4.13	Error-corrected simulated transmission with $p_{\text{add}} = 10\%$ and $p_{\text{loss}} = 0\%$. The plot shows the average number of successfully received (green) vs transmitted (pink) vs successfully received and error-corrected (orange) information bits per pulse for each super-block of size n . The number of transmitted super-blocks are 10 000 for each super-block size of n , out of which there are about as many of each super-block permutation.	59
4.14	The table shows the size n of the transmitted super-blocks and the respective percentage of super-blocks that are not distorted during the transmission, vs the percentage of super-blocks that are successfully corrected, vs the percentage of super-blocks that can not be corrected using EC.	59
4.15	The table shows the size n of the transmitted super-blocks and the respective average number of transmitted information bits per pulse, vs the average number of bits per pulse that are correctly received with and without EC, vs the ratio between the two.	60
4.16	Error-corrected simulated transmission with $p_{\text{add}} = 10\%$ and $p_{\text{loss}} = 0\%$. The plot shows the average number of successfully received (green) vs transmitted (pink) vs successfully received and error-corrected (orange) information bits per pulse for each super-block of size n . The number of transmitted super-blocks are 10 000 for each super-block size of n . All super-blocks are constructed with lengths in declining order: 7,4,2,1,...	60

4.17	The table shows the size n of the transmitted super-blocks and the respective percentage of super-blocks that are not distorted during the transmission, vs the percentage of super-blocks that are successfully corrected, vs the percentage of super-blocks that can not be corrected with BPPM EC.	61
4.18	The table shows the size of the transmitted super-blocks n and the respective average number of transmitted information bits per pulse, vs the average number of bits per pulse that are correctly received with and without EC, vs the ratio between the two.	61
4.19	Error-corrected simulated transmission with $p_{\text{add}} = p_{\text{loss}} = 10\%$. The plot shows the average number of successfully received (green) vs transmitted (pink) vs successfully received and error-corrected (purple) information bits per pulse for each super-block size n . The number of transmitted super-blocks are 10 000 for each super-block size of n . All super-blocks are constructed with lengths in rising order: 1,2,4,7,...	63
4.20	The table shows the size n of the transmitted super-blocks and the respective percentage of super-blocks that are not distorted during the transmission, vs the percentage of super-blocks that are successfully corrected, vs the percentage of super-blocks that can not be corrected using EC.	64
4.21	The table shows the size n of the transmitted super-blocks and the respective average number of transmitted information bits per pulse, vs the average number of bits per pulse that are correctly received with and without EC, vs the ratio between the two.	64
4.22	Graph displaying the calculated dark-count probability (p_{add}) for the SPD of model ID210 (from ID Quantique) over detection efficiency span $\eta_{\text{eff}} = 5 - 25\%$	65
4.23	The probability for photon loss (p_{loss}) over a propagation distance of $L = 0 - 75$ km when $\eta_{\text{eff}} = 10\%$. The losses are simulated for pulse sizes of u number of photons.	66
4.24	The probability for photon loss (p_{loss}) over a propagation distance of $L = 0 - 75$ km when $\eta_{\text{eff}} = 20\%$. The losses are simulated for pulse sizes of u number of photons.	67
4.25	Polarization drift displayed in power level over time. Here, the horizontally polarized signal is high and the vertically polarized signal is low.	68
4.26	Polarization drift displayed in power level over time. Here, the vertically polarized signal is high and the horizontally polarized signal is low.	69
4.27	Error-corrected simulated transmission with $p_{\text{loss}} = 19.28\%$, $p_{\text{add}} = 0.05\%$ and 100 photons per pulse at a fiber distances of 0 km. The plot shows the average number of successfully received (green) vs transmitted (pink) vs successfully received and error-corrected (purple) bits per pulse for each super-block of size n	71
4.28	The table shows the size n of the transmitted super-blocks and the respective percentage of super-blocks that are not distorted during the transmission, vs the percentage of super-blocks that are successfully corrected, vs the percentage of super-blocks that can not be corrected using EC.	71
4.29	The table shows the size n of the transmitted super-blocks and the respective average number of transmitted information bits per pulse, vs the average number of bits per pulse that are correctly received with and without EC, vs the ratio between the two.	72
4.30	Error-corrected simulated transmission with $p_{\text{loss}} = 34.56\%$, $p_{\text{add}} = 0.05\%$ and 100 photons per pulse at a fiber distances of 5 km. The plot shows the average number of successfully received (green) vs transmitted (pink) vs successfully received and error-corrected (purple) bits per pulse for each super-block of size n	72

4.31	The table shows the size n of the transmitted super-blocks and the respective percentage of super-blocks that are not distorted during the transmission, vs the percentage of super-blocks that are successfully corrected, vs the percentage of super-blocks that can not be corrected using EC.	73
4.32	The table shows the size n of the transmitted super-blocks and the respective average number of transmitted information bits per pulse, vs the average number of bits per pulse that are correctly received with and without EC, vs the ratio between the two.	73
4.33	Error-corrected simulated transmission with $p_{\text{loss}} = 48.98\%$, $p_{\text{add}} = 0.05\%$ and 10 photons per pulse at a fiber distances of 0 km. The plot shows the average number of successfully received (green) vs transmitted (pink) vs successfully received and error-corrected (purple) bits per pulse for each super-block of size n	74
4.34	The table shows the size n of the transmitted super-blocks and the respective percentage of super-blocks that are not distorted during the transmission, vs the percentage of super-blocks that are successfully corrected, vs the percentage of super-blocks that can not be corrected using EC.	75
4.35	The table shows the size n of the transmitted super-blocks and the respective average number of transmitted information bits per pulse, vs the average number of bits per pulse that are correctly received with and without EC, vs the ratio between the two.	75
4.36	Error-corrected simulated transmission with $p_{\text{loss}} = 58.63\%$, $p_{\text{add}} = 0.05\%$ and 10 photons per pulse at a fiber distances of 5 km. The plot shows the average number of successfully received (green) vs transmitted (pink) vs successfully received and error-corrected (purple) bits per pulse for each super-block of size n	76
4.37	The table shows the size n of the transmitted super-blocks and the respective percentage of super-blocks that are not distorted during the transmission, vs the percentage of super-blocks that are successfully corrected, vs the percentage of super-blocks that can not be corrected using EC.	76
4.38	The table shows the size n of the transmitted super-blocks and the respective average number of transmitted information bits per pulse, vs the average number of bits per pulse that are correctly received with and without EC, vs the ratio between the two.	77
4.39	Error-corrected simulated transmission with $p_{\text{loss}} = 19.82\%$, $p_{\text{add}} = 6.48\%$ and 100 photons per pulse at a fiber distances of 0 km. The plots shows the average number of successfully received (green) vs transmitted (pink) vs successfully received and error-corrected (purple) bits per pulse for each super-block of size n	78
4.40	The table shows the size n of the transmitted super-blocks and the respective percentage of super-blocks that are not distorted during the transmission, vs the percentage of super-blocks that are successfully corrected, vs the percentage of super-blocks that can not be corrected using EC.	79
4.41	The table shows the size n of the transmitted super-blocks and the respective average number of transmitted information bits per pulse, vs the average number of bits per pulse that are correctly received with and without EC, vs the ratio between the two.	79
4.42	Error-corrected simulated transmission with $p_{\text{loss}} = 34.99\%$, $p_{\text{add}} = 6.48\%$ and 100 photons per pulse at a fiber distances of 5 km. The plots shows the average number of successfully received (green) vs transmitted (pink) vs successfully received and error-corrected (purple) bits per pulse for each super-block of size n	80

4.43	The table shows the size n of the transmitted super-blocks and the respective percentage of super-blocks that are not distorted during the transmission, vs the percentage of super-blocks that are successfully corrected, vs the percentage of super-blocks that can not be corrected using EC.	80
4.44	The table shows the size n of the transmitted super-blocks and the respective average number of transmitted information bits per pulse, vs the average number of bits per pulse that are correctly received with and without EC, vs the ratio between the two.	81
4.45	Error-corrected simulated transmission with $p_{\text{loss}} = 30.67\%$, $p_{\text{add}} = 6.48\%$ and 10 photons per pulse at a fiber distances of 0 km. The plots shows the average number of successfully received (green) vs transmitted (pink) vs successfully received and error-corrected (purple) bits per pulse for each super-block of size n	82
4.46	The table shows the size n of the transmitted super-blocks and the respective percentage of super-blocks that are not distorted during the transmission, vs the percentage of super-blocks that are successfully corrected, vs the percentage of super-blocks that can not be corrected using EC.	83
4.47	The table shows the size n of the transmitted super-blocks and the respective average number of transmitted information bits per pulse, vs the average number of bits per pulse that are correctly received with and without EC, vs the ratio between the two.	83
4.48	Error-corrected simulated transmission with $p_{\text{loss}} = 43.79\%$, $p_{\text{add}} = 6.48\%$ and 10 photons per pulse at a fiber distances of 5 km. The plots shows the average number of successfully received (green) vs transmitted (pink) vs successfully received and error-corrected (purple) bits per pulse for each super-block of size n	84
4.49	The table shows the size n of the transmitted super-blocks and the respective percentage of super-blocks that are not distorted during the transmission, vs the percentage of super-blocks that are successfully corrected, vs the percentage of super-blocks that can not be corrected using EC.	84
4.50	The table shows the size n of the transmitted super-blocks and the respective average number of transmitted information bits per pulse, vs the average number of bits per pulse that are correctly received with and without EC, vs the ratio between the two.	85
4.51	Error corrected simulated image transmission, at a transmission distance of $L = 0$ km (transmitter and receiver placed back-to-back), with $p_{\text{add}} = 0.05\%$ and $p_{\text{loss}} = 19.28\%$	86
4.52	Error corrected simulated image transmission at a transmission distance of $L = 5$ km, with $p_{\text{add}} = 0.05\%$ and $p_{\text{loss}} = 34.56\%$	87
4.53	Ratios of super-blocks of size $n=2$ that are successfully received (green), successfully error corrected (yellow) and non-correctable (red).	87
4.54	Error corrected simulated image transmission, at a transmission distance of $L = 0$ km, with $p_{\text{add}} = 0.05\%$ and $p_{\text{loss}} = 19.28\%$ and transmitter and receiver placed back-to-back.	88
4.55	Error corrected simulated image transmission, at a transmission distance of $L = 5$ km, with $p_{\text{add}} = 0.05\%$ and $p_{\text{loss}} = 34.56\%$	88
4.56	Ratios of super-blocks of size $n = 3$ that are successfully received (green), successfully error corrected (yellow) and non-correctable (red).	89
4.57	Error corrected simulated image transmission at a transmission distance of $L = 0$ km, with $p_{\text{add}} = 0.05\%$ and $p_{\text{loss}} = 19.28\%$. The image shows the successfully error corrected pixel data (green) and the non-correctable pixel data (red).	90

4.58	Error corrected simulated image transmission at a transmission distance of $L = 5$ km, with $p_{\text{add}} = 0.05\%$ and $p_{\text{loss}} = 34.56\%$. The image shows the successfully error corrected pixel data (green) and the non-correctable pixel data (red).	90
4.59	Ratios of super-blocks of size $n=4$ that are successfully received (green), successfully error corrected (yellow) and non-correctable (red).	91
4.60	Error corrected simulated image transmission at a transmission distance of $L = 0$ km, with $p_{\text{add}} = 0.05\%$ and $p_{\text{loss}} = 19.28\%$. The image shows the successfully error corrected pixel data (green) and the non-correctable pixel data (red).	92
4.61	Error corrected simulated image transmission at a transmission distance of $L = 5$ km, with $p_{\text{add}} = 0.05\%$ and $p_{\text{loss}} = 34.56\%$. The image shows the successfully error corrected pixel data (green) and the non-correctable pixel data (red).	92
4.62	Ratios of super-blocks of size $n=5$ that are successfully received (green), successfully error corrected (yellow) and non-correctable (red).	93
4.63	Repeated error corrected image transmission simulation with super-block size of $n = 3$ at a transmission distance of $L = 5$ km, with $p_{\text{add}} = 0.05\%$ and $p_{\text{loss}} = 34.56\%$. The image shows the percentage of properly received data (with and without error correction) for each iteration. Non-correctable pixel data is illustrated using red pixels for each iteration. The average photon number per pulse is $u = 100$	94
4.64	Repeated error corrected image transmission simulation with super-block size of $n = 3$ at a transmission distance of $L = 5$ km, with $p_{\text{add}} = 6.48\%$ and $p_{\text{loss}} = 43.79\%$. The image shows the percentage of properly received data (with and without error correction) for each iteration. Non-correctable pixel data is illustrated using red pixels for each iteration. The average photon number per pulse is $u = 10$	95
4.65	Repeated error corrected image transmission simulation with super-block size of $n = 5$ at a transmission distance of $L = 5$ km, with $p_{\text{add}} = 0.05\%$ and $p_{\text{loss}} = 34.56\%$. The image shows the percentage of properly received data (with and without error correction) for each iteration. Non-correctable pixel data is illustrated using red pixels for each iteration. The average photon number per pulse is $u = 100$	96
4.66	Repeated error corrected image transmission simulation with super-block size of $n = 5$ at a transmission distance of $L = 5$ km, with $p_{\text{add}} = 6.48\%$ and $p_{\text{loss}} = 43.79\%$. The image shows the percentage of properly received data (with and without error correction) for each iteration. Non-correctable pixel data is illustrated using red pixels for each iteration. The average photon number per pulse is $u = 10$	97
A.1	Scheme describing the experimental setup for single photon transmission.	104

List of Tables

3.1	Table showing performed transmission simulations using arbitrarily chosen values for loss probability (p_{loss}) and addition probability (p_{add}).	47
3.2	Table showing performed transmission simulations using experimentally derived values for loss probability (p_{loss}) and addition probability (p_{add}), at detection efficiency $\eta_{\text{eff}} = 10\%$. In the table, L is the propagated distance and u is the average number of photons per pulse.	48
3.3	Table showing performed transmission simulations using experimentally derived values for loss probability (p_{loss}) and addition probability (p_{add}), at detection efficiency $\eta_{\text{eff}} = 20\%$. In the table, L is the propagated distance and u is the average number of photons per pulse.	49
3.4	Table showing performed image transmission simulations using experimentally derived values for loss probability (p_{loss}) and addition probability (p_{add}), at detection efficiency $\eta_{\text{eff}} = 10\%$. In the table, n is the number of sub-blocks per super-block, L is the propagated distance and u is the average number of photons per pulse.	50
3.5	Table showing repeated transmission simulations of images using experimentally derived values for loss probability (p_{loss}) and addition probability (p_{add}), at detection efficiencies $\eta_{\text{eff}}=10$ and 20%. In the table, n is the size of the used super-blocks, L is the propagated distance and u is the average number of photons per pulse.	50

Todo list

■ lägg till refractive index värden	13
■ kommentera/förtydliga någonstans att BPPM protokollet är designat för singelfotoner men jag kör med ljuspulser istället	15



1 Introduction

1.1 Motivation

The search for energy efficient optical communication techniques is an important matter in modern time. The reason for this is the ever increasing amount of internet data traffic, i.e. the amount of network data that is constantly being transmitted all over the world[Lundberg2019PowerCommunication]. This, in combination with the fact that every pulse of classical light used for classical optical communication contains billions of photons, means that there is a need for more energy efficient techniques. This fact lays the foundation for the existence of the beyond pulse position modulation (BPPM) protocol. Namely, the BPPM protocol suggests a way of using single photons for conveying more than one bit of information per photon and thereby providing a much more energy efficient solution for optical communication than using classical light pulses.

For encoding messages using optical communication, implementation of modulation techniques are required. These are used to shape the light into pulses carrying the encoded information. One of the most commonly used modulation techniques today is On-off keying (OOK)[Jarzyna2015IncoherentLight]. Just like OOK, BPPM is a modulation technique. The BPPM protocol is an extension of the regular pulse position modulation (PPM) technique, which in current time is not commonly used for optical communication. The advantage that techniques such as PPM (and BPPM) however have over more widespread modulation techniques such as OOK, is in regards to energy efficiency, as only one pulse of light is needed to describe each symbol. Therefore, the encoding utilizes only the temporal placement of the one pulse for the variations in the codewords, instead of applying variations to the amount of used energy per encoded symbol.

It is well known that optical signals propagating over long distances suffer attenuation and dispersion. This in turn can lead to errors in the received data. However, there is at this time a lack of available error correction methods involved with the PPM technique. Namely, the commonly used Reed-Solomon error correction code does not recover a significant amount of data when used in optical communication systems that experience high levels of fading in combination with low energy transmission[ericssonpatent][Aspreas2023ReedReceivers]. Therefore, in addition to tackling the issue of energy consumption in optical communication,

the BPPM error correction protocol was invented to provide more options for error correction in the field of modulation techniques which utilize temporal encoding of pulses[ericssonpatent].

1.2 The Project Goal

The goal of this feasibility study is to implement and test the functionality and capabilities of the BPPM error correction protocol invented at Ericsson. Note however that the scope of this thesis project is to test the protocol while simulating pulses containing more than one photon, which therefore demands a higher energy consumption than what was originally intended.

The implementation of the study consists of two parts: i) a software implementation and ii) a hardware implementation. The hardware implementation consists of an optical communication system that is used to experimentally derive the probabilities of loss- and addition errors in a setup where horizontally and vertically polarized light pulses are generated for long distance transmission. The experimental setup consists of a transmitter and a receiver side, connected over a single-mode fiber communication channel. The software implementation consists of the BPPM error correction protocol described in section 2.9, as well as simulated error generation using the experimentally derived probabilities for errors.

1.3 Related work

Optical communication utilizing single photons is of great interest in the world of data transfer, as it makes it possible to send as much information as possible using as little energy as possible. The idea of being able to transmit more than one bit of information per photon can be explored in many different ways.

Although pulse position modulation is not one of the most widely used modulation techniques for optical communication, there is a current interest for exploration of PPM using polarized single photons. Just like the BPPM protocol, these studies explore the possibility of reducing data loss during optical communication and increase the amount of information that can be conveyed using very few photons, both in free space and in fiber communication. In a study published in 2021, free-space optical communication with polarized photons encoded using PPM was utilized to explore the possibility of expanding channel capacity and thereby sending more information using less energy. The polarized PPM encoding utilized $\log_2(M) + 1$ bits of information per symbol, in contrast to the $\log_2(M)$ bits of information that is standard when using regular PPM. Here M is the number of available time-slots used for the encoding. The polarized PPM encoding of this study was tested during free-space long distances transmission with high levels of background noise. The results of the study were that each polarized pulse could carry 50% more information than for regular non-polarized PPM. Thereby, adding polarization as a degree of freedom in the encoding made it possible to suppress some of the background noise[Zhang2021HighModulation].

In another study which was published in 2017, free-space transmission of single photons from a heralded single photon source were used to experimentally verify the possibility of successfully detecting 10.5 bits of information per transmitted photon. The experiment utilized a spatial resolving photon counting detector of intensified charge coupled device type (ICCD), in combination with a pixel grid of 9072 spatial positions. Using a spatial light modulator (SLM), the transmitted photons were spatially encoded by being directed at different points on the detection surface of the ICCD[Tentrup2017TransmittingPhoton].

In regards to error correction in optical communication systems, different protocols have been studied and utilized over the years, amongst the most prevalent ones being Reed-Solomon (RS) and low density parity checking (LDPC). Another type of more recently explored error correction codes within optics are so called fountain codes. These types of error correction codes differ from codes like Reed-Solomon in the way that they have no fixed rates, meaning that their rates of transmission change with the transmission systems capacity. In a study published in 2020, a type of fountain code called Luby transform (LT) codes are used to attempt improving the bit error rate (BER) for optical fiber transmission. LT codes have a less complex encoding and decoding process than some other types of fountain codes, which is the reason why it was chosen for the study. The result of the study showed that using LT code, the transmission errors could be reduced no matter the channel noise level. The use of LT code was compared to both a case with no attempt at error correction, as well as a case of error correction using LDPC (with fixed transmission rate), in both cases the error correction with LT code exceeded the results of the opposing techniques[Ndiaye2020ImpactCode]. In an article from as early as 2010, the possibility of using a version of fountain codes in combination with PPM transmission and a photon counting receiver is described, suggesting that because of the characteristics of the errors involved with this type of optical communication encoding, fountain codes would provide efficient error correction[Fletcher2010High-EfficiencyCounting].

1.4 Research questions

- How can the BPPM error-correction protocol be implemented and tested using software simulations?
- How can an optical communication system be built so that it can be used to test the BPPM protocol?
- What are the error probabilities for photon losses and additions in the available experimental setup? Also, what is the polarization behaviour of the propagating light?
- How well does the BPPM error-correction protocol perform when errors are applied to its input?



2 Background and Theory

In this chapter, techniques and phenomena related to the thesis work are explained. This includes topics such as the behaviour of light propagation in fiber, light distribution, polarization, transmission errors etc. In addition, techniques such as error correction and signal modulation are described.

2.1 Electromagnetic Waves

Electromagnetic waves make up what is more commonly referred to as light. All the observations that are made by the human eye are due to reflections of electromagnetic waves as they propagate in different directions. The catalysts of electromagnetic waves are accelerations or vibrations of charged particles such as for example protons, electrons or ions[Bhattacharjee2023FundamentalWaves]. One way of creating this type of movement of charges is by de-excitation of electrons inside of atoms. Meaning that a previously excited electron is leaving a higher energy state for a lower one and simultaneously emitting the excess energy from the transition, which turn into rays of light[Zubairy2016ALight]. The movement of the charge, makes it so that its electric field starts to vibrate. The electric fields are vector fields that are specifically related to the charged property of the particle. The electric field is described by equation 2.1, expressing the field based on its temporal and spatial state. From the oscillations of the electric field, a magnetic field is generated, which moves perpendicularly to the electric field. The magnetic field is described by equation 2.2, which just like the electric field, changes over time and space. The electromagnetic wave is the result of the vibrating perpendicular motions of the electric and magnetic fields, as they alternately influence the motion of one another[Bhattacharjee2023FundamentalWaves]. The direction of the electromagnetic wave propagation is perpendicular to the two fields and therefore light is a so called *transverse* wave. The perpendicular relationship between the electric- and magnetic field, as well as the propagation direction, is expressed using equation 2.3, called the **Poynting vector**[Stutzman2018WavePrinciples].

$$\vec{E}(t, z) = E_0 \cos(\omega t - \beta z) \hat{x} \quad [\text{V/m}] \quad (2.1)$$

$$\vec{H}(t, z) = \frac{E_0}{\eta} \cos(\omega t - \beta z) \hat{y} \quad [\text{A/m}] \quad (2.2)$$

$$\vec{S}(t, z) = \vec{E}(t, z) \times \vec{H}(t, z) \quad (2.3)$$

The motions of the electric- and magnetic fields can be understood from equations 2.1 and 2.2. In these equations, \vec{E} is the electric field vector and \vec{H} is the magnetic field vector. Furthermore, w is the angular frequency in rad/s, t is the time elapsed [s], k is the distance propagated [m] and β is the phase constant in rad/m. Finally, the intrinsic medium impedance is $\eta = \sqrt{\mu/\epsilon} [\Omega]$, where μ is the medium permeability [H/m] and ϵ is the medium permittivity [F/m] [Stutzman2018WavePrinciples].

2.1.1 Polarization

Polarization is the unique property of electromagnetic waves which describes the behaviour of the electric field vector (and thereby the field oscillations) over time. The notations used to describe the electric field components of the polarization in the \hat{x} - and \hat{y} -direction are here given by equation 2.4 and 2.5 respectively. These equations are related via the combined electric field described by equation 2.6[Stutzman2018WavePrinciples].

$$E_x(t, z) = E_1 \cos(\omega t - \beta z) \quad (2.4)$$

$$E_y(t, z) = E_2 \cos(\omega t - \beta z + \delta) \quad (2.5)$$

$$\vec{E}(t, z) = E_x(t, z)\hat{x} + E_y(t, z)\hat{y} \quad (2.6)$$

In these equations, E_1 and E_2 are the amplitudes of the electric field components and δ is the relative phase between the two components. The values of E_1 , E_2 and δ determine the behaviour of the polarization. In figure 2.1, an illustration can be seen of the three main types of polarizations: elliptical, linear and circular in the cartesian coordinate system[Stutzman2018WavePrinciples].

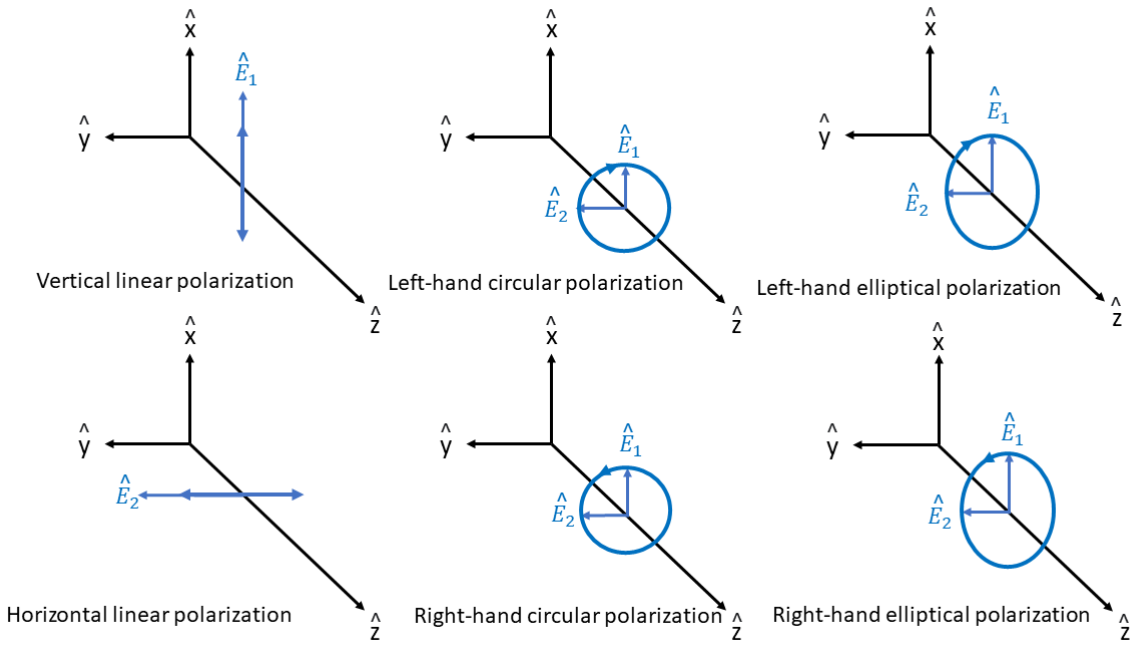


Figure 2.1: Illustration of elliptical-, circular- and linear polarization in the cartesian coordinate system ($\hat{x}, \hat{y}, \hat{z}$), with electric field vectors \hat{E}_1 and \hat{E}_2 .

The polarization types illustrated in figure 2.1 can be represented by different surface positions on the so called Poincaré sphere in figure 2.2. Therefore the Poincaré sphere is a helpful tool for visualization of different polarizations [Walkenhorst2020RevisitingState].

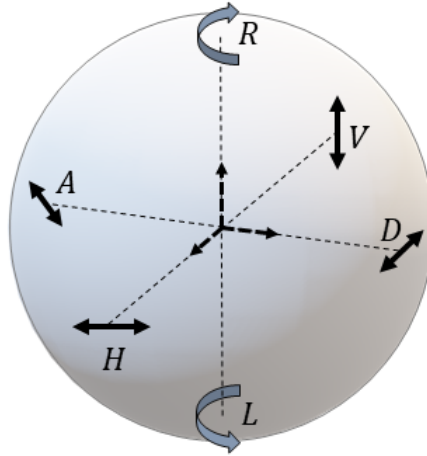


Figure 2.2: Illustration of the Poincaré sphere, where the linear polarizations: horizontal (H), vertical (V), diagonal (D), anti-diagonal (A) are illustrated as different spatial point on the sphere surface. At the top and bottom of the figure, right (R) and left (L) rotation are included.

2.1.1.1 Elliptical Polarization

Elliptical polarization is the umbrella term for all types of polarizations. It describes an electromagnetic wave for which the electric field components $E_x(t, z)$ and $E_y(t, z)$ do not necessarily have the same amplitude (E_1 and E_2) at a given point in time. There can also be a relative phase $\delta \neq 0^\circ$ differentiating the two. Different combinations of amplitude- and phase differences results in a rotation of the electric field over time which creates elliptical polarization. In figure 2.1, an illustration of two types of elliptical polarizations can be seen. In these cases, the amplitudes are $E_1 \neq E_2$ and the relative phases are either $\delta = 90^\circ$ (left-hand elliptical polarization) or $\delta = -90^\circ$ (right-hand elliptical polarization). Light can also be elliptically polarized if the relative phase is $\delta \neq 90^\circ$ [[Stutzman2018WavePrinciples](#)].

2.1.1.2 Linear Polarization

Linear polarization is a special case of elliptical polarization for which the phases of the electric-and magnetic fields are equal ($\delta = 0^\circ$). This makes it so that the electric field only oscillates in one dimension, meaning that it does not rotate[[Stutzman2018PolarizationPolarization](#)][[Stutzman2018WavePrinciples](#)]. An illustration of the electric- and magnetic fields of the linearly polarized electromagnetic wave can be seen in figure 2.3.

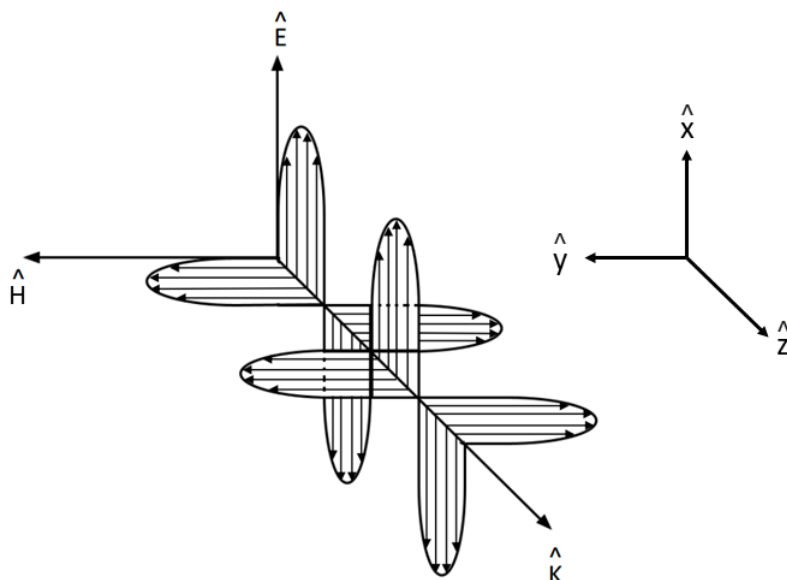


Figure 2.3: Illustration of the relation between the electric field \hat{E} (direction \hat{x}), magnetic field \hat{H} (direction \hat{y}), and wave propagation direction \hat{K} (direction \hat{z}) of a linearly polarized electromagnetic wave.

The relevance of polarization in regards to the thesis project specifically concerns the two linear polarization states called *horizontal* (H) and *vertical* (V) polarization[[ericssonpatent](#)]. For the horizontal linear polarization illustrated in figure 2.1, the electric field component amplitudes are $E_1 = 0$ and $E_2 \neq 0$. For the vertical linear polarization illustrated in the same figure, $E_2 = 0$ and $E_1 \neq 0$. Thereby, they are distinguished by their respective direction of oscillation in the \hat{x} - and \hat{y} -plane, meaning that they have the associative property of being perpendicular to one another. This property is utilized in the BPPM error correction protocol

since it makes them separable. For example, if light with vertical linear polarization passes through a horizontal linear polarizer, none of the light will reappear on the other side of the polarizer and vice versa [Stutzman2018WavePrinciples]. This process is illustrated in figure 2.4.

Note that the linear polarization can for example also be diagonal (D) and antidiagonal (A), for which the amplitudes are $E_1 = E_2$ [Stutzman2018WavePrinciples]. Because the diagonal and antidiagonal polarizations are also a duo of linear orthogonal polarization states, they can just as well be used instead of the horizontal and vertical combination of states. The difference lies in the experimental setup, as the D- and A- states require the use of a half-wave plate (HWP) to rotate the polarization to the horizontal and vertical polarization states before separating them using a polarizing beam splitter (PBS). Utilizing more components for the light to pass through contributes to additional loss of light and crosstalk between the polarized signals. Therefore, the usage of H- and V- states are used in order to avoid unnecessary system complications. The relationship between horizontal-, vertical-, diagonal- and antidiagonal-linear polarizations can be seen in the Poincaré sphere in figure 2.2.

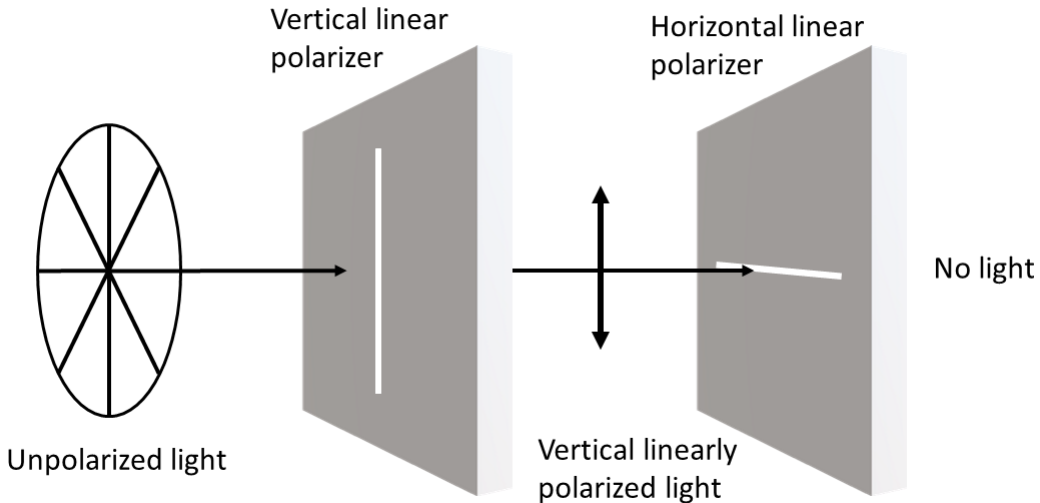


Figure 2.4: Illustration of unpolarized light passing through a vertical linear polarizer followed by a horizontal linear polarizer. At the first polarizer, only the vertically polarized portion of the light will pass through to the other side. After the second polarizer, none of the remaining light will have passed through. Because the vertical and horizontal polarizations are orthogonal, their respective polarizer will cancel out the light of the other.

2.1.1.3 Circular Polarization

Circular polarization is another special case of elliptical polarization, in which the amplitudes of the two electric field components are equal, $E_1 = E_2$. In figure 2.1, both the so called right-hand circular ($\delta = -90^\circ$) and the left-hand circular polarization ($\delta = +90^\circ$) can be seen [Stutzman2018WavePrinciples]. In figure 2.2, the right-and left-hand rotations are represented as R and L at the top and bottom of the Poincaré sphere.

In theory, also left- and right-hand circularly polarized light could be used instead of linear H- and V-polarization states in the system implementation. However, just like for diagonal and antidiagonal linear polarization states, this would contribute to the need for extra components

in the experimental setup and therefore result in more light losses and a low polarization extinction ratio. In this case, a quarter-wave plate (QWP) would be needed to rotate the circular polarization before the light is separated using a PBS[[Stevens2002PolarisationSystems](#)].

2.2 Signal Modulation

In order to transmit information during optical communication, the light signals must be encoded using some kind of modulation technique. Modulation theory is the technique of encoding data using energy states (light pulses) inside of time-bins. In this section, a couple of different modulation techniques are described.

2.2.1 On-off Keying

On-off keying (OOK) is one of the simplest and most commonly used modulation techniques for optical fiber communication[Jarzyna2015IncoherentLight]. The reasons for this is amongst other things OOK's comparatively high spectral efficiency (meaning that it can produce a high information rate for low bandwidth), as well as the fact that it is a cheap modulation option[Chitkara2014ComparativeModulator]. OOK utilizes only two energy states for encoding, meaning that a time-bin is either empty or occupied[Jarzyna2015IncoherentLight]. OOK modulation uses temporal binary encoding of pulses amongst x possible time-bins. The binary property of the encoding makes it so that with the x number of available time-bins, 2^x different data values can be expressed. The signal encoding of OOK can be either return to zero (RT) or non-return to zero (NRZ). In RT, the signal must return to zero between each encoded bit. This means that the duration of the light pulse does not cover the whole temporal duration of an information bit, simply because there is not enough time between that bit and the one after it. Therefore, RZ is more power efficient than NRZ, for which the signal does not have to go to zero between each encoded bit, meaning that the pulse covers the whole duration of the bit. One advantage that NRZ however has over RZ is the increased bandwidth efficiency that comes along with a longer pulse duration[Kim2018SuitableCoding]. An illustration of the OOK encoding, where $x = 3$, can be seen in figure 2.5.

2.2.2 Pulse Position Modulation

Pulse position modulation (PPM) is one of modulation techniques which are not commonly used for optical communication, one of the reasons being that it requires a large bandwidth. Also, during implementation of PPM, a lot of circuitry complications come along with creating a proper signal synchronization at the receiver[Kim2018SuitableCoding].

The PPM encoding is based on sending optical pulses of consistent width and amplitude, while using time as the variable for encoding. In modulation, the width of the pulse refers to its duration in time and the amplitude of the pulse corresponds to its power consumption. Thereby, PPM can be used to keep energy demand at a minimum. The advantage of PPM over more commonly used techniques such as OOK, is that it requires only one pulse of light to encode a symbol. In contrast, OOK can require several to transmit the same amount of information. However, this also means that communication using PPM is more time-consuming than other modulation techniques. Just like OOK, PPM utilizes only two energy states for encoding, wherein a time-bin is either empty or occupied[Jarzyna2015IncoherentLight].

For PPM, the temporal placement of a pulse amongst a number of $M = 2^x$ possible time-bins is the variable that allows for the encoding of the information. The transmission rate for PPM is measured in bits per second[Tang2022TheModulation]. Given the M number of possible time-bins, the encoded information per said pulse is $\log_2(M)$ number of bits[Mendez2010PulseArchitectures]. The BPPM protocol is an extension of regular PPM. Therefore, it too utilizes temporal encoding of optical signals, but with polarized single photons[ericssonpatent][Kim2018SuitableCoding].

Figure 2.5 illustrates how PPM differs from OOK. In this example $x = 3$ and there are therefore $M = 8$ available time-bins for the PPM encoding (one for each symbol), and $x = 3$ available time-bins for the OOK encoding (which can be used to create $2^x = 8$ different symbols). In this figure, the temporal position of the one pulse in the PPM encoding corresponds to the same decimal value that is expressed in binary temporal pulse encoding according to OOK[[Kim2018SuitableCoding](#)].

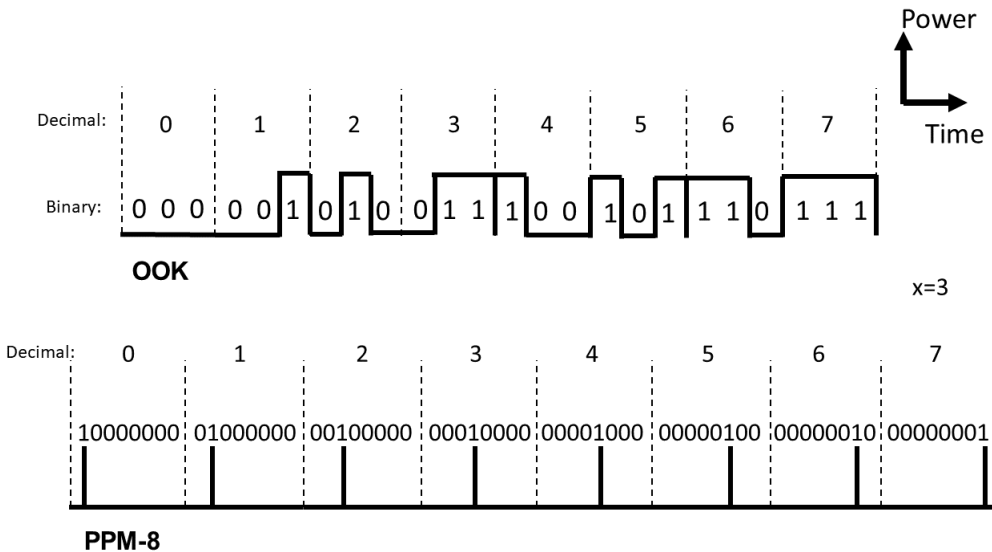


Figure 2.5: Signal illustrations of pulse position modulation using 8 time-slots (PPM-8) and on-off keying using 3 time-slots (OOK).

2.2.3 Pulse Amplitude Modulation and Pulse Width Modulation

There are other types of pulse modulation techniques than just PPM. Two examples are Pulse Amplitude Modulation (PAM) and Pulse Width Modulation (PWM). As the names would suggest, for PAM the pulse amplitude is the modulated variable while position and width are kept constant. For PWM, the pulse width is varied while amplitude and position are kept constant. In contrast to for example PAM, PPM generally has little interference of noise, which makes it an appropriate option when dealing with noisy channels[[Sacko2017TechniquesModulation](#)]. The three signal structures associated with PAM, PWM and PPM are illustrated in figure 2.6.

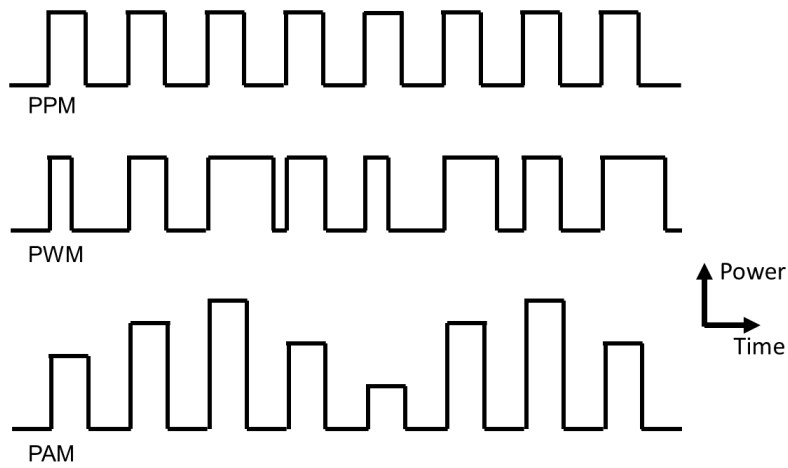


Figure 2.6: Signal illustrations of the pulse modulation techniques: pulse position modulation (PPM), pulse width modulation (PWM), pulse amplitude modulation (PAM).

In addition to OOK, two of the most commonly used modulation technique for optical fiber communication are PAM-2 and PAM-4. PAM-2 means that there are two available energy states for encoding (light/no light) and PAM-4 describes an encoding of 4 different available energy states [Apena2018PerformanceMATLAB]. PAM-2 is actually the same as NRZ OOK modulation because there are only two energy states and the pulse duration covers the whole bit [Kim2018SuitableCoding]. The encodings of PAM-2 and PAM-4 are displayed in figure 2.7.

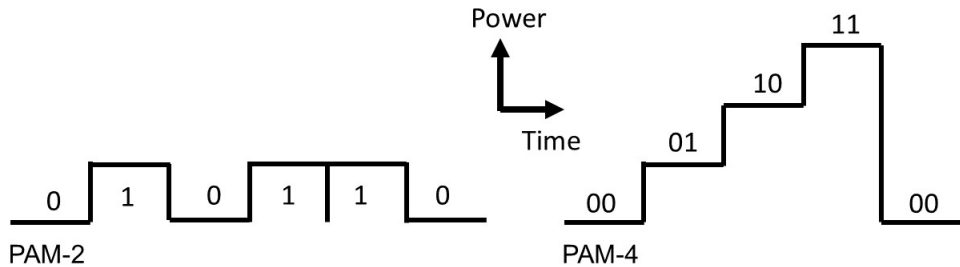


Figure 2.7: Signal illustrations of the pulse amplitude modulation techniques: PAM-2 and PAM-4.

2.3 Light Propagation in Single-mode Fiber

Optical communication over long distances require transmission of light, either through fiber propagation or in a free-space medium. Free-space transmission means that light is transmitted without an optical medium guiding it, therefore the light travels at a speed of $3 \cdot 10^8$ m/s. Communication via fiber on the other hand provides the light with an optical path through a fiber medium, which somewhat slows down the speed of the light propagation due to the refractive index of the fiber medium. During the thesis project, optical fiber of single-mode type is utilized.

An optical fiber is made up of a waveguide construction consisting of the so called core and cladding. The core is the middle portion of the fiber in which the light propagates, which is surrounded by the cladding. As the name suggests, the waveguide "guides" the electromagnetic wave in the direction of light propagation, with the light moving in a zigzag pattern inside the fiber as in figure 2.8. The light zigzags inside the fiber using total internal reflection (TIR), which is a phenomenon caused by the difference in the refractive indices of the core and cladding. If the core and cladding have refractive indices n_1, n_2 respectively, their relation should be such that $n_1 > n_2$ [Kasap2013SymmetricWaveguide].

For TIR to be possible, the incident angle of the light between core and cladding must be larger than the so called critical angle, θ_c . The critical angle is calculated according to equation 2.7.

$$\sin(\theta_c) = \frac{n_2}{n_1} \quad \Rightarrow \quad \theta_i > \theta_c = \arcsin \frac{n_2}{n_1} \quad (2.7)$$

At total internal reflection, the entirety of the incident wave is reflected inside the fiber. This means that none of the light is transmitted into the cladding and therefore there is no loss[Kasap2013SnellsTIR].

During the thesis project, single-mode fiber of type SMF-28 is used, for which the refractive index of the core is $n_1 = ??$ and the refractive index of the cladding is $n_2 = ??$.

lägg till
refractive
index värden

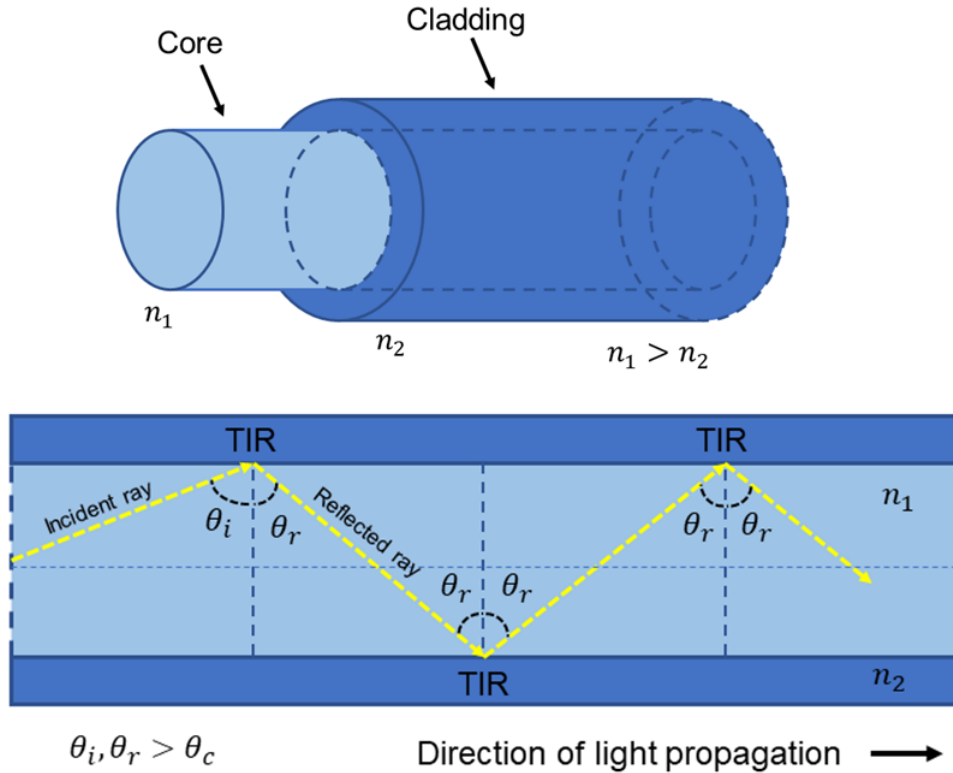


Figure 2.8: Illustration of light propagation in single-mode fiber. In this figure, n_1 and n_2 are the refractive indices of the core and cladding respectively. The angles θ_i and θ_r are the incident and reflected angles of light and θ_c is the critical angle.

A single-mode fiber is a fiber which only guides one beam of light, multi-mode fibers on the other hand has multiple paths for light to propagate through. The different modes of a multi-mode fiber do not interact with each other. Information propagating in multi-mode fiber moves slower than in single-mode fiber because of modal dispersion, which means that the light propagating in each mode has its own group velocity. The different group velocities make it so that the combined signal at the receiver covers/consists of a span of different information rates. Since single-mode fiber has only one mode, there is no modal dispersion to slow down the information rate[[Daendliker2000ConceptPhotonics](#)]. Single-mode fiber is suitable for transmission over long distances because of this lack of modal dispersion. Multi-mode fiber is better suited for short distance transmission because the modal dispersion gets progressively worse with the increased propagation distance[[Kasap2013WaveguideVelocity](#)]. Note however that multi-mode fiber in general is no longer used for telecommunication, aside for in some data center interconnections. In these cases, it is often for short to medium distance transmission up to 1 km. However, multi-mode fiber is still invariably used in local area networks (LAN:s)[[Kasap2013Telecommunications](#)].

2.4 Transmission Errors in Optical Communication

As previously mention, during optical communication via fiber, different types of signal errors can occur. Some of these errors (photon losses and photon additions) are covered by the BPPM protocol. The most common errors in optical communication via fiber is: attenuation, dispersion and non-linear effects[[M.Binjumah2017ErrorTransmission](#)].

Since the thesis project involves experimentation using single-mode fiber, there can be no intermodal dispersion, as this is an error that is specific to the existence of several modes in the multi-mode fiber. However, there will be some intramodal dispersion[Kasap2013WaveguideVelocity]. According to the product specifications of the single-mode fiber that is used during the thesis work (type: SMF-28), the dispersion is at a maximum $18.0 \text{ ps}/(\text{nm} \cdot \text{km})$ at the operating wavelength of the laser source at 1550 nm. This means that the dispersion is estimated to be quite low during the experiments, since the bit rate is slow[Kasap2013DispersionCompensation]. The non-linear effects will also be quite insignificant because of the low power of the transmitted signals[Kasap2013NonlinearDWDM]. This leaves only attenuation as the primary impairment during the optical fiber transmissions of this thesis project. Namely, light intensity decreases with propagated distance, which means that losses through attenuation are unavoidable.

2.4.1 Attenuation in Fiber and Loss of Light

Photon losses occur in an optical fiber when the intensity of the light propagating through it decreases with distance. This is called attenuation and has to do with a weakening of the electric field along the path of propagation. Attenuation can happen due to both extrinsic factors (such as bending of the fiber) and intrinsic factors (such as absorption and scattering). Bending losses arise from the fiber being curved in such a way that the internal reflections of the light inside the fiber are not TIR. Therefore, some of the light rays will exit the fiber through the cladding, as the angle of incidence is smaller than the critical angle θ_c . This transmission of light into the fiber wall will lead to overall attenuation of the signal power[Kasap2013AttenuationFibers]. An illustration of this phenomenon can be seen in figure 2.9.

kommentera/förty
någonstans
att BPPM
protokollet är
designat för
singelfotoner
men jag
kör med
ljuspulser
istället

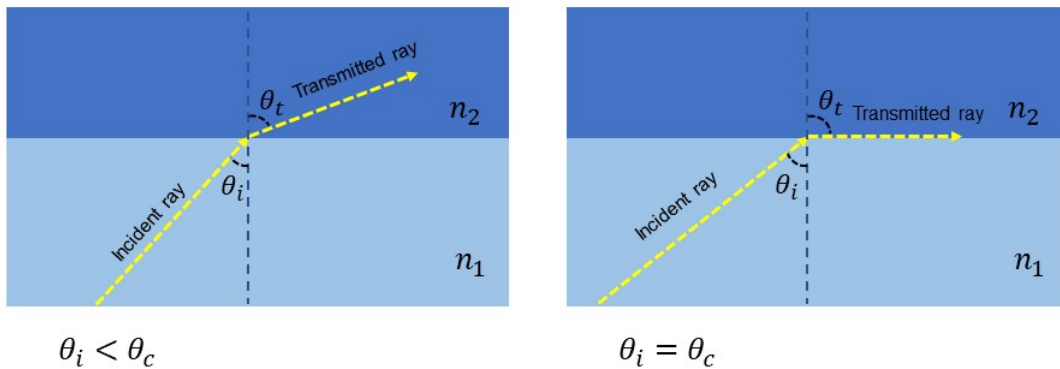


Figure 2.9: Illustration of loss of light in fiber due to angle of incidence (θ_i) being smaller than the critical angle θ_c . In this figure, θ_t is the angle of the transmitted light and n_1, n_2 are the refractive indices of the core and cladding respectively.

Attenuation caused by absorption occurs when some of the energy of the light is transformed into heat. This can happen during propagation through the fiber, when molecules in the medium are polarized, which in turn causes lattice vibrations [Kasap2013AbsorptionIndex].

Attenuation caused by scattering occurs when parts of the light ray are forced to propagate in other directions than that of the intended propagation path. This happens when a ray encounters changes in the refractive index throughout the medium, as can be the case in inhomogeneous materials. These scattered rays of light are called secondary electromagnetic waves and the specifics of the scattering is wavelength dependent[Kasap2013ScatteringLight][Kasap2013AttenuationFibers]. The attenuation over a distance can be expressed using the attenuation coefficient α according to equation 2.8.

$$\alpha = -\frac{1}{P} \frac{dP}{dz} \quad (2.8)$$

in which z is the distance propagated and P is the power of the signal at that distance. Given a fiber length L , an input optical power P_{in} and an output optical power P_{out} , the attenuation in dB per unit length of fiber can be expressed according to equation 2.9.

$$\alpha_{\text{dB}} = \frac{10}{L} \cdot \log_{10}(P_{\text{in}} / P_{\text{out}}) \quad (2.9)$$

This expression can be rewritten and used to create equation 2.10, describing the probability of not losing a photon on its way through the fiber channel or over the optical system components in the experimental setup. In this expression L is the propagated distance. During the thesis work, equation 2.10 is one of the components needed to model the estimated loss probabilities for the optical system p_{loss} .

$$P_{\text{channel_loss}} = 10^{(-\alpha_{\text{dB}} \cdot L - P_{\text{in}} + P_{\text{out}})/10} \quad (2.10)$$

2.5 False Detections and Detector Losses

In an optical communication system, there can be signal errors and distortions occurring both during channel transmission and at the receiver. In a single photon detector (SPD), the errors that occur at the receiver are related to the detection efficiency of the detector and the photoelectric activity inside it. In the SPD, the probability of detecting a transmitted signal properly is given by equation 2.11[Zhang2021HighModulation].

$$P_{\text{detect}} = \exp(-T_{\text{dt}} \cdot (f_{\text{dc}} + f_{\text{sl}})) \cdot (1 - \exp(-\eta_{\text{eff}} \cdot u)) \quad (2.11)$$

Where T_{dt} is the deadtime of the SPD [s], f_{dc} is the dark-count rate [Hz], f_{sl} is the stray light rate [Hz], η_{eff} is the detection efficiency [%] and u is the average number of photons per transmitted pulse[Zhang2021HighModulation].

2.5.1 Detector Losses

The losses occurring at the detector are related to the set detection efficiency of the SPD (η_{eff}), which makes it so that the detector can register a maximum of $\eta_{\text{eff}} \cdot u$ photons per pulse. Here, each pulse contains u number of photons. Since equation 2.11 described the probability of signal detection, the probability of not detecting the incoming signal is naturally given by 2.12. During the thesis work, equation 2.12 is the other component needed to model the estimated loss probabilities p_{loss} for the optical system.

$$P_{\text{no_detect}} = 1 - P_{\text{detect}} \quad (2.12)$$

2.5.2 Detector Additions

During the thesis project, the term "addition errors" will be used interchangeably with "dark-counts". The reason for this being that the photon additions that could potentially occur during transmission through the fiber channel, are estimated to be much smaller than the

dark-count contributions occurring at the detector (stray light << dark-counts).

During light detection, as incoming photons are registered at the receiver, the energy they carry is passed over to electrons inside the detector. This causes a discharge of electrons inside the detector, and an "electron avalanche" is created. The phenomena is called the photoelectric effect and it is the process that transforms an optical signal to an electrical signal. However, due to factors such as thermal effects, quantum tunneling and afterpulsing inside the detector, there can be false detections without any actual incident photons. These false detections are called dark-counts and cause an excessive amount of released electrons which are then registered as signal input[Spagnolo2019LEDEffect][Panglosse2020DarkDiodes]. The thermal effects are caused by the heat being generated in the detector during use and afterpulsing is caused by delayed release of electrons that have been stuck in the junction depletion region of the semiconductor material [Panglosse2020DarkDiodes].

Quantum tunneling is a phenomena related to quantum mechanics, just as the name suggests. It is the process of having a particle (of energy E_1) pass through a potential barrier of higher energy (E_2), such that $E_1 < E_2$. According to classical mechanics this should not be possible. However, due to quantum tunneling, the particle manages to do so anyways. Quantum tunneling can thereby cause dark-counts in a detector by making it so that an electron of energy level E_1 passes through the energy barrier in the detector (of energy level E_2) which is supposed to stop false detections from happening. Because of quantum tunneling, the activity of the electron is then misread as an incoming photon[Martin-Palma2020QuantumPhotons].

Equation 2.13 describes the probability for dark-counts occurring in the detector. It is therefore the formula that is used to model the addition error probability p_{add} during the thesis work. In this expression T is the sampling time [s], f_{dc} is the dark-count rate [Hz] and f_{sl} is the stray light rate [Hz][Zhang2021HighModulation].

$$P_{\text{noise}} = 1 - \exp(-T \cdot (f_{\text{dc}} + f_{\text{sl}})) \quad (2.13)$$

2.6 Bit-flips

The loss- and addition errors described in sections 2.5 and 2.4.1 can also be called binary bit-flip errors. Depending on whether the channel is binary symmetric or asymmetric, losses and additions are more or less likely to occur[Kl1995ErrorChannel].

2.6.1 Binary Bit-flips

Bit-flips are errors in binary communication systems which mean that a value of 0 can become a 1 and vice versa. This flip occurs with a variable probability p . In figure 2.10, the binary symmetric channel (BSC) and the binary asymmetric channel (z-channel) can be seen. For the BSC, the probability p of a $0 \rightarrow 1$ transition is the same as for a $1 \rightarrow 0$ transition. For the z-channel on the other hand, the probability of a $0 \rightarrow 1$ bit-flip is negligible or non-existent compared to a $1 \rightarrow 0$ bit-flip[Kl1995ErrorChannel].

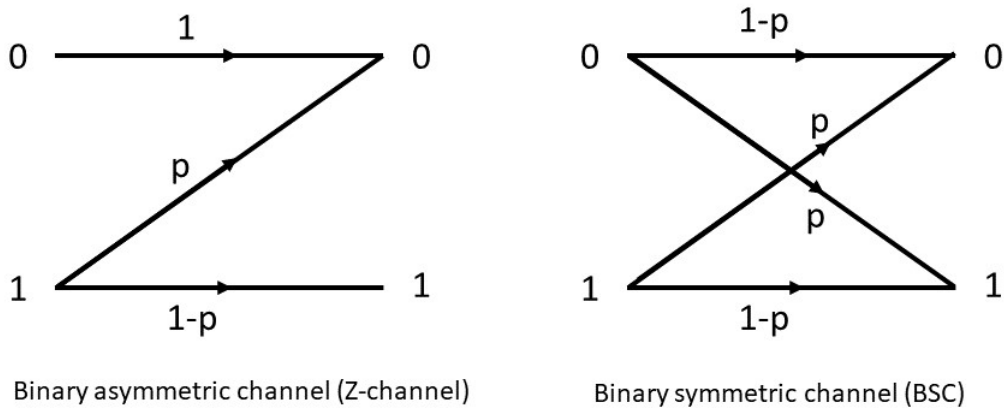


Figure 2.10: Illustrations of bit-flips in the BSC and z-channel, where p is the bit-flip probability.

2.6.2 Polarization Bit-flips

During the thesis project, there is yet another dimension to the potential bit-flips to be aware of. That is the polarization of any addition error photons in a system of BSC type. Since the encoding of the protocol incorporates the use of horizontal (H) and vertical (V) linear polarization states, there can be additive bit-flips of either type $0 \rightarrow H$ or $0 \rightarrow V$.

Theoretically, there can also occur combinations of losses and additions of photons in such a way that ultimately only the polarization of the photon occupying a particular time-bin is changed. Meaning that, a horizontally polarized photon is lost ($H \rightarrow 0$) and after that another photon with vertical polarization is added to the exact same now empty time-bin ($0 \rightarrow V$). Naturally, the process can also happen the other way around, so that ultimately $V \rightarrow 0 \rightarrow H$. Because of the low probability for this type of loss- and addition error combination in the same time-slot, scenarios such as this are not taken into account in the software implementation of the BPPM error correction protocol.

Another type of bit-flip to be aware of is in regards to polarization drift in the system, in this case meaning that $V \rightarrow H$ and $H \rightarrow V$. In a system with stable polarization states (H and V) this is not an issue. The BPPM protocol assumes stable polarization throughout transmission and therefore this type of error is not taken into account either during the software implementation of the protocol. However, during actual optical transmission, the polarization drift is a phenomena to be aware of and is should be counteracted if possible.

2.6.2.1 Polarization Drift

Polarization drift occurs in optical fiber when the fiber structure is imperfect in such a way that the electric field components E_x and E_y are not completely orthogonal. By then, the electric field components eventually start to exchange power. The fiber can be damaged during manufacturing, installation or through bending. The damage causes the core radius to become asymmetric, in turn creating birefringence and therefore polarization drift. [1]. In the case of using horizontal and vertical polarization states, which are utilized during the thesis work, the impact of polarization drift ultimately means that the polarization will no longer be linear, but instead elliptical.

Polarization drift is not a particularly quick process and can be compensated for using the right equipment, such as for example polarization-maintaining fiber or electronic stabilization. Regarding transmission of single photons in particular, a feedback signal in combination with electronic polarization controllers (EPC) can be used to continuously stabilize the polarization by rotation of the EPC:s. The feedback signal is in this case created using an extra laser source sending classical light pulses. By measuring and correcting for the drift in the classic light beam, the single-photon signal can be stabilized as well[[Chen2007ActiveDistribution](#)]. Because polarization is the degree of freedom used to aid in the error correction of BPPM, it is important that a communication system utilizing this protocol has stable enough polarization.

2.7 Photon Statistics

Depending on which type of light source is used during optical transmission, the probability distribution of the light is either Poissonian, sub-Poissonian or super-Poissonian[Fox2006PhotonStatistics]. During this thesis project, a laser source is used, which means that the light distribution is Poissonian. The three distribution types are briefly described in this section to give an understanding of how they differ and most importantly, what is the nature of the light distribution that is observed during the thesis work.

2.7.1 Poisson Distribution

The Poisson distribution of light is applicable to coherent sources of light, such as lasers. Therefore, Poissonian light distribution is the relevant type of photon statistic for this thesis project. Poisson distribution describes the probability of registering a number of photons k within a light pulse, provided that the average number of photons per pulse is u . This probability is described by equation 2.14, which is used in figure 2.11 to model the distributions for pulses containing between (on average) 1 and 10 photons[Zhang2021HighModulation]. Poisson distribution is consistent with the behaviour of classical light[Fox2006PhotonStatistics].

$$P_{\text{poisson}}(u, k) = \frac{u^k}{k!} e^{-u} \quad \text{where } u = \bar{k}, \quad k \in \{0, 1, 2, \dots\} \quad (2.14)$$

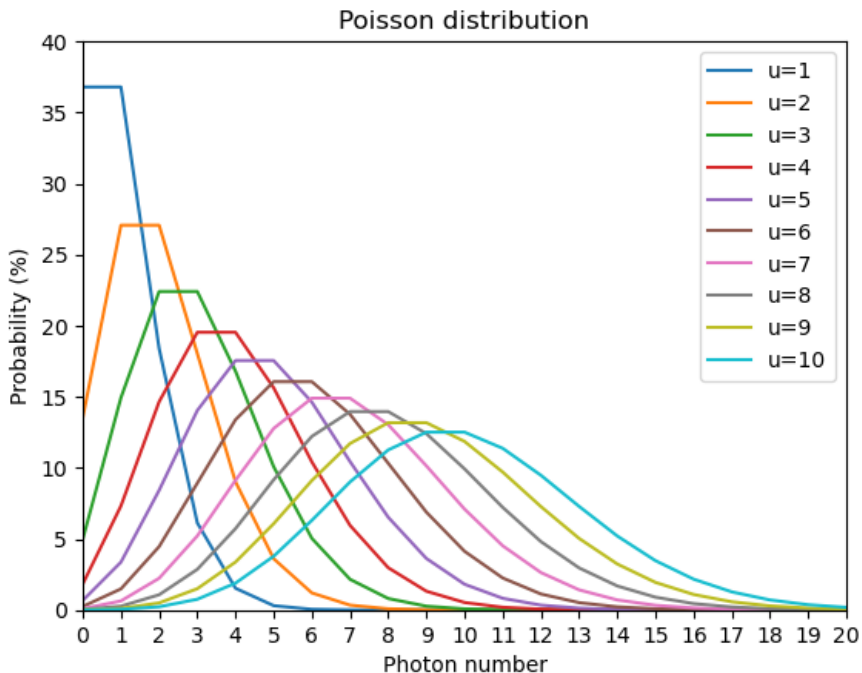


Figure 2.11: Poisson distribution: Event registering probability (P_{poisson}) over photon number (k) for an average number of photons per pulse $u = 1, 2, 3, 4, 5, 6, 7, 8, 9, 10$.

2.7.2 Super-Poissonian Distribution

The super-Poissonian light distribution is applicable to thermal light (also called black-body radiation) and is therefore just like Poisson distribution consistent with the behaviour of classical light. The super-Poissonian statistics follow the Bose-Einstein distribution described by equation 2.15, which is used in figure 2.12 to model the distributions for u - values between on average 1 and 10 photons per pulse[Fox2006PhotonStatistics]. Similar to Poisson distribution, super-Poissonian distribution describes the probability of registering a number of photons k within a pulse, provided that u is the average number of photons per pulse[Zhang2021HighModulation].

$$P_{\text{super_poisson}}(u, k) = \frac{u^k}{(u + 1)^{k+1}} \quad \text{where} \quad u = \bar{k}, \quad k \in \{0, 1, 2, \dots\} \quad (2.15)$$

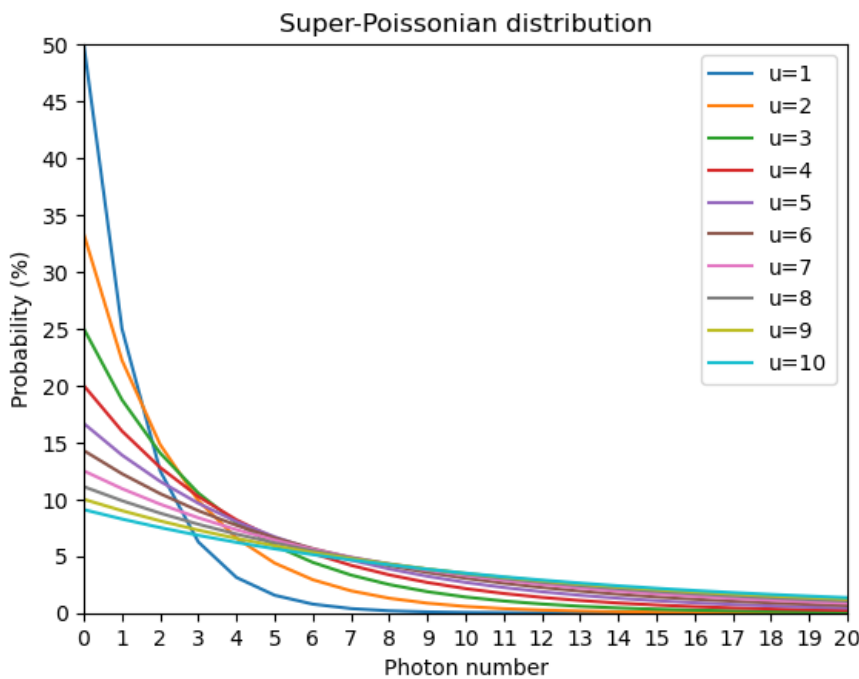


Figure 2.12: Super-Poissonian distribution: Event registering probability ($P_{\text{super_poisson}}$) over photon number (k) for an average number of photons per pulse $u = 1, 2, 3, 4, 5, 6, 7, 8, 9, 10$.

2.7.3 Sub-Poissonian Distribution

In contrast to Poisson distribution and super-Poissonian distribution, sub-Poissonian statistics is more consistent with the quantum optical way of viewing light, rather than the classical theory. In other words, sub-Poissonian distribution is relevant when light is not regarded as a classical electromagnetic wave, but rather as a stream of photons [Fox2006PhotonStatistics]. Therefore, had the light source used during the thesis work been of single photon emitter type, the distribution would have been sub-Poissonian. Sub-Poissonian distribution describes the probability of registering a number of photons k within a pulse, provided that the average number of photons per pulse is u . This probability is described by equation 2.16, which is used in figure 2.13 to model the distributions for u - values between on average 1 and 10 photons per pulse [Zhang2021HighModulation][Fox2006PhotonStatistics].

$$P_{\text{sub_poisson}} = \begin{cases} 1, & k = u \\ 0, & k \neq u \end{cases} \quad \text{where } u = \bar{k}, \quad k \in \{0, 1, 2, \dots\} \quad (2.16)$$

As can be seen in figure 2.13, the sub-Poissonian distribution describes the Fock state for each photon number, in which the probability of detection is 100% when $k = u$ and 0% when $k \neq u$ [Deng2023Heisenberg-limitedStates].

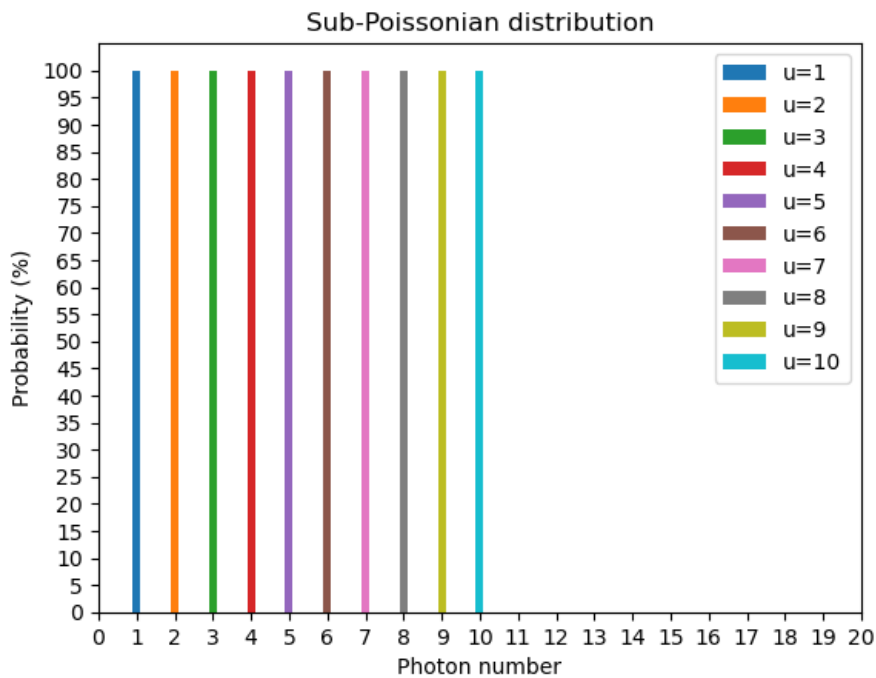


Figure 2.13: Sub-Poissonian distribution: Event registering probability ($P_{\text{sub_poisson}}$) over photon number (k) for an average number of photons per pulse $u = 1, 2, 3, 4, 5, 6, 7, 8, 9, 10$.

2.8 Error-correction

Another aspect to the BPPM protocol is the capacity to perform error correction on erroneous received data. In sections 2.4.1 and 2.5 errors that can occur during optical transmission are described in the form of addition- and loss errors. These are the error types in focus for the BPPM protocol.

To increase the amount of successfully transmitted information over noisy and unreliable optical transmission channels, error correction codes can be used to detect and/or restore some of the lost data at the receiver side of the system. Error correction codes are an important aspect of coding theory as they lessen the need to re-send information, thereby decreasing the required amount of energy needed for transmission. Coding theory is the study of arranging information in ways which makes it possible to perform error correction[Dumas2015ErrorCorrection]. This can be done using a set of algorithmic rules governing the data encoding at the transmitter, which can later be used for decoding and error correction at the receiver[Alabady2021AnNetworks]. An important coding theory term is *error rate*, which describes the ratio between the amount of data that was lost during transmission and the amount of data that was originally transmitted. The error rate can thereby be reduced by the use of error correction codes. The error rate for communication via optical fiber is approximately 10^{-9} [Dumas2015ErrorCorrection].

2.8.1 Reed-Solomon Codes

There are many different types of error correction codes, one of the most well known ones being Reed-Solomon. Reed-Solomon is a type of forward error correction code (FEC) and it is widely used because of its prominent error-correction capabilities regarding burst errors[TelecommunicationStandardizationSectorITU2000ForwardSystems]. FEC codes are often used when information for whatever reason cannot be resent or when it is very expensive to do so. In some ways, the BPPM error correction protocol is also a type of FEC, because of its ability to retrieve lost transmission data at the receiver[Alabady2021AnNetworks].

The Reed-Solomon encoding (often written as RS[n,k]) utilizes implementation of some extra information bits in addition to the transmitted data, so called parity bits. The extra parity bits can be used to recover information in erroneous codewords. In Reed-Solomon, codewords consisting of $n = 2^s - 1$ number of symbols are made, where each symbol consists of s number of bits. Furthermore, out of the n number of symbols in the codeword, k number of symbols make out the data that is to be conveyed. The variables n and k are related via the expression $2t = n - k$, where $2t$ are the number of added parity symbols used for error correction of the codeword and t is the maximum number of solvable symbol errors per said codeword. Naturally, this means that a large t -value implies more solvable errors, but at the cost of a larger number of required parity symbols $2t$. Therefore, the improvement of the error correction capabilities comes at the cost of heightened consumption of computational power. The trade-off then becomes a matter of power versus data accuracy[Alabady2021AnNetworks].

An example of commonly used Reed-Solomon encoding is RS[255, 239]. In this particular encoding, the codeword is $n = 255$ symbols long and there are $s = \log_2(n - 1) = 8$ information bits per symbol, i.e. 1 symbol = 1 byte. Therefore, each codeword consists of 255 bytes and $k = 239$ of these bytes are made up of data. The added parity symbols that can be used for error correction make up $n - k = 16$ bytes of the codeword. This means that a maximum of $t = (n - k)/2 = 8$ bytes of data can be recovered through error correction[Alabady2021AnNetworks].

Using single photon encoded PPM combined with Reed-Solomon is one way of performing optical transmission and error correction. The need for research into newer modulation techniques and error correction protocols such as BPPM stems from the need for even better and more energy efficient solutions. This is especially true in optical communication systems that experience high levels of fading in combination with low energy transmission, for which Reed Solomon has not proven to provide a significant amount of data recovery[ericssonpatent][Aspreas2023ReedReceivers].

2.9 The BPPM Error Correction Protocol Description

In this section, the BPPM protocol invented at Ericsson is explained. In short, the BPPM protocol utilizes single photon for encoding, with linear polarization (horizontal and vertical states) as a degree of freedom. The use of single photons in orthogonal polarization states and with temporal encoding, allows for corrections of loss- and addition errors that are common during optical communication. The BPPM protocol is especially applicable to asymmetric channels, meaning that the probability of loss is greater than the probability of addition[Kl1995ErrorChannel][ericssonpatent].

2.9.1 Definitions

- **Super-block:** A sequence of data values encoded using photons in particular temporal arrangements, i.e. photons in time-bins. There is a sequential dependence between the temporal encoding of the photons and their polarizations[ericssonpatent].
- **Sub-block:** The components that make up a super-block. Each sub-block contains exactly one photon which is either horizontally or vertically polarized. The photon in a sub-block always occupy its very first time-bin. The rest of the sub-block consists of a variable number of empty time-bins, depending on the length of the sub-block[ericssonpatent].

2.9.2 Data Representation

In the BPPM error correction protocol, data is structured in separate codewords that are here called **super-blocks**. The super-blocks are independent of each other in regards to the error correction. A super-block is the combination of n number of **sub-blocks**, wherein each sub-block length x is gathered from a number sequence such that $x \in \{1, 2, 4, 7, 12, 20, \dots\}$ [Hoey2016SequenseSequences]. Note that no matter the value of n , the corresponding super-block must be constructed using the first n sub-blocks in the sequence and no sub-block length can be used more than once in a super-block. The order of the n number of sub-blocks within the super-block can however be arranged in any one of the $n!$ available permutations. The number of available permutations is therefore a consequence of the length of the super-block and the amount of possible permutations is what gives versatility to the data. Therefore, the longer the super-block, the larger is the amount of information that can be transmitted using that super-block size. The amount of information bits that can be transmitted using this data representation is calculated using: $\log_2(n!)$ [ericssonpatent].

Example 1

Assume a super-block size of $n = 3$ sub-blocks. With this, it is possible to construct $n! = 3! = 6$ different super-block permutations: (1,2,4), (1,4,2), (2,1,4), (2,4,1), (4,1,2), (4,2,1). With these, it is possible to transmit a maximum of $\log_2(3!) = 1.585\dots$ bits of information per super-block.

The values in the sequence of allowed lengths $x \in \{1, 2, 4, 7, 12, 20, \dots\}$ each correspond to a length x of a sub-block, which is the same as its temporal duration. Every sub-block consists of a single photon occupying a time-bin, followed by a number of empty time-bins ($x - 1$). For example, a sub-block of length 4 consists of a photon followed by three empty time-bins (see sub-block 3 in figure 2.15). In the sequence of allowed lengths, any summation of two values will result in a length that is not already in the sequence, meaning that the summation is distinct. This is a fact that can be used for error correction. This also means that the summation of any two elements from the sequence will result in a value that can't be produced by the summation of any other two sequence values, meaning that the summation of two sequence

values is always distinct. In addition, since each sub-block length should be found only once in a super-block, any potential duplicates can be used to identify errors in the super-block. For the sake of error correction, the number of sub-block lengths n in a super-block are assumed to be known on both the transmitter and receiver side[ericssonpatent].

Each sub-block photon in a super-block is linearly polarized either horizontally (H) or vertically (V) (see section 2.1.1.2 for description of linear polarization states). Bit-flips between the two polarization states are assumed to be highly unlikely according to the protocol and are not covered by BPPM. Namely, the polarization is important for the error correction as the polarization of a sub-block photon is dependent on the length of the sub-block that comes after it. If the following sub-block is shorter, the polarization of the previous sub-block will be vertical (V). If the following sub-block on the other hand is longer than its predecessor, the polarization of the former will be horizontal (H). The polarization of the last sub-block in the super-block will, in the same manner, be dependent on the length of the very first sub-block in the super-block[ericssonpatent].

Example 2

In figure 2.14 the correlation between polarization and order of sub-block lengths within a super-block is displayed using super-block permutations of size $n=2$. Let's first study super-block permutation (1,2). Since $1 < 2$, the sub-block of length 1 will be horizontally polarized. Furthermore, because $2 > 1$, the sub-block of length 2 will have vertical polarization. This means that the full sequence of polarization is (H,V). By using the same logic, the sequence of polarization for super-block permutation (2,1) is (V,H).

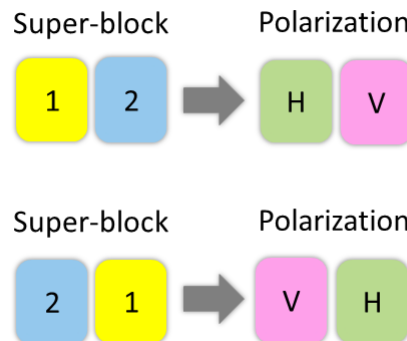


Figure 2.14: Illustration of the dependence between polarization and order of sub-block lengths within super-blocks of size $n=2$, i.e. for permutations (1,2) and (2,1). In the figure, H=horizontal polarization and V=vertical polarization.

Example 3

Assume a super-block consisting of four sub-blocks, with its lengths arranged in the order: (1, 2, 4, 7). The corresponding sequence of polarizations is then: (H,H,H,V), since $1 < 2 < 4 < 7$ and $7 > 1$. The super-block is then transmitted as: HH0H000V000000. In which, the 0:s correspond to the empty time-bins which define the temporal length of the sub-blocks. Note that all time-bins are of the same width in this encoding, regardless of whether they contain a polarized photon (H or V) or no photon at all. In figure 2.15, the super-block is illustrated using signal power over time.

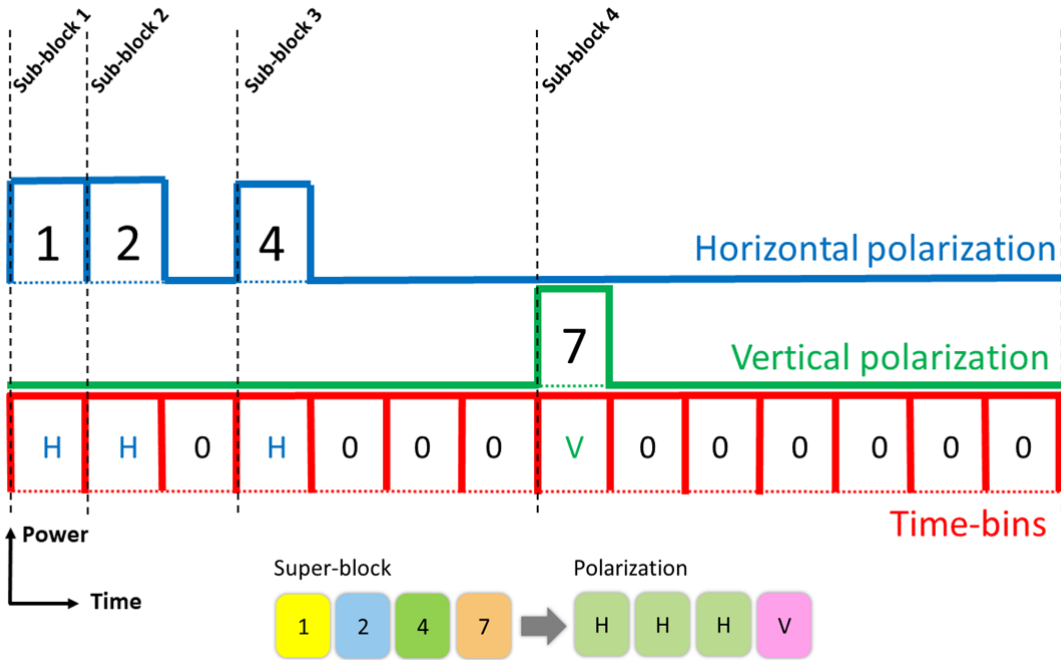


Figure 2.15: Illustration of super-block permutation (1,2,4,7), displaying signal power over time. In the figure, H=horizontal polarization and V=vertical polarization.

2.9.3 Error Correction

The BPPM error correction protocol describes solutions for two types of errors: additions of photons (from stray light or dark-counts) and losses of photons (due to attenuation). The specific rules concerning the correction of these two error types are presented in sections 2.9.3.2 and 2.9.3.1 respectively. Instances where there are non-correctable errors in super-blocks are discussed in 2.9.3.3. Note that for error correction to be possible, the length of the transmitted super-blocks must be known to both sender and receiver[ericssonpatent].

2.9.3.1 Loss of a Photon

Let's assume that there has been a photon loss in a super-block during transmission. Then, one of the indicators to the receiver that this has happened is the fact that the super-block will contain one less sub-block than expected. In some loss error cases, some of the sub-block lengths within the erroneous super-block will not be included in the sequence of allowed lengths. In other cases, one or more values from the sequence of allowed lengths, that should be in the super-block, are not present. The reason for this is the fact that the loss of a photon will conclude in the temporal elongation of the sub-block before it[ericssonpatent].

Example 4

As an example of this type of error, assume that super-block HH0H000V000000 (1,2,4,7) is transmitted, see figure 2.15. The received erroneous super-block is HH00000V000000 (1,6,7), see figure 2.16. In other words, the sub-block of length 4 has disappeared throughout transmission and the sub-block length now replacing the 2 and the 4, is of length 6. Since the recipient can be assumed to know the length of the complete

super-block to be $n = 4$, they will know that it is missing one sub-block value. In addition to this, the length of 6 is not in the sequence of allowed lengths. Also, it is known that the super-block must contain the lengths: 1,2,4 and 7. Therefore, the 6 must be an addition of 2 and 4. Now, the question remaining is in what order they should be placed in the corrected super-block. This part of the solution will require knowledge about the polarization. Namely, if the polarization corresponding to the disallowed length of 6 is horizontal, then the 2 must be placed before the 4, as $2 < 4$. If on the other hand, the polarization is vertical, the 4 must be placed before the 2. In this particular example, since the polarization of the sub-block with length 6 is horizontal, the corrected super-block will be HH0H000V000000 (1,2,4,7).

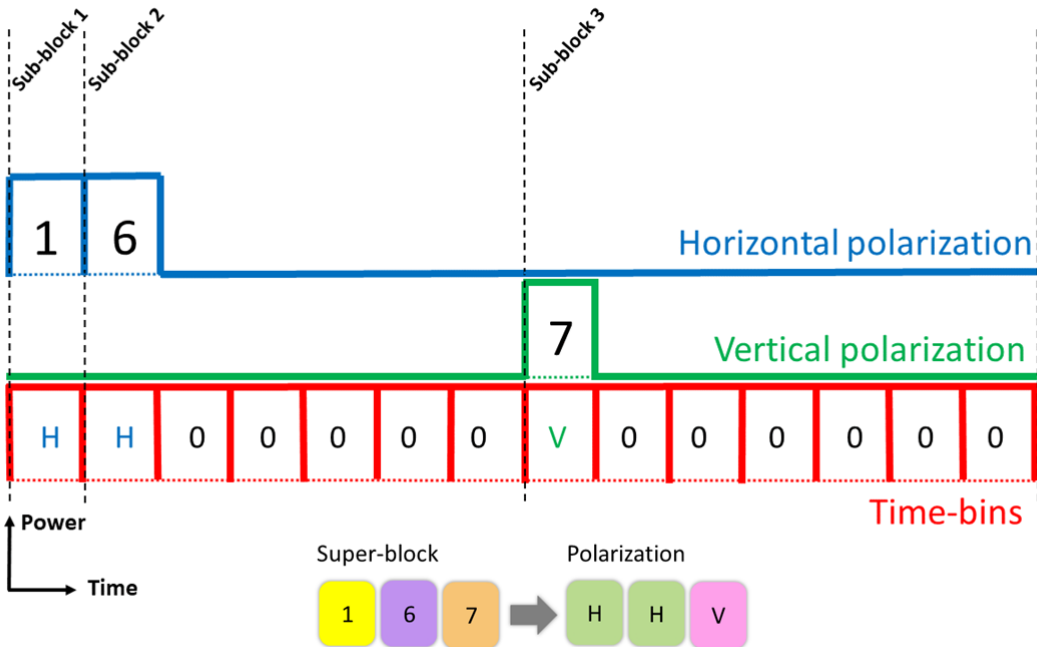


Figure 2.16: Illustration of the erroneous super-block (1,6,7), displaying signal power over time. In the figure, H=horizontal polarization and V=vertical polarization.

The same method as above can be applied for any number of loss errors in a super-block, provided that the loss errors don't occur in two directly adjacent sub-blocks.

Example 5

For example when transmitting super-block HH0H000V000000 (1,2,4,7) (see figure 2.15) and receiving H00H000000000 (3,11) (see figure 2.17). In this case, it is only possible to split the 3 into 1 and 2, and the 11 into 4 and 7 when looking amongst the values in the sequence of allowed lengths. Now, just like before, to get the correct order of the lengths, the polarization of the respective erroneous sub-blocks must be studied. Since both sub-block of length 3 and 11 have horizontal polarization, the correct order must be (1,2,4,7), as $1 < 2 < 4 < 7$ and $7 > 1$.

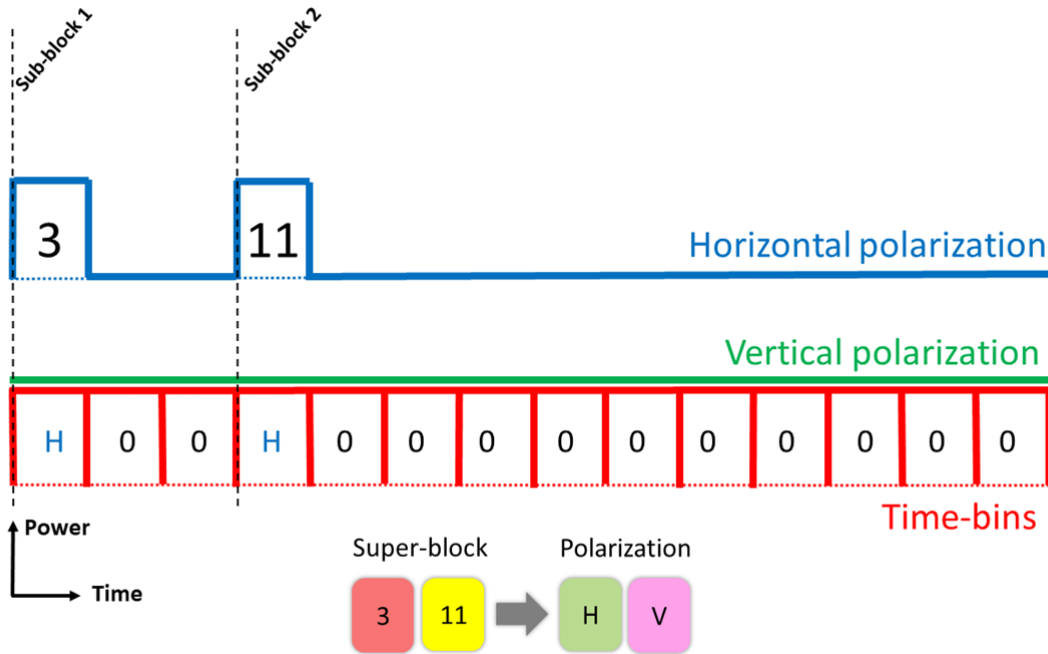


Figure 2.17: Illustration of the erroneous super-block (3,11), displaying signal power over time. In the figure, H=horizontal polarization and V=vertical polarization.

Let's now study a special case where it is the first sub-block in the super-block that is missing.

Example 6

Let's assume that during transmission of a super-block, only the very first sub-block length is lost. In these situations there are no disallowed lengths present in the detected super-block, however the super-block will contain one less sub-block than expected. This type of error is corrected by inserting the missing value at the beginning of the super-block. An example of this type of error would be receiving 0H0H000V000000 (2,4,7), which would then be corrected as HH0H000V000000 (1,2,4,7). In contrast to this, if the missing length of 1 instead for example was originally placed at the end of the super-block, so that the original super-block was (2,4,7,1). Then the sequence H0H000V0000000 (2,4,8) would be received instead. In this case, the polarization of the 4, and the fact that 1 and 7 are both missing from the super-block, are used to solve the error. Namely, since $4 > 1$ and $4 < 7$, the horizontal polarization of the 4 makes it so that the correct super-block is H0H000V000000H (2,4,7,1).

2.9.3.2 Addition of a Photon

In the cases where there appears an addition of a photon in a super-block, the error correction protocol will make note that the super-block contains more sub-blocks than expected. The addition of a photon in a super-block results in a cut-off of the length of an already existing sub-block, by having an extra photon placing itself in one of the empty time-bins of that sub-block. In the examples below, an "X" is used to represent the polarized added photon in

the super-block. In reality however, the "X" will always represent either an "H" for horizontal- or a "V" for vertical polarization[ericssonpatent].

Example 7

As an example of this type of error, assume that the super-block HH0H000H000000V000000000000 (1,2,4,7,12) is transmitted. The received erroneous super-block in this particular case happens to be HH0H000H000000V00X00000000 (1,2,4,7,3,9). In cases such as this, where the added photon results in two disallowed adjacent sub-block lengths, the error is solved by summing them up directly to create the allowed length 12.

If there is a doublet of an allowed length placed adjacent to a disallowed length, then these can be directly summed up as well.

Example 8

An example of this is when transmitting the super-block HH0H000V000000 (1,2,4,7) (see figure 2.15) and instead receiving the erroneous super-block HH0HX00V000000 (1,2,1,3,7) (see figure 2.18). Here, the only possible solution is to combine the adjacent 1 and 3 to correct the super-block error.

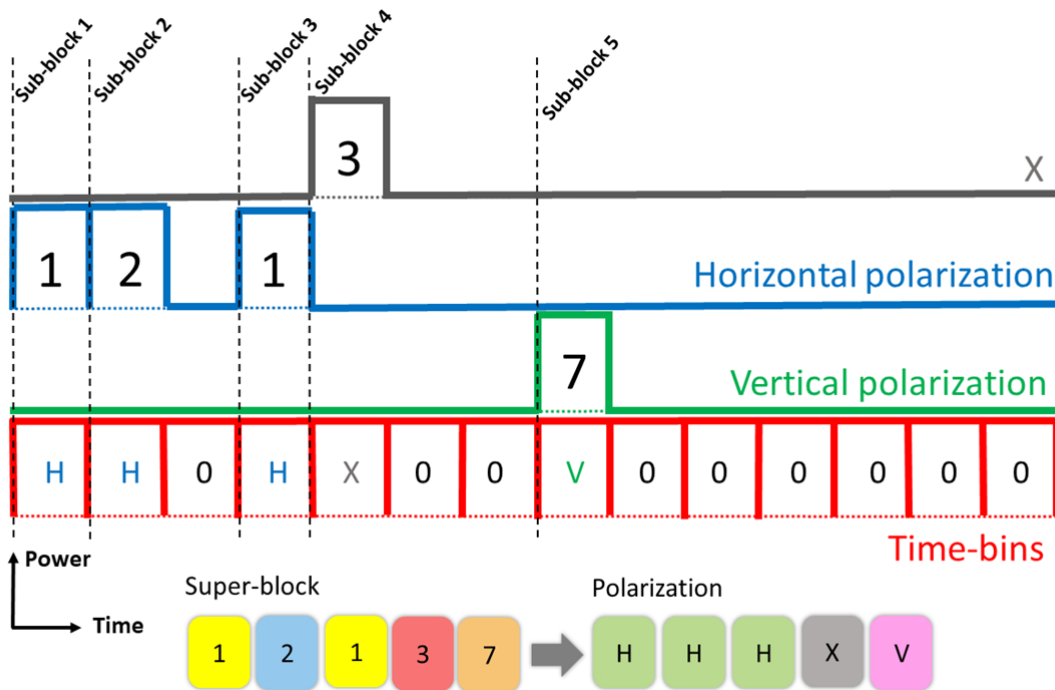


Figure 2.18: Illustration of the erroneous super-block (1,2,1,3,7), displaying signal power over time. In the figure, H=horizontal polarization, V=vertical polarization and X is either H- or V-polarization.

There are also so called “symmetric” error cases, which are situations where there is a disallowed length directly adjacent to duplicate allowed lengths, one on each side of

it[ericssonpatent].

Example 9

An example of this type of error is when transmitting the super-block HH0H000H000000V000000000000 (1,2,4,7,12) and receiving HH0H000H00X000V000000000000 (1,2,4,3,4,12). In this instance, knowledge of the polarization is needed to solve the error. Since the polarization corresponding to the first allowed duplicate length 4 is horizontal, the following two lengths of 3 and 4 should be summed up to create a 7. If instead the same first sub-block of length 4 in the super-block had been vertically polarized, then the length of 3 had been combined with that sub-block and the solution would have been HH0V00000H000V000000000000 (1,2,7,4,12).

Regarding the density of solvable addition errors in one super-block, the protocol makes it possible to solve for all singular additions per every other sub-block in the super-block. Meaning that, there can only be one photon addition in a given sub-block meanwhile the two sub-blocks directly adjacent to it must remain intact during transmission for the error correction to work[ericssonpatent].

Example 10

An example of such a solvable case, is when transmitting HH0H000H000000V000000000000 (1,2,4,7,12) and receiving HHXH000H00X000V000000000000 (1,1,1,4,3,4,12). Since there are three lengths of 1 in a row present in the erroneous super-block and no length of 2, the protocol will assume that two of them should be summed up. Since the polarization of the first 1 is horizontal, the following two lengths of 1 will be combined. Since the sub-block length following them in the sequence is a 4, the corrected length of 2 will be given a horizontal polarization. The result of this first iteration is HH0H000H00X000V000000000000 (1,2,4,3,4,12). Now, the disallowed sub-block length of 3 must be combined with the length of 4 either before or after it, creating either (4,7) or (7,4). As the corresponding polarization of the first length 4 is horizontal, it is assumed that the sequence must be of order (4,7), as 4<7. The corrected super-block is then HH0H000H000000V000000000000 (1,2,4,7,12).

2.9.3.3 Non-correctable Errors

Instances where there are combinations of both loss- and addition errors within the same super-block are not covered by the error correction protocol. Also, the protocol can in general not correct for situations where there are directly adjacent sub-block additions or losses. For loss errors, this means that the protocol cannot correct errors where two neighbouring sub-block lengths are lost. In the case of addition errors, this means that i) several addition errors within one sub-block cannot be corrected and ii) addition errors within directly adjacent sub-blocks cannot be corrected[ericssonpatent].

Example 11

Assuming for example that the transmitted super-block is HH0H000V000000 (1,2,4,7) (see figure 2.15), and the received super-block is H000000V000000 (7,7) (see figure 2.19). In this situation, both the second and third sub-block have been lost during transmission. From the polarization, one can decipher that the first 7 in the super-block is the one that should be sectioned of into lengths 1,2 and 4. However, there is no way for the recipient to know in what order these 3 lengths were placed in the original super-block. Based

on the given information, the solution could either be one of permutations: (2,4,1,7), (1,4,2,7) and (1,2,4,7).

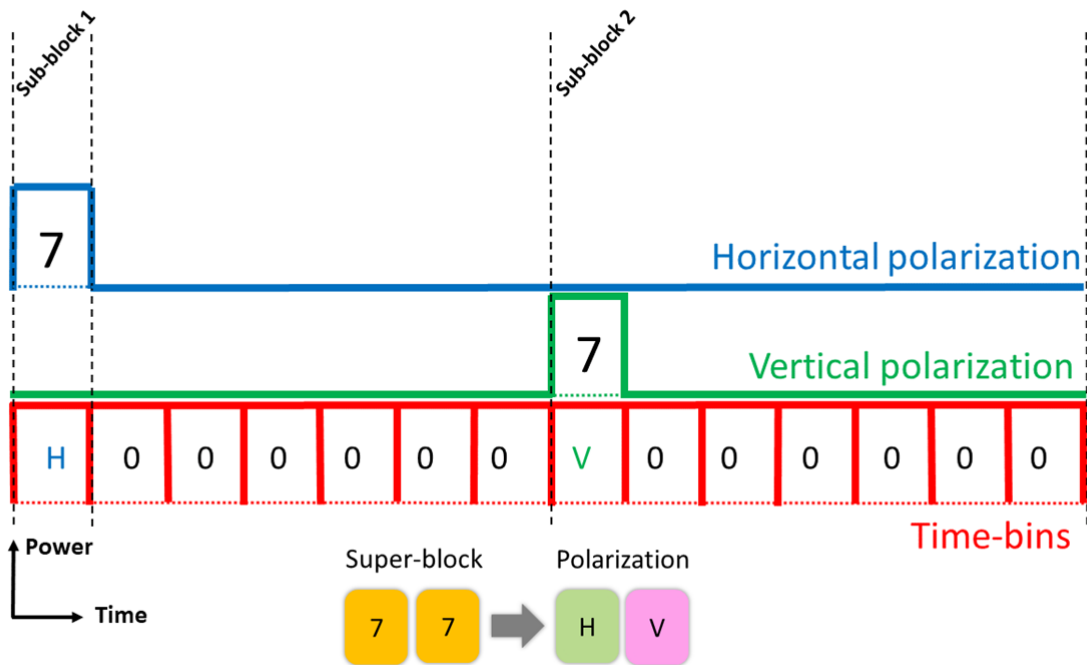


Figure 2.19: Illustration of the erroneous super-block (7,7), displaying signal power over time. In the figure, H=horizontal polarization and V=vertical polarization.

Just like in example 11, the errors that are not covered by the protocol content can at least in most cases be detected. In some instances, there can be combined loss- and addition errors such that the result is an acceptable super-block structure that however differs from the original super-block (see section 2.6.2). In situations such as these, the protocol will not be able to catch the error and the received data will be incorrect. These types of errors are however highly unlikely to occur[ericssonpatent].

Example 12

For example, receiving (1,2,4) HH0V000, when the transmitted super-block is (1,4,2) HV000H0. In this scenario there has occurred two losses and two additions. However, as previously stated, these types of errors have very low probability.

An important piece of information in regards to detecting both solvable and unsolvable errors is the fact that the receiver is assumed to have knowledge of the length of the transmitted super-block. Therefore, in each one of the cases where the received super-block is either longer or shorter than what is to be expected, the receiver will know that there has been at least one error. In the instances where the error correction protocol cannot reconstruct the original super-block, the missing information can instead be requested to be re-sent[ericssonpatent].

2.9.3.4 Error Probabilities

The errors that occur during the super-block transmission are dependent on the loss probability of a photon (p_{loss}), the addition probability (p_{add}) and the size of the super-block. Equation 2.17 describes the joint probability of having l losses and a additions in a super-block consisting of n number of sub-blocks and N time-bins[ericssonpatent].

$$P(l, a) = \binom{n}{l} p_{\text{loss}}^l (1 - p_{\text{loss}})^{n-l} \cdot \binom{N-n}{a} p_{\text{add}}^a (1 - p_{\text{add}})^{N-n-a} \quad (2.17)$$

Here, the notation $\binom{n}{l}$ is the binomial coefficient $\binom{n}{l} = \frac{n!}{l!(n-l)!}$.

2.9.3.5 BPPM Protocol Delimitations Summary

The delimitations of the BPPM error correction protocol are listed in this section.

- The BPPM protocol does not solve for photon losses or addition errors in directly adjacent sub-blocks within a super-block.
- The BPPM protocol does not correct for several additions within the same sub-block.
- The BPPM protocol does not correct for combinations of both loss- and addition errors within the same super-block. It can only correct erroneous super-blocks with either loss- or addition errors.
- The type of bit-flip errors where horizontal polarization becomes vertical polarization and vice versa, are assumed to be highly unlikely and are not handled by the BPPM protocol. See section 2.6 for elaboration regarding bit-flip errors.



3 Method

In this chapter, the methods used during the thesis work are described. This includes a description of the optical communication system design, consisting of the experimental setup as well as the corresponding electronic control system. This chapter also includes a description of the software implementation of the error simulation and error correction processes, as well as the data translation process made between super-block representation to hardware representation of data. Finally, the experimental process is described.

3.1 Project Process

The thesis work consists of a mixture of laboratory work and software simulations. The laboratory work includes experimentally deriving the probabilities of photon loss (p_{loss}) and dark-counts (p_{add}) respectively. In addition to this, a measurement of the polarization drift in the setup is performed over time. The experimentally derived values for p_{loss} and p_{add} are used for software simulation of errors that are ultimately attempted to be solved using the BPPM error correction protocol.

3.2 Delimitations

During the thesis work, some delimitations are established to set the framework for the project. The delimitations are presented in this section.

- The experiments are limited to short transmission distances over non-polarization maintaining single-mode fiber (type SMF-28) as well as the system components listed in sections 3.3.1.1 and 3.3.1.2.
- The laser source is of telecom CW-DFB type (1550 nm).
- For the detection of photons/light pulses, a single photon detector (SPD) is available, as well as two 1.2 GHz InGaAs photodetectors. The photodetectors are of model DET01CFC (from Thorlabs) and the SPD is of avalanche photodiode type, model ID210 from ID Quantique and has detection efficiency span $\eta_{\text{neff}} = 5 - 25\%$.

- During the dark-count rate experiment, the SPD settings are: 12 ns gate width, 1 MHz gate rate, 0.10 μ s dead time and 1.65 ns trigger delay.
- During the making of the addition error probability model, the terms "photon additions" and "dark-counts" are used interchangeably. The reason being that the stray light rate << dark-count rate. Therefore, since the rate of additions occurring in the fiber are negligible in comparison to the dark-counts at the detector, the probabilities of photon addition and dark-counts are treated as equal.
- During the power loss measurement over the experimental setup, the limiting nodes for measurement are set up between a) the end of the transmitter and b) the end of the receiver.
- The utilized oscilloscope has a bandwidth of 300 MHz.
- The simulated transmission is limited to pulses made up of more than one single photon because of the limitations of the available optical components.

3.3 System Design

The optical communication system consists of the experimental setup illustrated in figures 3.1 and 3.2 as well as the control system in the form of FPGA and software described in sections 3.4 and 3.5.1 respectively. The system was designed to be able to test the feasibility of the error correction protocol using classical pulses of light instead of single photons. This system design therefore implement photodetectors for detection of the linearly polarized light pulses.

3.3.1 Experimental Setup

The experimental setup consists of a transmitter and a receiver side, with a single-mode optical fiber communication channel connecting them. How these two parts of the setup are composed can be seen in figure 3.1. How light propagates through the setup is described in sections 3.3.1.1 and 3.3.1.2.

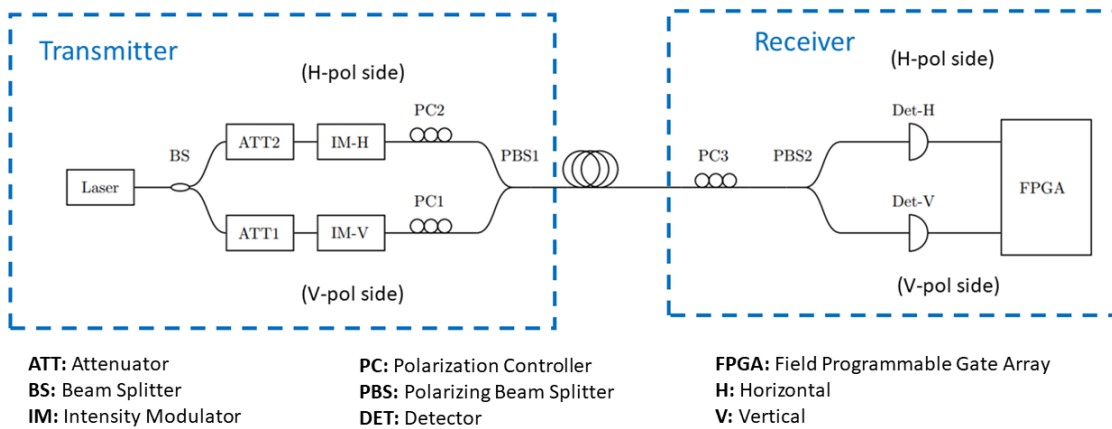


Figure 3.1: Scheme describing the experimental setup.

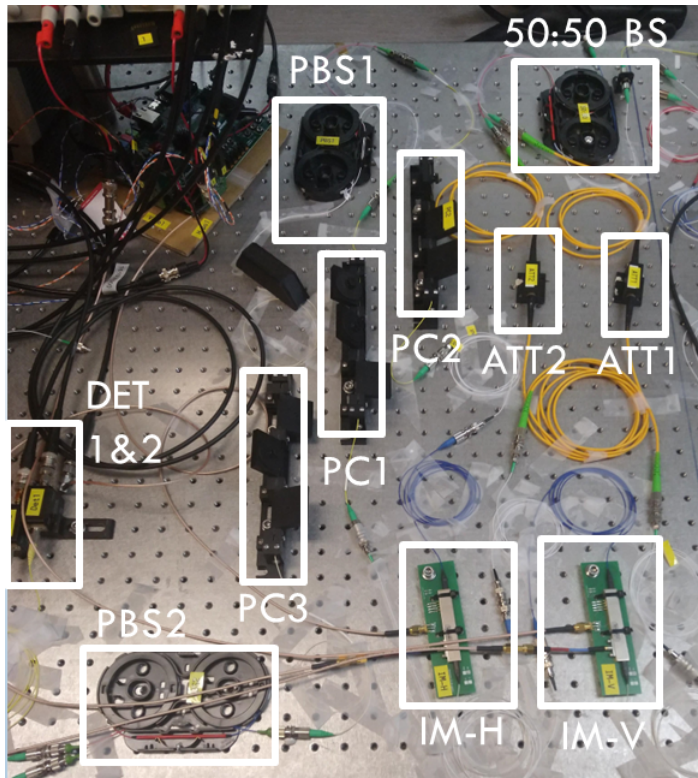


Figure 3.2: Photo of the experimental setup from the laboratory.

3.3.1.1 Transmitter

The transmitter side of the experimental setup includes the following components:

- 1 Telecom continuous wave DFB laser source (1550 nm) (Laser in figure 3.1)
- 1 50:50 non-polarizing beamsplitter (BS in figure 3.1)
- 2 variable attenuators (ATT1, ATT2 in figure 3.1)
- 2 intensity modulators (IM-V, IM-H in figure 3.1), type: lithium niobate (LiNbO_3)
- 2 manual fiber polarization controllers (PC1, PC2 in figure 3.1)
- 1 polarizing beamsplitter (PBS1 in figure 3.1), model: PBC1550SM-APC

The transmitter can be seen on the left side of figure 3.1. The transmission process starts with a 1550 nm telecom continuous wave (CW) DFB laser emitting light. The continuous wave is split into two fiber paths by a non-polarizing 50:50 beamsplitter (BS). The light passing through each fiber path is manually attenuated to the appropriate power levels using the variable attenuators ATT1 and ATT2 respectively. Attenuation of the light is used in order to transmit as little energy as possible through the setup, while still achieving a detectable signal. Since there is no single photon source, the attenuation is a way to simulate much weaker signals during the transmission in comparison to those that are generated by the source. Naturally this is not an appropriate solution for an optical communication system intended for actual energy efficient transmission, since it is a waste of energy. However, since the thesis work is a feasibility study of the BPPM protocol, this is an appropriate solution for the task at hand.

Next, the intensity modulators IM-H and IM-V are used to section of the continuous wave of light into 0.1 ms long pulses of classical light. Just like the attenuators, the intensity modulators are used to aid in the simulation of a single photon source, by turning the continuous wave into pulses. The IM-components are also used to polarize the incoming light, as they have built in polarizers. The polarized light pulses then pass through the manual polarization controllers (MPC) PC1 and PC2, where their polarization is rotated into the respective horizontal/vertical states. The three paddles of each MPC component are set to angles that allow for maximum power passage in both fiber paths. The paddles function as wave plates that rotate the polarization of the passing light through stress-induced birefringence. Subsequently, the two fiber paths are combined into a single mode transmission fiber channel of model SMF-28, via the polarizing beamsplitter (PBS1).

3.3.1.2 Receiver

The receiver side of the experimental setup includes the following components:

- 1 manual fiber polarization controller (PC3 in figure 3.1)
- 1 polarization beam splitter, model: PBC1550SM-APC (PBS2 in figure 3.1)
- 2 Photodetectors from Thorlabs, model: DET01CFC (Det-H, Det-V in figure 3.1)

The receiver can be seen to the right in figure 3.1. At the receiver side of the setup, the incoming light pulses from the single-mode transmission fiber channel passes through the PC3 component, which corrects any potential rotation to the coordinate system of the linear polarization states. This rotation occurs due to birefringence in the fiber as the light propagates through the channel between transmitter and receiver. The horizontal and vertical polarizations are separated by a polarizing beamsplitter (PBS2). Finally, the polarized classical pulses of light are detected by the photodetectors Det-V and Det-H respectively.

3.3.1.3 Equipment

In this section, the specifications of the utilized laboratory equipment is listed.

- The used laser source is a Yenista Optics OSICS continuous wave DFB with operating wavelength 1550 nm. During laboratory measurements, it is run on a power of 12 dBm (and current 3.17 mA).
- Intensity modulator bandwidth: 10 GHz

3.4 Control System and Transmission Process

During the thesis work, both the software implementation of the transmitter control system, and the experimental setup of transmitter and receiver are developed. Therefore, their current functionality is described in this section. The description of the receiver control system software however is merely a suggestion for any potential future implementation of the BPPM protocol, as it was not finished during the project duration.

The control system consists of a field programmable gate array (FPGA) ZedBoard and a Python Jupyter-interface. FPGA:s are adaptable chips used for signal control within integrated circuits and they are made up of logic blocks. The FPGA chip is programmed using very high-speed integrated circuit hardware description language (VHDL)[[Sulaiman2009DesignReview](#)].

3.4.1 Control System: Transmitter

At the start of the transmission process, the user enters the super-block data to be transmitted into the Jupyter-interface. There, it is translated into the correct input format for the FPGA driver code. The FPGA driver generates a continuous stream of an electrical square waveform signal. These square waves are the time-bins within which light pulses can be temporally transmitted. In the FPGA driver code, the length of each sub-block within the super-block is translated into the description of a classical light pulse, followed by a temporal duration of the zero-state corresponding to the rest of the sub-block length. The meaning of the zero-state is that no signal is transmitted during it. Therefore, the interruption of the zero-state corresponds to the end of the sub-block, using the next sub-block light pulse as a marker. It is the IM-components in the experimental setup, that controlled via the FPGA, chops the incoming continuous wave light into pulses and polarizes them.

As was previously mentioned in section 2.9.3.3, both sender and receiver are assumed to know the length of the transmitted super-blocks. Without this knowledge, it is very difficult to distinguish the super-blocks from one another. Therefore, naturally, this is information that must be shared between the two nodes beforehand[[ericssonpatent](#)].

3.4.2 Control System: Receiver

On the receiver side, once an incoming light pulse has been registered using the photodetectors, the temporal gap between the incoming pulses can be used to interpret the length of each sub-block. The polarization of an incoming light pulse will determine in which one of the two photodetectors (Det-H, Det-V) it will be detected. Since the length of an incoming super-block is assumed to be known by the receiver (see section 2.9), the temporal duration of a super-block registration can be set accordingly. By combining knowledge about the time it takes to collect a complete super-block, with information of the starting time of the transmission, as well as duration of transmission over the fiber channel, it should be possible to section off the incoming super-blocks into separate entities. By doing this at the correct temporal intervals there will not be a risk of the sub-block data "bleeding" over to the adjacent sub-blocks even if they are erroneous in some way. The detected sub-block information is saved in the memory of the FPGA. From the memory, the sub-block data can be retrieved by the Jupyter-interface, where it is translated back into software sub-block representation before it is sent through the error correction process. For the software implementation of both the data translation and error correction processes, Python was used. The process described above is briefly illustrated in figure 3.3.

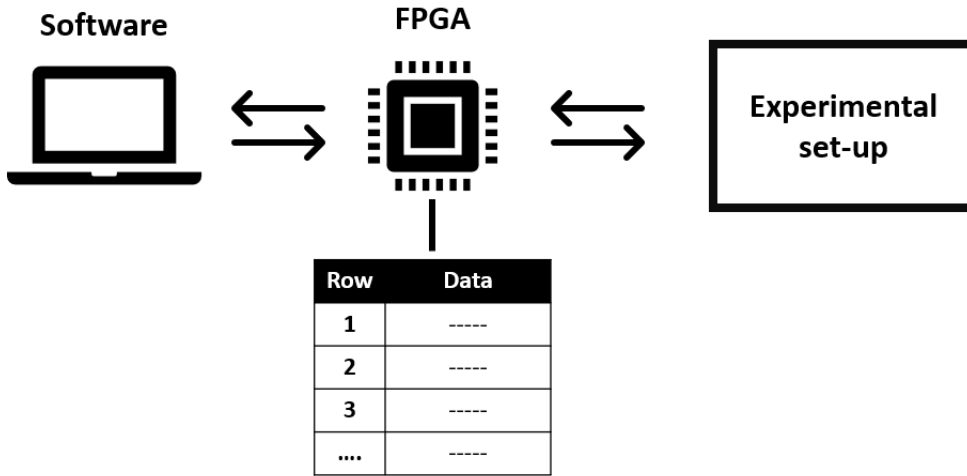


Figure 3.3: Illustration of the communication scheme between the control system, consisting of the software and the field programmable gate array (FPGA) with memory (row/data), and the experimental setup.

A detailed description of the FPGA hardware architecture can be seen in figure 3.4. The connection between figure 3.4 and the experimental setup in figure 3.1 is such that the H-out and V-out (in 3.4) are the output driver signals controlling the IM-components in figure 3.1 (which cut the light into pulses and polarizes them). Also, the DET-H and DET-V components (in figure 3.4) are the FPGA inputs of the detected light signals at the receiver in the experimental setup in figure 3.1.

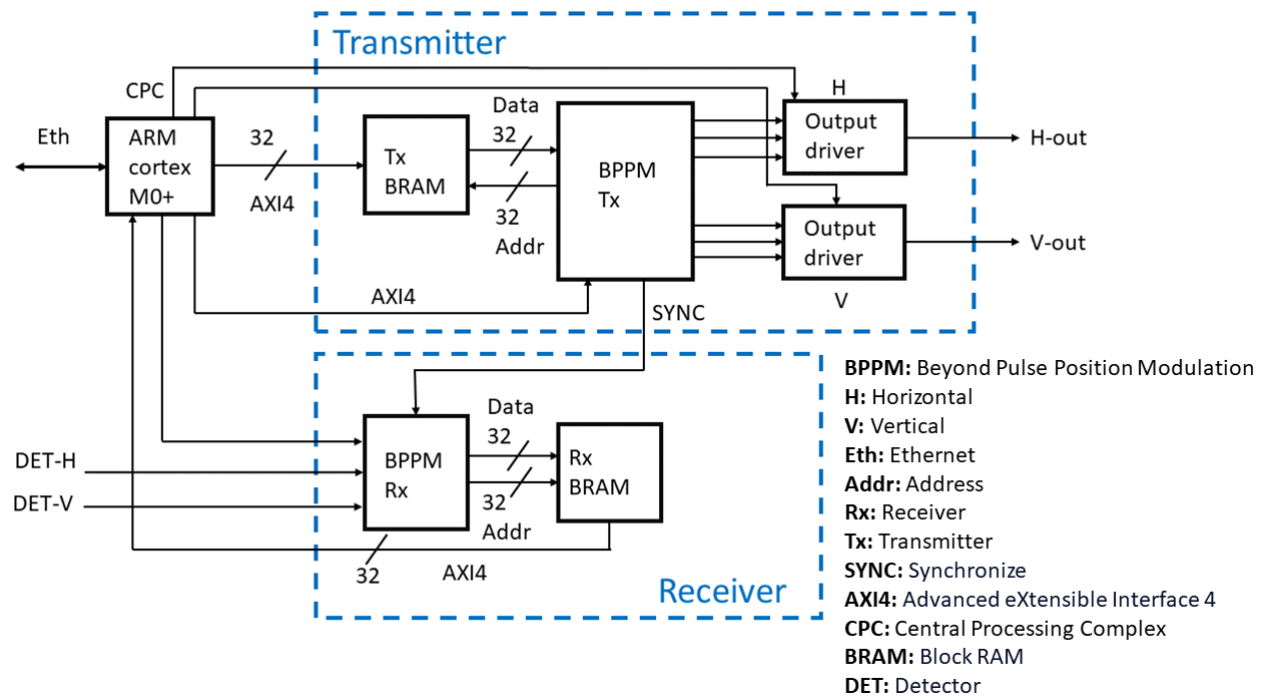


Figure 3.4: Detailed illustration of the hardware communication scheme between transmitter and receiver. The arrows in the figure illustrate the direction of the signals.

3.5 Software

As was previously mentioned in section 3.4, both the software implementation of the transmitter control system, and the experimental setup of transmitter and receiver are developed during the thesis project. Therefore, the current functionality of the transmitter software is described in section 3.5.1. The description of the receiver control system software however is merely a suggestion for potential future implementation, as it was not finished during the project duration.

3.5.1 Data Translation Between Hardware and Software

In order for the Jupyter-interface and the FPGA driver code to communicate, the data that passes between them must be translated appropriately. The input to the Python Jupyter-interface is in super-block representation. In this code, each sub-block in the super-block is represented as an integer describing a binary 10 bit long sequence. The 9 least significant bits (LSB) in such a sequence are used to describe the length of the sub-block in binary and the last and most significant bit (MSB) is used to represent its polarization. The terms **most** and **least** significant bits refer to the size of the decimal value corresponding to the bit placement in the binary 10 bit sequence, with the most significant bit having the largest value and the least significant bit having the smallest value[Bansal2019BinarySystemb]. If the value of the MSB bit is 1, then the polarization is vertical and if the value is 0, then the polarization is horizontal. Therefore, the integer representing the sub-block length as it enters the VHDL FPGA driver code (hardware representation), will be larger than $2^9 = 512$ if the polarization is vertical, and less than 512 if the polarization is horizontal (see figure 3.5).

	MSB				LSB					
Bit index	9	8	7	6	5	4	3	2	1	0
Binary	2^9	2^8	2^7	2^6	2^5	2^4	2^3	2^2	2^1	2^0
Decimal	512	256	128	64	32	16	8	4	2	1

Horizontal polarization → MSB=0 → Decimal value=0
 Vertical polarization → MSB=1 → Decimal value=512

Figure 3.5: Table showing the binary, decimal and bit index values for most significant bit (MSB) and least significant bit (LSB), which are used to construct sub-block values in hardware representation.

The motivation behind describing each sub-block using exactly 10 binary bits, is based on a tradeoff between efficient FPGA memory usage, while still being able to create longer sub-blocks (with up to 475 time-slots each). Namely, the idea is to fit 3 sub-blocks per FPGA memory row (of 32 bits), leaving 2 bits per row unused. In figure 3.6, the different data representations of all permutations of super-block size $n = 3$ can be seen. The super-block data structure is thoroughly described in section 2.9.

Data representations (n=3)			
Super-block	Polarization	Encoding	Hardware
1, 2, 4	H, H, V	HH0V000	1, 2, 516
1, 4, 2	H, V, V	HV000V0	1, 516, 514
2, 1, 4	V, H, V	V0HV000	514, 1, 516
2, 4, 1	H, V, H	H0V000H	2, 516, 1
4, 1, 2	V, H, H	V000HH0	516, 1, 2
4, 2, 1	V, V, H	V000V0H	516, 514, 1

Figure 3.6: Table showing the different data representations of super-block (size n=3) information. In this figure, H=horizontal polarization and V=vertical polarization.

As the optical signals pass through the experimental setup and are received by the photodetectors, they are grouped into packets corresponding to the temporal duration of the expected super-block size, containing N number of time-bins. After that, the packets are sectioned off into sub-block lengths based on the temporal duration between the detections of light pulses. Once the data has been sectioned off into smaller segments, they are translated back into the integer representation containing length and polarization information in the VHDL code (i.e. as integers larger or smaller than 512). This information is stored in the memory of the FPGA, three sub-blocks per memory row, where from they can be retrieved by the Jupyter-interface. In the Python code, they are once again translated back into super-block representations of the correct size n , before being sent through the error correction process.

3.5.2 Error Generation for Feasibility Test of Error-correction Code Implementation

It is important to make sure that no loss- and addition errors that are solvable according to the protocol are missed during the software implementation of the error correction codes. Therefore, additional error generating code is written, which produces every type of maximum complexity solvable error combination according to BPPM. In these codes, erroneous super-blocks are produced with exactly one addition/loss error per every other sub-block in each super-block. Namely, the error correction protocol is able to correct for all error combinations with complexity below- and including single non-adjacent loss/addition errors. These types of tests are made for all the permutations of a given super-block of size n . Regarding addition errors, the placement of the added sub-block length is tested for all different time-bin placements within each sub-block. Note that loss- and addition errors are not combined within the same super-blocks in these particular error simulating codes, as these codes were specifically developed to only generate solvable errors for losses and additions separately. As has been mentioned previously, the BPPM protocol cannot correct for both losses and additions within the same super-block, since the combination of the two error types dramatically increases the complexity of the error correction. During the development and testing of the error-correction codes, the codes are continuously updated, as errors that should be solvable according to the protocol, are sometimes flagged as uncorrectable due to misses in the code implementation.

Naturally, these types of controlled error combinations cannot be expected during a real optical transmission. Therefore, more realistic error combinations (of both losses and additions) are simulated as well (see section 3.5.3).

3.5.3 Probabilistic Error Simulation in Software for Testing of Error-correction Protocol

In order to test the error correction protocol in a way that is similar to an actual optical transmission, code for simulated error generation is written. This code is produced in the Python Jupyter interface and it first calculates the joint probabilities of all the possible combinations of ($a=0,\dots,N-n$) addition- and ($l=0,\dots,n$) loss errors in a given super-block of size n sub-blocks using equation 2.17. Secondly, there is a code portion written that probabilistically applies these error combinations to a super-block input based on the joint error probabilities $P(l, a)$. Naturally, the density and combinations of occurring loss- and addition errors are dependant on the size of the super-block n as well as the values of the p_{loss} and p_{add} variables.

3.5.4 Error Correction

In order to correct for the loss- and addition errors that occur during a data transmission process, the error correction protocol needs to be implemented into software code. This code is written in Python. During the correction process, firstly, the error type is evaluated. If the incoming super-block is longer/shorter than expected, it is categorized as having addition/loss errors. This conclusion can be drawn because the length of the received super-blocks are assumed to be known. Based on the assumed error type, the super-block will be handled using the respective error correction process for either loss or addition errors. Both types of errors are approached iteratively, solving for one error at a time. If the encountered errors are within the bounds of the protocol (see section 2.9), the error correction process will be successful. Note again that the error-correction codes cannot correct for combinations of additions and losses within the same super-block, the errors must be of either loss **or** addition type.

Once a super-block has passed through the error correction process, it is sent through a code section which verifies that all of the super-block is of a valid structure. This means, verifying that the combinations of lengths and polarizations in the corrected super-blocks are in accordance with the error correction protocol. In the cases where error correction was performed, this process of double checking is done to make sure that error correction was successful. In situations where the received super-block was always of the correct length, this is done to make sure that there are no combinations of losses and addition errors such that the data would be disrupted meanwhile the length was kept the same. In figure 3.7, this sequence of events is illustrated. Once the error correction process has finished, the resulting super-blocks will be partitioned into three categories:

- Successfully received super-blocks
- Successfully error corrected super-blocks
- Non-correctable super-blocks

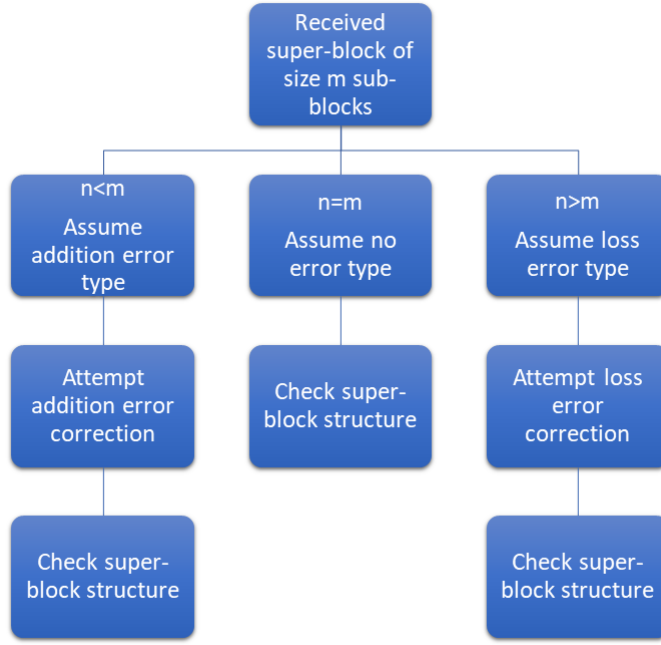


Figure 3.7: Flow chart of the error correction process in software. In this figure, m is the actual number of sub-blocks in the received super-blocks and n is the expected number of sub-blocks in the super-block.

3.5.5 Interfaces for Transmission of Image Data

As an extension of the software interface where super-blocks are directly fed into the system by the user, there is also an interface developed for transmission of image data. This image transmitting interface is programmed to map the pixel data of an input image to permutations of super-blocks of size n before the transmission. The mapping is made with one super-block permutation per pixel value. At the receiver side of this software interface for image translation, the received super-blocks are mapped back to pixel data after error-correction. Amongst the erroneous data, the pixels whose corresponding super-blocks are successfully corrected using BPPM, are marked as green pixels in the restored image. The pixel super-blocks that are however uncorrectable, are instead replaced by red pixels in the restored image.

3.6 Experimental Process

The goal of the experimental process is to test the functionality of the error correction protocol as well as the experimental setup. The idea is to make models describing addition- and loss error probabilities that are applicable to actual long distance optical transmission and use the BPPM protocol to attempt error correction. In order to do this, the capabilities of the software implementation of the error correction codes need to be tested to make sure that they are up to protocol standard (see section 3.5.2). Also, tests need to be performed that provide realistic values for error probabilities (p_{loss} and p_{add}), that can be used for software simulations of realistic transmission errors. In addition to this, tests need to be performed to measure the polarization drift in the experimental setup over time.

3.6.1 Error Probability Test

In order to make realistic error generating software simulations, the probabilities of photon loss (p_{loss}) and photon addition (p_{add}), are established experimentally. The values for p_{loss} and p_{add} are then implemented in equation 2.17, which is used to generate the error combinations.

3.6.1.1 Determining Dark-count Probability (p_{add})

The false photon detections due to detector noise of the SPD are experimentally determined at different detection efficiencies in range $\eta_{\text{eff}} = 5 - 25\%$, by covering the fiber input of the detector and reading the dark-count rate on the SPD display for the different detection efficiency values (η_{eff}). The measured results were then used to make a model of p_{add} over η_{eff} using equation 2.13, where $p_{\text{add}} = P_{\text{noise}}$, which gives equation 3.1 for addition probability. The resulting model can be found in section 4.2.1.

$$p_{\text{add}} = 1 - \exp(-T \cdot (f_{\text{dc}} + f_{\text{sl}})) \quad (3.1)$$

During the experiment, the gating frequency is set to 1 MHz, giving a sampling time of $T = 10^{-6}$ s and the dead time of the SPD is 0.10 μs . The dark-count rate f_{dc} is displayed on the SPD.

3.6.1.2 Determining Loss Probability (p_{loss})

The loss probability (p_{loss}) during transmission is determined by making a model combining both measured and expected losses. Losses occurring over the system components with transmitter and receiver back-to-back are measured with a power meter. The expected losses occurring due to added fiber distance of length L km between sender and receiver are estimated based on the maximum attenuation found in the specification sheet of the utilized single-mode fiber. The model for p_{loss} over distance is described by equation 3.2.

$$p_{\text{loss}} = 1 - P_{\text{detect}} \cdot 10^{(-\alpha_{dB} \cdot L - P_{\text{in}} + P_{\text{out}}) / 10} \quad (3.2)$$

Where P_{detect} is calculated using equation 2.11 for different average number of photons per pulse u . According to the specification sheet of the utilized single-mode fiber (model: SMF-28), $\alpha_{dB} = 0.18$ [dB/km] is the maximum expected attenuation for a laser operating at wavelength 1550 nm. The power values P_{in} and P_{out} are the measured intensities in dBm at the output of the transmitter and at the output of the receiver when they are placed back-to-back. The dark-count rate $f_{\text{dc}} \approx f_{\text{dc}} + f_{\text{sl}}$, in equation 2.11 is deducted from figure 4.22 (showing the addition error probability) depending on the set value of detection efficiency η_{eff} of the SPD. The losses are simulated for $\eta_{\text{eff}} = 10\%$ and $\eta_{\text{eff}} = 20\%$. The value for SPD deadtime is set to $T_{\text{dt}} = 0.1 \mu\text{s}$. The results of these combined experiments and simulations are presented as the model for loss probability in section 4.2.2.

3.6.2 Polarization Drift Test

Since knowledge about the polarization of the transmitted light is crucial for the error correction process, it is important to know how stable the respective horizontal/vertical polarization states are throughout transmission. Therefore, a test is performed using the available experimental setup to see how the polarization changed over time. Before this experiment is performed, the polarization states are aligned once. During the experiment, no polarization stabilizing intervention is made.

Aligning the polarization states is done through positioning the three paddles of each PC in positions that allow for maximum power for the respective linear polarizations (horizontal and vertical). In addition to this, the power supply to the IM-components is set to values that maximized the optical signals. During the test, data is collected of the optical signals, which is then used to plot the signal power over time for the horizontally/vertically polarized light pulses.

3.6.3 Correction of Software Simulated Errors Test

In this section, error correction using BPPM is described for different simulated values for addition- and loss error probabilities.

3.6.3.1 Arbitrary Values for p_{loss} and p_{add}

Using the error generating simulation code described in section 3.5.3, the performance of the error correction codes is tested using arbitrarily chosen values for p_{loss} and p_{add} (either at 0% or 10%). This is done partly to be able to study losses and additions separately, but also in order to see how the error types affect the error-correction capabilities if they are given the same probability of occurring (so that $p_{\text{add}} = p_{\text{loss}}$). Studying the three scenarios:

- Only loss errors,
- Only addition errors and
- Equal probability for addition- and loss errors,

makes it possible to evaluate which type of error is most difficult to correct for and therefore which error type is preferable in regards to restoring the largest amount of lost data. This information can later be used to decide what detection efficiency (η_{eff}) should be set on the SPD during actual transmission, as well as during error simulation of loss- and addition probability values. Namely, a high η_{eff} -value can decrease losses and increases dark-counts, while a low η_{eff} -value can increase losses and decreases dark-counts.

After letting the input super-blocks pass through the error simulation code (implementing the arbitrarily chosen values for loss- and addition errors), the erroneous super-blocks are sent through the error correction codes described in 3.5.4. The simulated transmission and error-correction using arbitrarily chosen values are described in table 3.1.

Simulation	p_{loss} (%)	p_{add} (%)	Result section
1	10	0	4.1.1
2	0	10	4.1.2
3	10	10	4.1.3

Table 3.1: Table showing performed transmission simulations using arbitrarily chosen values for loss probability (p_{loss}) and addition probability (p_{add}).

The results of these simulations are presented in section 4.1, using graphs displaying the average number of information bits per pulse over different super-blocks of size n . The average number of information bits per pulse are calculated using equation 3.3.

$$\text{Bits}_{\text{per_pulse}} = \frac{\log_2(n!)}{n} \cdot P_{\text{perc}} \quad [\text{Bits/pulse}] \quad (3.3)$$

where P_{perc} is the percentage of super-blocks of size n that were either received correctly without error-correction, properly error-corrected or non-correctable.

3.6.3.2 Experimentally Derived Values for p_{loss} and p_{add}

By applying experimentally derived values for p_{loss} and p_{add} (from the result sections 4.2.1 and 4.2.2) in the error generating simulation code described in section 3.5.3, the performance of the error correction codes can be tested for scenarios that are similar to an actual optical transmission. The density and combinations of loss- and addition errors are dependant on the size n of the super-block as well as the values of the p_{loss} and p_{add} variables. In turn p_{loss} is dependent on the average number of photons per pulse u (see equation 2.11) and detection efficiency η_{eff} of the SPD. By looking at figure 2.11 (for Poissonian light distribution), it can be derived that for an average photon number $u \geq 10$, the probability of registering $k < 1$ events is $P = 0\%$. Therefore, the pulse sizes used for the simulated error generation and correction will also be larger than or equal to $u = 10$.

Naturally, having a larger number of average photons per pulse causes the probability of losing a pulse detection (p_{loss}) to decrease as the average number of photons per pulse (u) increases. The reason for this is that all photons in a pulse need to be lost in order to lose a complete sub-block in the super-block. The idea is that for detection, a single photon is all that is needed. Therefore, p_{add} will not be affected by the average number of photons per pulse.

The values that are ultimately used for p_{loss} and p_{add} during the following simulations, are used to calculate the joint probabilities for different error combinations using equation 2.17. By applying the possible joint errors probabilistically to a super-block input, erroneous data is simulated. After the simulation of errors is complete, the erroneous super-blocks were passed through the error correction codes described in 3.5.4. The specific transmission simulations with error correction that are performed, are listed below.

For a detection efficiency setting of $\eta_{\text{eff}} = 10\%$, the simulations presented in table 3.2 are performed. The results of these tests are presented in section 4.3.1, using graphs displaying the average number of information bits per pulse over different super-blocks of size n (calculated using equation 3.3).

Simulation	$p_{\text{loss}} (\%)$	$p_{\text{add}} (\%)$	L	u	Figure
1	19.28	0.05	0	100	4.27
2	34.56	0.05	5	100	4.30
Simulation	$p_{\text{loss}} (\%)$	$p_{\text{add}} (\%)$	L	u	Figure
3	48.98	0.05	0	10	4.33
4	58.63	0.05	5	10	4.36

Table 3.2: Table showing performed transmission simulations using experimentally derived values for loss probability (p_{loss}) and addition probability (p_{add}), at detection efficiency $\eta_{\text{eff}} = 10\%$. In the table, L is the propagated distance and u is the average number of photons per pulse.

For a detection efficiency setting of $\eta_{\text{eff}} = 20\%$, the simulations presented in table 3.3 were performed. The results of these tests are presented in section 4.3.2, using graphs displaying the average number of information bits per pulse over different super-blocks of size n (calculated using equation 3.3).

Simulation	$p_{\text{loss}} (\%)$	$p_{\text{add}} (\%)$	L	u	Figure
5	19.82	6.48	0	100	4.39
6	34.99	6.48	5	100	4.42
Simulation	$p_{\text{loss}} (\%)$	$p_{\text{add}} (\%)$	L	u	Figure
7	30.67	6.48	0	10	4.45
8	43.79	6.48	5	10	4.48

Table 3.3: Table showing performed transmission simulations using experimentally derived values for loss probability (p_{loss}) and addition probability (p_{add}), at detection efficiency $\eta_{\text{eff}} = 20\%$. In the table, L is the propagated distance and u is the average number of photons per pulse.

3.6.3.3 Transmission of Image Data: Single Iteration

For the simulated transmission of image data, pixel values are mapped to super-block permutations. In the simulations listed in table 3.4, the transmitted image is a pixelated black- and white Ericsson logo with only two different pixel values. The pixel values are mapped to one each of two permutations of super-block sizes $n = 2, 3, 4, 5$. The black pixels are mapped to super-blocks of rising length order (1,2,4,7,...) and the white pixels are mapped to super-blocks of declining length order (...,7,4,2,1).

At the receiver part of the code, the received and error corrected super-blocks are compared to the transmitted list of super-blocks and the results can be seen in section 4.4. In the resulting images which are labeled with a c), the green squares represent the successfully corrected super-blocks and the red squares belong to the super-blocks that could not be successfully corrected. The rest of the squares (black and white) represent the data that was successfully received without the need for error correction. The simulated detection efficiency during the image transmissions was set to $\eta_{\text{eff}} = 10\%$ and the average number of photons per pulse was set to $u = 100$.

Generally, when transmitting an image made up of only two types of data values (i.e. black and white pixels), using super-blocks of size $n > 2$ is unnecessary. The reason being that the required energy/pixel becomes larger without gaining any bits/pulse with such limited data diversity (see section 2.9.2). The idea of the different super-block sizes is to transmit data with different levels of versatility and therefore, as the super-block size increases, so does also the number of information bits per pulse. The reason why the larger super-blocks ($n > 2$) are not used in a more efficient way during the simulations listed in table 3.4 is simply a matter of illustrating the transmission results as an image that is easily understood. The utilization of all the permutations of a super-block of size n , requires $n!$ number of different pixel values. As each pixel value is a description of a distinct color, this can for larger super-blocks lead to a restored image in which it is hard to distinguish between the pixels that are transmitted without errors, vs the pixels that are successfully recovered using the BPPM error correction protocol (green pixels), vs the pixels that are lost (red pixels).

Simulation	n	$p_{\text{loss}} (\%)$	$p_{\text{add}} (\%)$	L	u	Figure
9	2	19.28	0.05	0	100	4.51
10	2	34.56	0.05	5	100	4.52
Simulation	n	$p_{\text{loss}} (\%)$	$p_{\text{add}} (\%)$	L	u	Figure
11	3	19.28	0.05	0	100	4.54
12	3	34.56	0.05	5	100	4.55
Simulation	n	$p_{\text{loss}} (\%)$	$p_{\text{add}} (\%)$	L	u	Figure
13	4	19.28	0.05	0	100	4.57
14	4	34.56	0.05	5	100	4.58
Simulation	n	$p_{\text{loss}} (\%)$	$p_{\text{add}} (\%)$	L	u	Figure
15	5	19.28	0.05	0	100	4.60
16	5	34.56	0.05	5	100	4.61

Table 3.4: Table showing performed image transmission simulations using experimentally derived values for loss probability (p_{loss}) and addition probability (p_{add}), at detection efficiency $\eta_{\text{eff}} = 10\%$. In the table, n is the number of sub-blocks per super-block, L is the propagated distance and u is the average number of photons per pulse.

3.6.3.4 Transmission of Image Data: Several Iterations

In addition to the simulations listed in table 3.4 wherein the super-block mapped image data is transmitted only once per super-block size and propagation distance, another simulated transmission process is performed using several iterations. During this test, the unrecovered super-blocks from each iteration of transmission are re-sent to study how many pixels are recovered for every repeated transmission. The purpose of this is to make a comparison between using more photons/pulse (where $u = 100$) and a lower detection efficiency ($\eta_{\text{eff}} = 10\%$) vs fewer photons/pulse (where $u = 10$) and a higher detection efficiency ($\eta_{\text{eff}} = 20\%$) and see how these factors impact the results for different super-block lengths. This is done for two different super-block sizes, $n = 3$ and $n = 5$ och the process is repeated seven times for each scenario. The performed transmissions are listed in table 3.5. The results of these simulations can be seen in section 4.4.2.

Simulation	n	$p_{\text{loss}} (\%)$	$p_{\text{add}} (\%)$	L	u	Figure
17	3	34.56	0.05	5	100	4.63
18	3	43.79	6.48	5	10	4.64
19	5	34.56	0.05	5	100	4.65
20	5	43.79	6.48	5	10	4.66

Table 3.5: Table showing repeated transmission simulations of images using experimentally derived values for loss probability (p_{loss}) and addition probability (p_{add}), at detection efficiencies $\eta_{\text{eff}}=10$ and 20% . In the table, n is the size of the used super-blocks, L is the propagated distance and u is the average number of photons per pulse.



4

Results and Discussion

In this chapter, the results produced during the thesis project are presented. In section 4.1, are the results of the error simulation and correction process using arbitrarily chosen values for p_{loss} and p_{add} . In section 4.2, the results of the experimental part of the project can be found. Lastly, in section 4.3 are the results of the error simulation and correction processes utilizing experimentally derived values for p_{loss} and p_{add} .

4.1 Results of Software Simulated Transmissions of Super-blocks: Arbitrary Values for p_{loss} and p_{add}

The results presented in this section correspond to the tests described in section 3.6.3.1. During these simulations, 10 000 super-blocks of size n number of sub-blocks, taken from the sequence of allowed lengths $\{1, 2, 4, 7, 12, 20, \dots\}$ are transmitted. Addition- and loss errors are both simulated separately and in combination in the three different scenarios presented in sections 4.1.1, 4.1.2 and 4.1.3. Note that the values for p_{loss} and p_{add} in these cases are arbitrarily chosen values used to show the capabilities of the BPPM protocol in different error scenarios. In order to study whether the choice of super-block permutation (meaning the order of the sub-block lengths in the super-block) affects the error correction capabilities, the simulations are performed three times for each error combination (only losses, only additions, both losses and additions). The utilized super-block permutations are:

- Rising sub-block length order: 1,2,4,7,...
- Mixed sub-block length order utilizing all different permutations
- Declining sub-block length order: ...7,4,2,1

4.1.1 Loss Error Generation and Correction results

During these simulations, only loss errors are tested. The separate probabilities for losses and additions are $p_{\text{loss}} = 10\%$ and $p_{\text{add}} = 0\%$.

4.1.1.1 Sub-block Lengths in Rising Order

In this section, the results of simulated transmission and error correction for only loss errors are presented. The sub-block lengths within the super-blocks are in rising order: shortest → longest. In figure 4.1, the average number of information bits per pulse are plotted over the super-block size of n sub-blocks. In figure 4.2 and 4.3, the results of the transmission and error correction process are laid out in tables for closer inspection of the numbers.

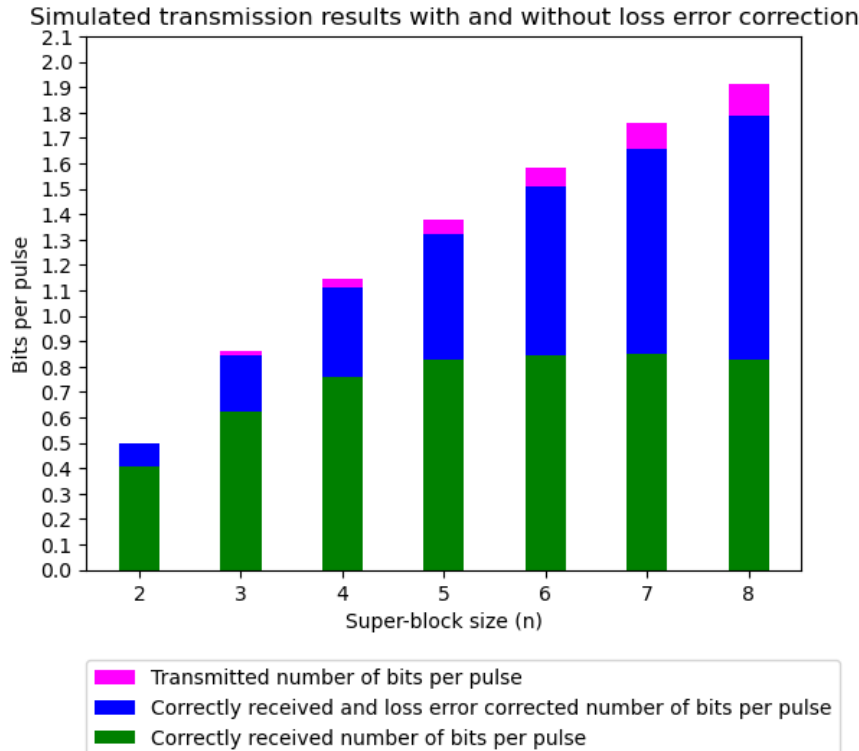


Figure 4.1: Error corrected simulated transmission with $p_{\text{add}} = 0\%$ and $p_{\text{loss}} = 10\%$. The plot shows the average number of successfully received (green) vs transmitted (pink) vs successfully received and error-corrected (blue) information bits per sub-block for each super-block of size n . The number of transmitted super-blocks per super-block size of n is 10 000 and all super-blocks are constructed with lengths in rising order: 1,2,4,7,....

n	Transmitted without errors (%)	Solved addition and loss errors (%)	Unsolved errors (%)
2	80.97	18.14	0.89
3	72.53	25.64	1.83
4	66.1	31.07	2.83
5	59.98	35.85	4.17
6	53.26	42.03	4.71
7	48.41	45.76	5.83
8	43.26	50.27	6.47

Figure 4.2: The table shows the size n of the transmitted super-blocks and the respective percentage of super-blocks that were not distorted during the transmission, vs the percentage of super-blocks that were successfully corrected, vs the percentage of super-blocks that could not be corrected using EC.

4.1. Results of Software Simulated Transmissions of Super-blocks: Arbitrary Values for p_{loss} and p_{add}

n	Transmitted (bits/pulse)	Correctly received and EC (bits/pulse)	Ratio (%)
2	0.5	0.5	99.11
3	0.86	0.85	98.17
4	1.15	1.11	97.17
5	1.38	1.32	95.83
6	1.58	1.51	95.29
7	1.76	1.65	94.17
8	1.91	1.79	93.53

Figure 4.3: The table shows the size n of the transmitted super-blocks and the respective average number of transmitted information bits per pulse, vs the average number of bits per pulse that were correctly received with and without EC, vs the ratio between the two.

4.1.1.2 Sub-block Lengths in Mixed Order

In this section, the results of simulated transmission and error correction for only loss errors are presented. The sub-block lengths in the super-blocks are in mixed order. This means that all available super-block permutations are used. In figure 4.4, the average number of information bits per pulse are plotted over the super-block size of n sub-blocks. In figure 4.5 and 4.6, the results of the transmission and correction process are laid out in tables for closer inspection of the numbers.

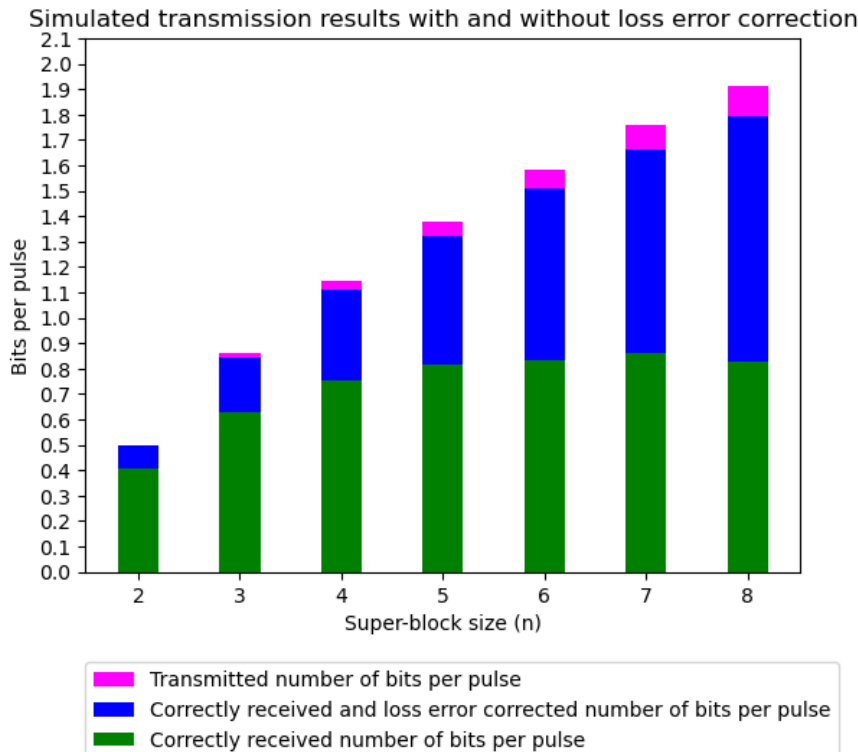


Figure 4.4: Error-corrected simulated transmission with $p_{\text{add}} = 0\%$ and $p_{\text{loss}} = 10\%$. The plot shows the average number of successfully received (green) vs transmitted (pink) vs successfully received and error-corrected (blue) information bits per pulse for each super-block of size n . The number of transmitted super-blocks per super-block size of n is 10 000, out of which there are about as many of each super-block permutation.

4.1. Results of Software Simulated Transmissions of Super-blocks: Arbitrary Values for p_{loss} and p_{add}

n	Transmitted without errors (%)	Solved addition and loss errors (%)	Unsolved errors (%)
2	81.21	17.92	0.87
3	72.97	25.28	1.75
4	65.63	31.35	3.02
5	59.06	36.71	4.23
6	52.8	42.76	4.44
7	49.17	45.51	5.32
8	43.26	50.47	6.27

Figure 4.5: The table shows the size n of the transmitted super-blocks and the respective percentage of super-blocks that were not distorted during the transmission, vs the percentage of super-blocks that were successfully corrected, vs the percentage of super-blocks that could not be corrected using EC.

n	Transmitted (bits/pulse)	Correctly received and EC (bits/pulse)	Ratio (%)
2	0.5	0.5	99.13
3	0.86	0.85	98.25
4	1.15	1.11	96.98
5	1.38	1.32	95.77
6	1.58	1.51	95.56
7	1.76	1.66	94.68
8	1.91	1.79	93.73

Figure 4.6: The table shows the size n of the transmitted super-blocks and the respective average number of transmitted information bits per pulse, vs the average number of bits per pulse that were correctly received with and without EC, vs the ratio between the two.

4.1.1.3 Sub-block Lengths in Declining Order

In this section, the results of simulated transmission and error correction for only loss errors are presented. The sub-block lengths of the super-blocks are in declining order. In figure 4.7, the average number of information bits per pulse are plotted over the super-block size of n sub-blocks. In figure 4.8 and 4.9, the results of the transmission and correction process are laid out in tables for closer inspection of the numbers.

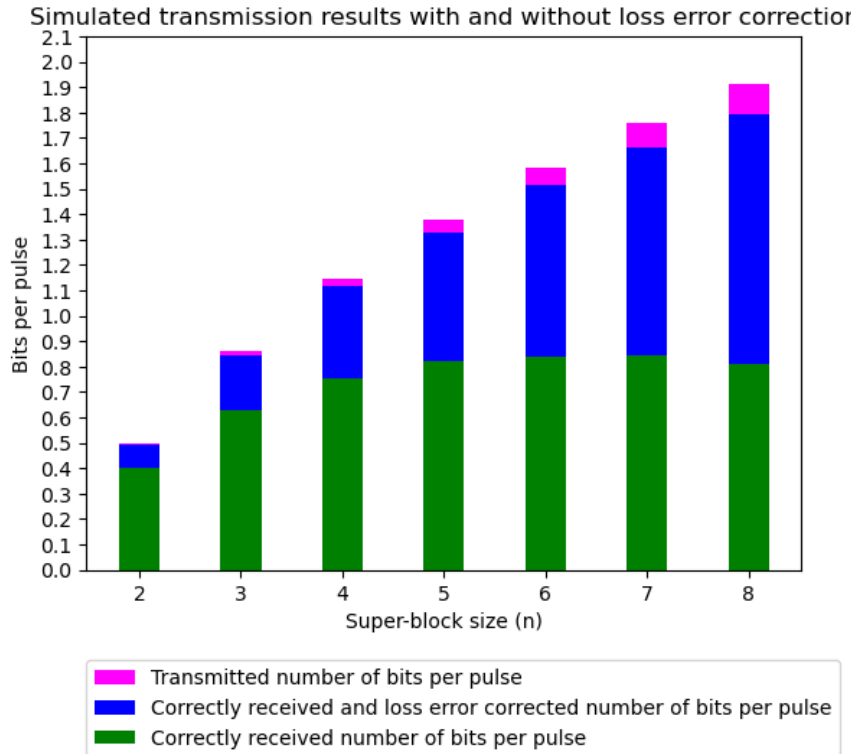


Figure 4.7: Error-corrected simulated transmission with $p_{\text{add}} = 0\%$ and $p_{\text{loss}} = 10\%$. The plot shows the average number of successfully received (green) vs transmitted (pink) vs successfully received and error-corrected (blue) information bits per pulse for each super-block of size n . The number of transmitted super-blocks per super-block size of n is 10 000. All super-blocks are constructed with lengths in declining order: 7,4,2,1,...

n	Transmitted without errors (%)	Solved addition and loss errors (%)	Unsolved errors (%)
2	80.83	18.06	1.11
3	72.88	25.17	1.95
4	65.67	31.67	2.66
5	59.44	36.82	3.74
6	53.2	42.5	4.3
7	48.11	46.63	5.26
8	42.24	51.39	6.37

Figure 4.8: The table shows the size n of the transmitted super-blocks and the respective percentage of super-blocks that are not distorted during the transmission, vs the percentage of super-blocks that are successfully corrected, vs the percentage of super-blocks that can not be corrected using EC.

4.1. Results of Software Simulated Transmissions of Super-blocks: Arbitrary Values for p_{loss} and p_{add}

n	Transmitted (bits/pulse)	Correctly received and EC (bits/pulse)	Ratio (%)
2	0.5	0.49	98.89
3	0.86	0.84	98.05
4	1.15	1.12	97.34
5	1.38	1.33	96.26
6	1.58	1.51	95.7
7	1.76	1.66	94.74
8	1.91	1.79	93.63

Figure 4.9: The table shows the size n of the transmitted super-blocks and the respective average number of transmitted information bits per pulse, vs the average number of bits per pulse that are correctly received with and without EC, vs the ratio between the two.

4.1.1.4 Discussion: Only Loss Errors

For the super-block sizes and error probabilities that are tested for in sections 4.1.1.1, 4.1.1.2 and 4.1.1.3, the conclusion can be drawn that the BPPM encoding with error correction improves the overall results of the transmission, when compared to usage of BPPM encoding with no EC (see the green and blue bars). Amongst the different super-block sizes $n = 2, \dots, 8$, the BPPM protocol manages to recover between 17.92-51.39% additional super-blocks. When comparing the three figures 4.1, 4.4 and 4.7, there is no significant visible difference in the percentage of successful error correction depending on the structure of the super-blocks. For super-blocks with sub-block lengths in rising order, the EC protocol gives between 18.14-50.27% improvement for all super-block sizes. For lengths in mixed order, the protocol gives between 17.92-50.47% improvement. For lengths in declining order, the EC improves the results with between 18.06-51.39%. In all three scenarios, the improvement is compared to using the BPPM encoding when there is no error correction. In conclusion, the software implementation of the BPPM protocol performs about as well for correcting any permutation of a super-block of size n .

4.1.2 Addition Error Generation and Correction Results

During these experiments, only addition errors are tested. The separate error probabilities for losses and additions are decided as $p_{\text{add}} = 10\%$ and $p_{\text{loss}} = 0\%$.

4.1.2.1 Sub-block Lengths in Rising Order

In this section, the results of simulated transmission and error correction for only addition errors are presented. The sub-block lengths of the super-blocks are in rising order. In figure 4.10, the average number of information bits per pulse are plotted over the super-block size of n sub-blocks. In figures 4.11 and 4.12, the results of the transmission and correction process are laid out in tables for closer inspection of the numbers.

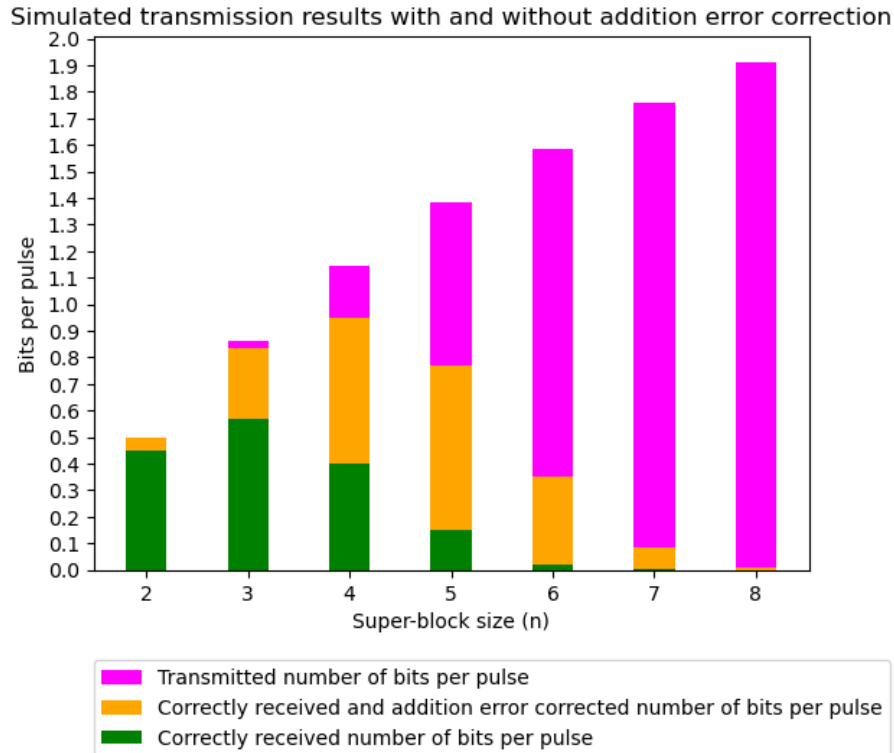


Figure 4.10: Error-corrected simulated transmission with $p_{\text{add}} = 10\%$ and $p_{\text{loss}} = 0\%$. The plot shows the average number of successfully received (green) vs transmitted (pink) vs successfully received and error-corrected (orange) information bits per pulse for each super-block of size n . The number of transmitted super-blocks per super-block size of n is 10 000. All super-blocks are constructed with lengths in rising order: 1,2,4,7,....

4.1. Results of Software Simulated Transmissions of Super-blocks: Arbitrary Values for p_{loss} and p_{add}

n	Transmitted without errors (%)	Solved addition and loss errors (%)	Unsolved errors (%)
2	89.65	10.35	0
3	65.76	31.35	2.89
4	34.8	48.16	17.04
5	10.87	44.71	44.42
6	1.35	20.84	77.81
7	0.09	4.61	95.3
8	0	0.55	99.45

Figure 4.11: The table shows the size n of the transmitted super-blocks and the respective percentage of super-blocks that are not distorted during the transmission, vs the percentage of super-blocks that were successfully corrected, vs the percentage of super-blocks that can not be corrected using EC.

n	Transmitted (bits/pulse)	Correctly received and EC (bits/pulse)	Ratio (%)
2	0.5	0.5	100
3	0.86	0.84	97.11
4	1.15	0.95	82.96
5	1.38	0.77	55.58
6	1.58	0.35	22.19
7	1.76	0.08	4.7
8	1.91	0.01	0.55

Figure 4.12: The table shows the size n of the transmitted super-blocks and the respective average number of transmitted information bits per pulse, vs the average number of bits per pulse that are correctly received with and without EC, vs the ratio between the two.

4.1.2.2 Sub-block Lengths in Mixed Order

In this section, the results of simulated transmission and error correction for only addition errors are presented. The sub-block lengths in the super-blocks are in mixed order. In figure 4.13, the average number of information bits per pulse are plotted over the super-block size of n sub-blocks. In figure 4.14 and 4.15, the results of the transmission and correction process are laid out in tables for closer inspection of the numbers.

4.1. Results of Software Simulated Transmissions of Super-blocks: Arbitrary Values for p_{loss} and p_{add}

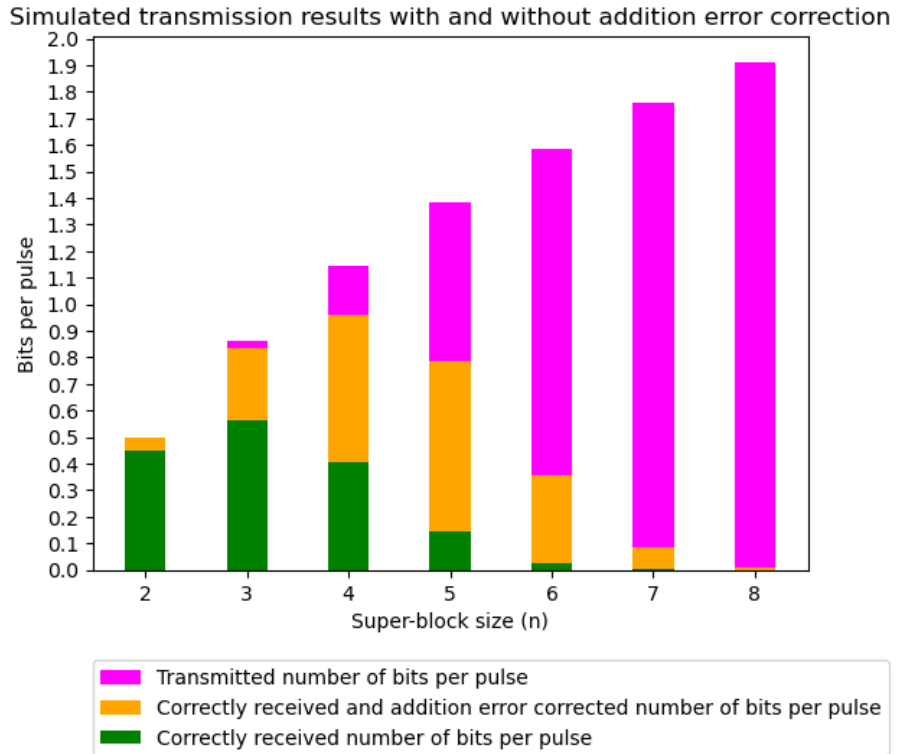


Figure 4.13: Error-corrected simulated transmission with $p_{\text{add}} = 10\%$ and $p_{\text{loss}} = 0\%$. The plot shows the average number of successfully received (green) vs transmitted (pink) vs successfully received and error-corrected (orange) information bits per pulse for each super-block of size n . The number of transmitted super-blocks are 10 000 for each super-block size of n , out of which there are about as many of each super-block permutation.

n	Transmitted without errors (%)	Solved addition and loss errors (%)	Unsolved errors (%)
2	89.92	10.08	0
3	65.55	31.17	3.28
4	35.21	48.5	16.29
5	10.48	46.45	43.07
6	1.46	21.1	77.44
7	0.13	4.6	95.27
8	0.01	0.49	99.5

Figure 4.14: The table shows the size n of the transmitted super-blocks and the respective percentage of super-blocks that are not distorted during the transmission, vs the percentage of super-blocks that are successfully corrected, vs the percentage of super-blocks that can not be corrected using EC.

4.1. Results of Software Simulated Transmissions of Super-blocks: Arbitrary Values for p_{loss} and p_{add}

n	Transmitted (bits/pulse)	Correctly received and EC (bits/pulse)	Ratio (%)
2	0.5	0.5	100
3	0.86	0.83	96.72
4	1.15	0.96	83.71
5	1.38	0.79	56.93
6	1.58	0.36	22.56
7	1.76	0.08	4.73
8	1.91	0.01	0.5

Figure 4.15: The table shows the size n of the transmitted super-blocks and the respective average number of transmitted information bits per pulse, vs the average number of bits per pulse that are correctly received with and without EC, vs the ratio between the two.

4.1.2.3 Sub-block Lengths in Declining Order

In this section, the results of simulated transmission and error correction for only addition errors are presented. The sub-block lengths are in declining order. In figure 4.16, the average number of information bits per pulse are plotted over the super-block size of n sub-blocks. In figure 4.17 and 4.18, the results of the transmission and correction process are laid out in tables for closer inspection of the numbers.

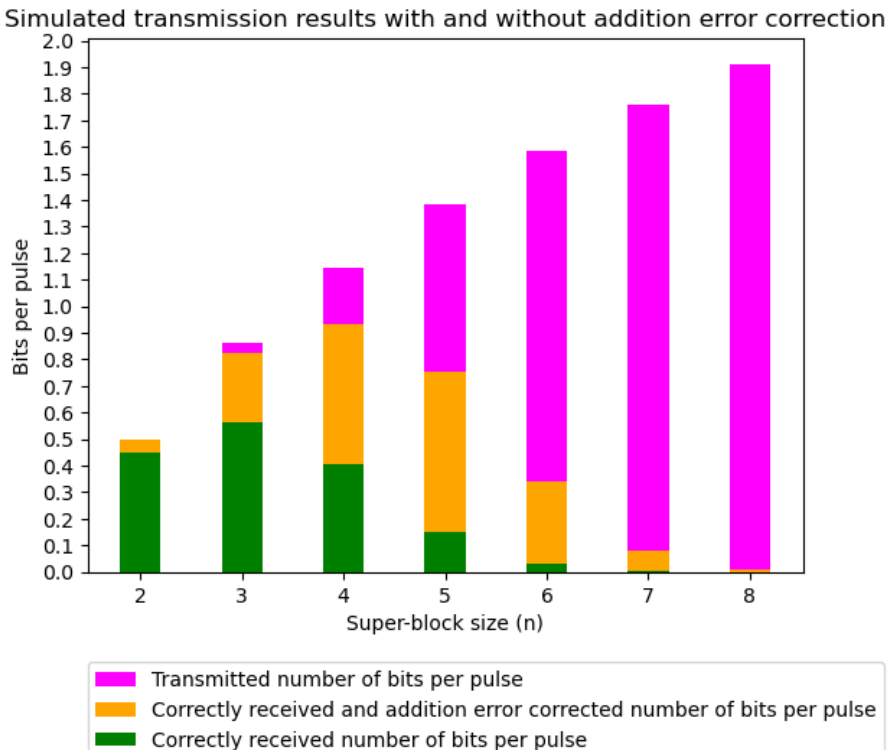


Figure 4.16: Error-corrected simulated transmission with $p_{\text{add}} = 10\%$ and $p_{\text{loss}} = 0\%$. The plot shows the average number of successfully received (green) vs transmitted (pink) vs successfully received and error-corrected (orange) information bits per pulse for each super-block of size n . The number of transmitted super-blocks are 10 000 for each super-block size of n . All super-blocks are constructed with lengths in declining order: 7,4,2,1,...

4.1. Results of Software Simulated Transmissions of Super-blocks: Arbitrary Values for p_{loss} and p_{add}

n	Transmitted without errors (%)	Solved addition and loss errors (%)	Unsolved errors (%)
2	90.29	9.71	0
3	65.52	29.92	4.56
4	35.17	46.38	18.45
5	10.86	43.51	45.63
6	2.02	19.55	78.43
7	0.08	4.52	95.4
8	0	0.49	99.51

Figure 4.17: The table shows the size n of the transmitted super-blocks and the respective percentage of super-blocks that are not distorted during the transmission, vs the percentage of super-blocks that are successfully corrected, vs the percentage of super-blocks that can not be corrected with BPPM EC.

n	Transmitted (bits/pulse)	Correctly received and EC (bits/pulse)	Ratio (%)
2	0.5	0.5	100
3	0.86	0.82	95.44
4	1.15	0.93	81.55
5	1.38	0.75	54.37
6	1.58	0.34	21.57
7	1.76	0.08	4.6
8	1.91	0.01	0.49

Figure 4.18: The table shows the size of the transmitted super-blocks n and the respective average number of transmitted information bits per pulse, vs the average number of bits per pulse that are correctly received with and without EC, vs the ratio between the two.

4.1.2.4 Discussion: Only Addition Errors

When looking at the simulation results presented in sections 4.1.2.1, 4.1.2.2 and 4.1.2.3, it can be understood that in all three cases, at super-block sizes of around $n \geq 8$, lost data is no longer recovered using the BPPM EC protocol at the proposed addition error probability. In other words, there is no longer any purpose to attempt error correction at this point. For an addition error probability of 10%, the maximum amount of data recovered using the EC protocol is obtained using super-blocks of size $n = 4$. For super-blocks with sub-block lengths ordered in rising order, this means an improvement in the recovered data amount of 48.16% compared to using BPPM without EC. For super-blocks with sub-block lengths in a mixed order, this means an improvement in recovered data of 48.50%. For super-blocks with sub-block lengths ordered in declining order, this means an improvement in recovered data of 46.38%. Just like for loss errors (see section 4.1.1.4), there is no significant difference in the addition EC capabilities of the protocol implementation when dealing with super-blocks of rising, mixed or declining sub-block length order.

In comparison with the results presented in section 4.1.1 (for only loss errors), it is clear for all three addition error simulations, that the addition error probability contributes to higher rates of error complexity than the loss error probability, as the super-block sizes increase. That is the case even though the probability for singular losses versus singular additions have the same value. This type of result is to be expected, since for each sub-block in a super-block, only one photon can be lost, no matter the length of that sub-block. However, the longer a sub-block is, the more empty time-bins there are that could potentially be occupied by one or several added photons.

For the super-block size of $n = 2$, the BPPM protocol is slightly better at performing error correction with a 10% probability for addition errors, than with the same error probability for loss errors. The results show that the ratio of successfully received super-blocks (with and without error correction) is 100% for only addition errors, and circa 99% for only loss errors. Even though the difference is very small, it is something worth noting and it has to do with the fact that this is the only super-block size in which there are naturally more occupied time-bins than there are empty ones (2 empty and 1 occupied).

4.1.3 Loss- and Addition Error Generation and Correction Results

During these simulations, the separate probabilities for loss- and addition errors are decided as $p_{\text{loss}} = p_{\text{add}} = 10\%$. The reason for testing a scenario where $p_{\text{loss}} = p_{\text{add}}$ is given in section 3.6.3.1. When simulating transmission for both losses and additions simultaneously, only super-blocks with sub-block length order: shortest → longest are used. The reason for this is that the choice of super-block permutation does not significantly affect the individual loss- and addition error correction results (see sections 4.1.1 and 4.1.2).

4.1.3.1 Sub-block Lengths in Rising Order

In this section, the results of the simulated transmission and error correction of both loss- and addition errors are presented. The sub-block lengths inside the super-blocks are in rising length order. In figure 4.19, the average number of information bits per pulse are plotted over the super-block size of n sub-blocks. In figure 4.20 and 4.21, the results of the transmission and correction process are laid out in tables for closer inspection of the numbers.

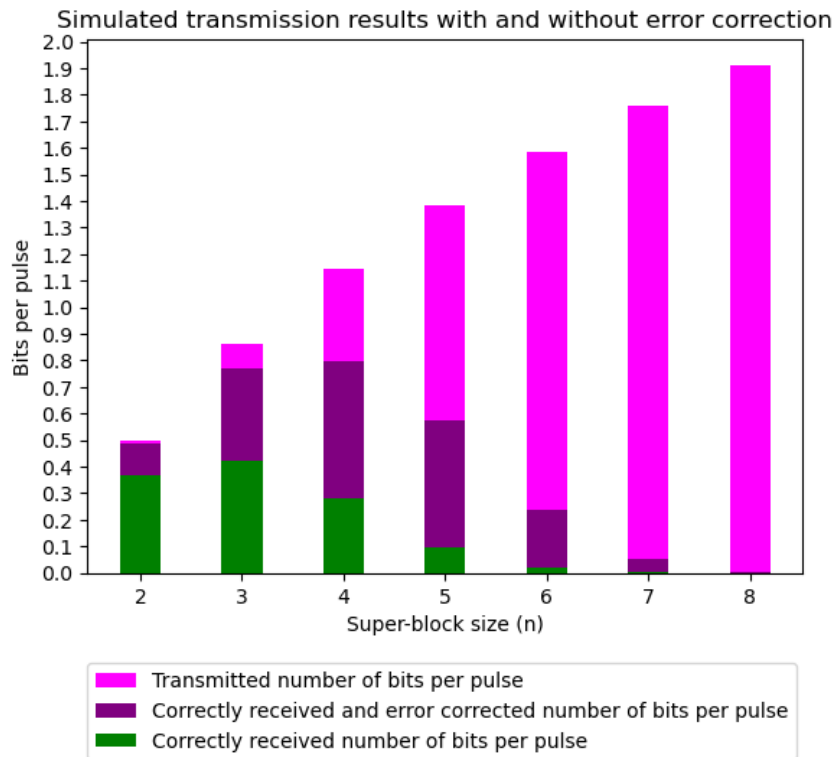


Figure 4.19: Error-corrected simulated transmission with $p_{\text{add}} = p_{\text{loss}} = 10\%$. The plot shows the average number of successfully received (green) vs transmitted (pink) vs successfully received **and** error-corrected (purple) information bits per pulse for each super-block size n . The number of transmitted super-blocks are 10 000 for each super-block size of n . All super-blocks are constructed with lengths in rising order: 1,2,4,7,....

4.1. Results of Software Simulated Transmissions of Super-blocks: Arbitrary Values for p_{loss} and p_{add}

n	Transmitted without errors (%)	Solved addition and loss errors (%)	Unsolved errors (%)
2	73.53	24.24	2.23
3	48.78	40.51	10.71
4	24.25	45.3	30.45
5	7.12	34.53	58.35
6	1.09	13.8	85.11
7	0.06	2.84	97.1
8	0	0.21	99.79

Figure 4.20: The table shows the size n of the transmitted super-blocks and the respective percentage of super-blocks that are not distorted during the transmission, vs the percentage of super-blocks that are successfully corrected, vs the percentage of super-blocks that can not be corrected using EC.

n	Transmitted (bits/pulse)	Correctly received and EC (bits/pulse)	Ratio (%)
2	0.5	0.49	97.77
3	0.86	0.77	89.29
4	1.15	0.8	69.55
5	1.38	0.58	41.65
6	1.58	0.24	14.89
7	1.76	0.05	2.9
8	1.91	0	0.21

Figure 4.21: The table shows the size n of the transmitted super-blocks and the respective average number of transmitted information bits per pulse, vs the average number of bits per pulse that are correctly received with and without EC, vs the ratio between the two.

4.1.3.2 Discussion: Loss- and Addition Errors

When looking at the results presented in section 4.1.3.1, it can be gathered that at super-block sizes of $n \geq 8$, and using the current error probabilities, the BPPM EC protocol is no longer of any benefit. From this section, it can be gathered that the maximum amount of successful error correction is obtained at super-block sizes of $n = 4$. At that super-block size, the error correction improves the over all transmission results with 45.30% (compared to when there is only BPPM encoding with no EC).

The transmission- and error correction results presented for simultaneously simulated loss- and addition errors (both at 10%), are much more alike the results of simulating for only addition errors (at 10%), than those of simulating for only loss errors at the same error probability. The conclusion is that the BPPM protocol is more effective at correcting for photon losses than photon additions at larger super-block sizes of n sub-blocks. As previously mentioned in section 4.1.2.4, the added complexity of multiple possible additions per sub-block vs the possibility of losing only one pulse per sub-block, makes loss errors easier to solve for in larger super-blocks. BPPM is therefore generally better suited for bit-flip errors of z-channel type over BSC type (see section 2.6.1). For actual transmissions of more versatile data and thereby a larger number of transmitted/encoded information bits per pulse (meaning: using longer super-blocks), it is therefore preferable to have error probabilities such that $p_{\text{loss}} \gg p_{\text{add}}$.

4.2 Experiments

In this section, the experimental results from measurements in the lab are presented. This includes: dark-count and photon loss measurements, as well as a polarization drift measurement.

4.2.1 Dark-count Probability (p_{add})

In figure 4.22, the model describing expected addition error probability (p_{add}) over detection efficiency η_{eff} can be seen. The available detection efficiency span of the SPD of model ID210 (from ID Quantique) is 5-25%. The addition error probability model is created according to the description in section 3.6.1.1. It utilizes the results of dark-count measurements from the lab. During the dark-count measurement, the minimum and maximum detected dark-count rates were 100 Hz and 135 kHz respectively, using gating frequency 1 MHz and SPD dead time 0.10 μs .

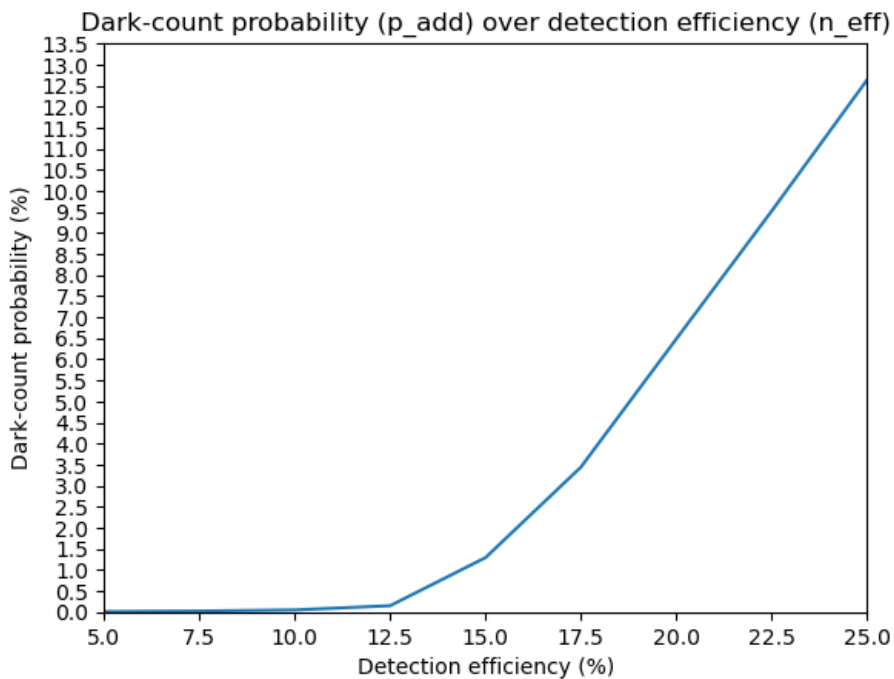


Figure 4.22: Graph displaying the calculated dark-count probability (p_{add}) for the SPD of model ID210 (from ID Quantique) over detection efficiency span $\eta_{\text{eff}} = 5 - 25\%$.

4.2.1.1 Discussion: Dark-counts

As expected, the value of addition error probability p_{add} increases with higher levels of detection efficiency. In figure 4.22, it can be seen that up until $\eta_{\text{eff}} = 10\%$, the addition probability level is quite low ($\leq 0.05\%$). For $\eta_{\text{eff}} > 12.5\%$ however, the probability of dark-counts increases significantly. Since the BPPM protocol is much more efficient at correcting for loss errors (at least when dealing with longer super-blocks), it is preferable to keep the probability p_{add} at a level that decreases the amount of losses at the detector and simultaneously keeps the addition errors at a minimum. Therefore, in the transmission simulation results presented in sections 4.3.1 and 4.4.1, the value of η_{eff} is set to 10%. This gives addition error probability $p_{\text{add}} = 0.05\%$. Because of the relatively low value of η_{eff} , it can be expected that the relationship between probability of photon addition vs photon loss is

such that $p_{\text{loss}} \gg p_{\text{add}}$.

For the simulation results presented in section 4.3.2, the detection efficiency η_{eff} is set to 20%. This is in an effort to study how the BPPM protocol performs during tests where there is a larger probability of having addition errors. Since the estimation of addition error contributions during the thesis work is such that stray light rate \ll dark-count rate, the most efficient way of simulating the behaviour of a noisy transmission channel is to increase the detection efficiency.

4.2.2 Loss Probability (p_{loss})

In this section, the simulated loss probability (p_{loss}) over a fiber distance of L km is presented. The model describes losses over propagation distance for different pulse sizes, containing on average a number of u photons. The construction of the loss probability model is described in section 3.6.1.2.

During the measurement of losses between the outputs of the transmitter and receiver, the laser source power is set to 12 dBm. The measured losses over the back-to-back system is $P_{\text{in}} - P_{\text{out}} = 0.93$ dB. Regarding the expected losses over an added fiber distance of L km between sender and receiver, the maximum attenuation specified in the single-mode fiber (SMF-28) specification sheet is $\alpha_{\text{dB}} = 0.18$ [dB/km] at the working wavelength of 1550 nm. This value is used for simulating the losses over 0 – 75 km. The losses are modelled separately for detection efficiencies $\eta_{\text{eff}} = 10\%$ (see figure 4.23) and $\eta_{\text{eff}} = 20\%$ (see figure 4.24).

Loss probability (p_{loss}) over fiber length (L) for different numbers of photons per pulse (u), using a detection efficiency (η_{eff}) of 10%

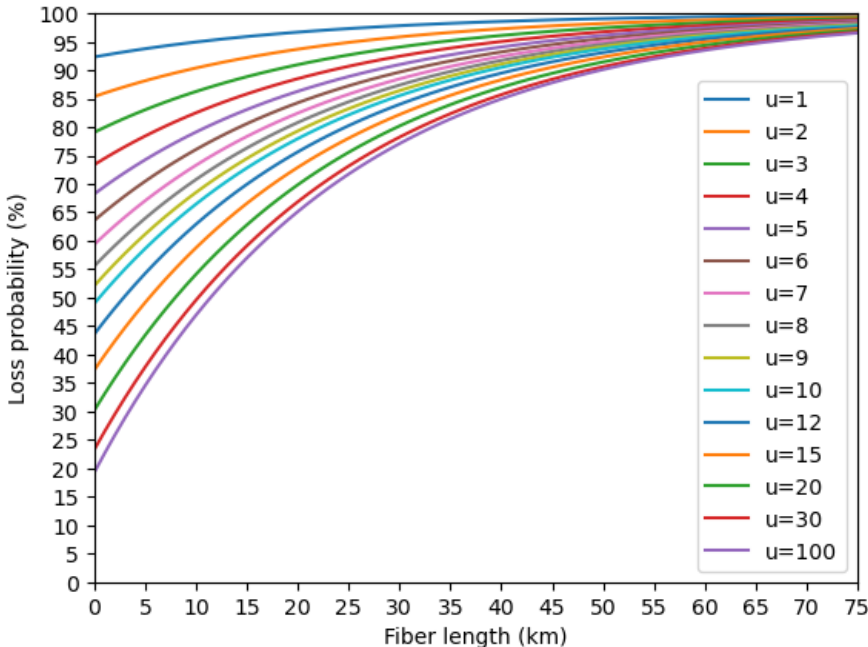


Figure 4.23: The probability for photon loss (p_{loss}) over a propagation distance of $L = 0 – 75$ km when $\eta_{\text{eff}} = 10\%$. The losses are simulated for pulse sizes of u number of photons.

Loss probability (p_{loss}) over fiber length (L) for different numbers of photons per pulse (u), using a detection efficiency (η_{eff}) of 20%

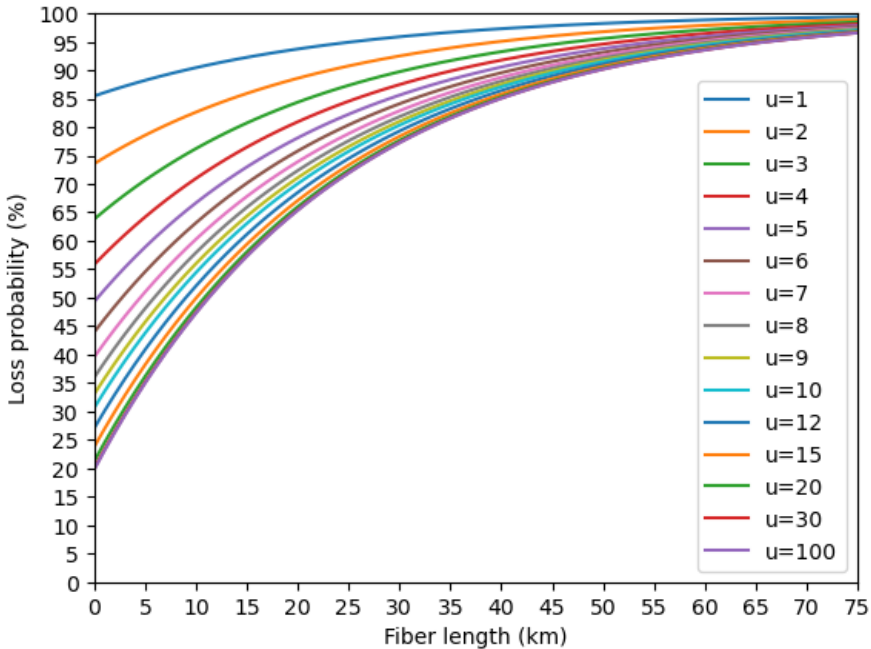


Figure 4.24: The probability for photon loss (p_{loss}) over a propagation distance of $L = 0 - 75$ km when $\eta_{\text{eff}} = 20\%$. The losses are simulated for pulse sizes of u number of photons.

4.2.2.1 Discussion: Photon Losses

As can be seen in figures 4.23 and 4.24, the average number of photons per pulse does impact the loss probability quite significantly. This is most notable at the $L = 0$ km distance. The more photons there are per pulse, the lower the loss probability. In both graphs, it is quite clear that using only one single photon per pulse in the available setup, will result in very high loss probabilities of between 85.47-92.32%, even in the back-to-back system. Therefore, it is of interest to model the loss probability for pulses $>> 1$ photon. Note however that at around $u = 100$, the loss probability reaches a minimum of circa $p_{\text{loss}} = 19\%$ losses. Meaning that pulse sizes > 100 photons do not change the loss probability for the better. It is therefore unnecessary to use higher energy light pulses in the available system. The minimum losses at $L = 0$ km originate from the measured losses between the ends of transmitter and receiver (of 0.93 dB), i.e. when the transmitter and receiver are placed back-to-back. When comparing the curves in figures 4.23 and 4.24, there is also a visible difference in loss probability created by the detection efficiency. The loss probability curves in figure 4.24 (using detection efficiency 20%) are closer to the minimum value of $p_{\text{loss}} \approx 19\%$ at a lesser number of average photons per pulse u , when compared to the curves in figure 4.23. However, as is displayed in figure 4.22, a greater detection efficiency results in a higher addition probability p_{add} .

It has previously been shown that the BPPM protocol is more prevalent at correcting for loss errors than addition errors when transmitting longer super-blocks (for example when $n > 2$, see section 4.1). For the simulations presented in sections 4.3.1 and 4.3.2, pulse sizes of $u = 100$ and $u = 10$ are used to study how the average photon number, detection efficiency of the SPD, and the propagation distance affects the transmission and error correction results. Although optical transmission using pulses containing on average 10 or 100 photons naturally requires more energy than using only 1 photon per pulse, these pulse sizes are still much

more energy efficient than the billions of photons per pulse that are normally involved with communication using classical light pulses.

4.2.3 Polarization Drift Test Results

The results presented in this section correspond to the experiment described in section 3.6.2. For measuring the polarization drift, a 1550 nm telecom cw-DFB laser source is used, with a power setting of 12 dBm. The duration of the experiment is 110 minutes, during which the polarized light pulses pass through the experimental setup with transmitter and receiver placed back-to-back, before being displayed on the oscilloscope. The results can be seen in figures 4.25 and 4.26, where the green curves represents the minimum/maximum power of the horizontally polarized light and the orange curves represents the minimum/maximum power of the vertically polarized light. When the vertically polarized signal is high, the horizontally polarized signal is low and vice versa.

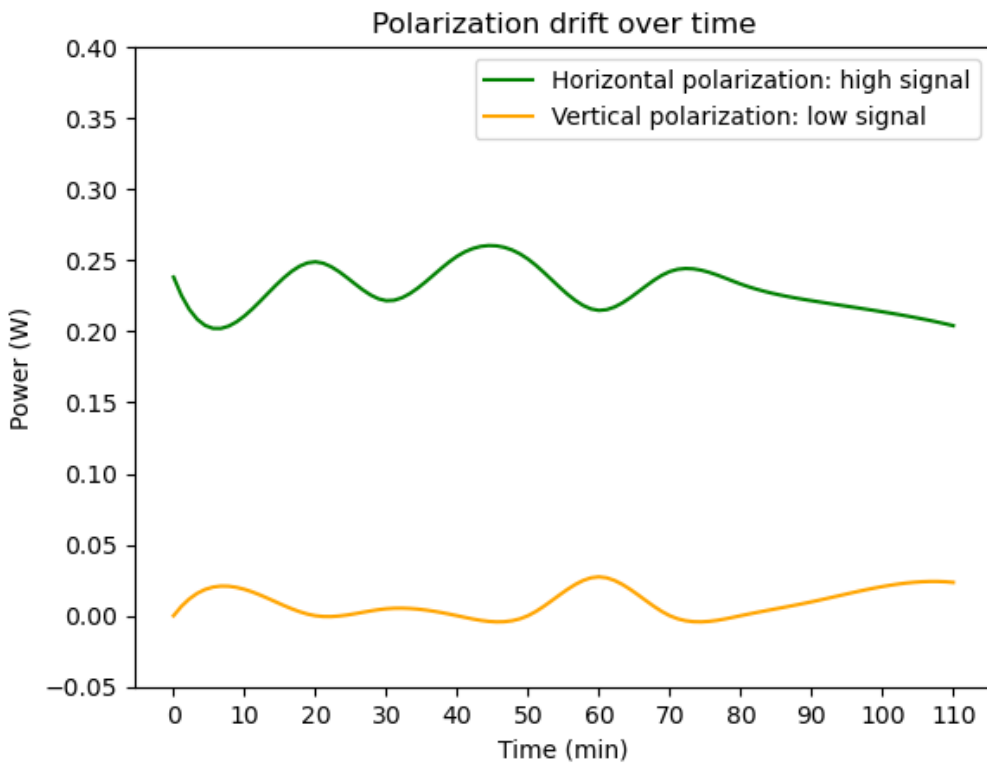


Figure 4.25: Polarization drift displayed in power level over time. Here, the horizontally polarized signal is high and the vertically polarized signal is low.

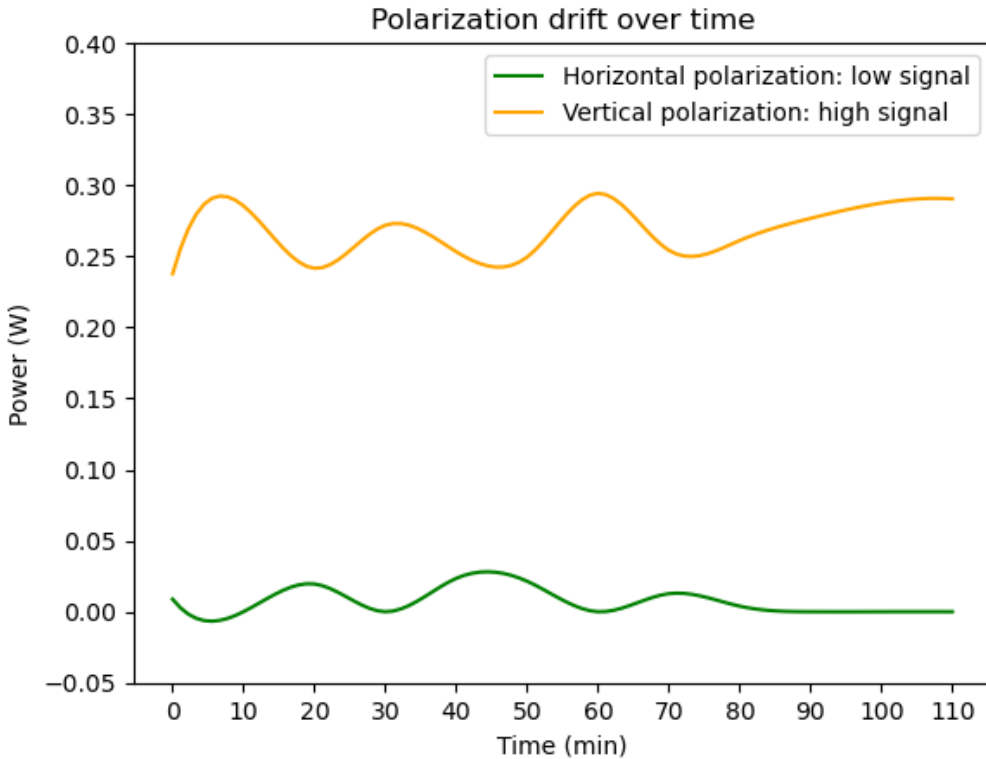


Figure 4.26: Polarization drift displayed in power level over time. Here, the vertically polarized signal is high and the horizontally polarized signal is low.

4.2.3.1 Discussion: Polarization Drift

As can be seen in figures 4.25 and 4.26, the high power polarized signals fluctuate with more than $\Delta = 0.05$ W over the duration of the experiment. The fluctuations in the graph represent how much of the light, which in the ideal case should all be on either the horizontally or vertically polarized curve, bleeds into the respective low power signals (which in an ideal case should be at zero power). However, the signals corresponding to the vertically- and horizontally polarized light never overlap, which means that the fluctuations are within some bounds.

In order to successfully be able to use the available laboratory setup to test the feasibility of the BPPM protocol, the bar for signal detection needs to be set well above the fluctuations of the lower signal (because it is not at zero power). Since the results imply that a system utilizing this sort of polarization alignment technique is quite unreliable over time, it is therefore recommended that for potential future laboratory testing of the BPPM protocol, either polarization maintaining fiber or some other type of active polarization stabilization should be used.

4.3 Results of Software Simulated Transmissions of Super-blocks: Experimentally Derived Values for p_{loss} and p_{add}

The results presented in this section correspond to the tests described in section 3.6.3.2. In section 4.3.1 the detection efficiency is set to $\eta_{\text{eff}} = 10\%$ and in 4.3.2 it is set to $\eta_{\text{eff}} = 20\%$. The data statistics is represented in graphs showing the average number of bit information per pulse (of sizes $u = 10$ and $u = 100$ photons) over a super-block size of n . Note that the values for p_{loss} and p_{add} in these simulations are experimentally derived from figures 4.23, 4.24 and 4.22.

4.3.1 Super-block Transmission with Detection Efficiency $\eta_{\text{eff}} = 10\%$

During these software simulated transmissions, 10 000 super-blocks of size n number of sub-blocks from the sequence of allowed lengths $\{1, 2, 4, 7, 12, 20, \dots\}$ are used. All super-blocks are constructed with lengths in rising order: shortest → longest. The probabilities for addition- and loss errors are derived from figures 4.22 and 4.23 respectively. The addition probability p_{add} is based on the SPD detection efficiency η_{eff} and the loss probability p_{loss} is based on a simulated propagation distance of L km, average pulse size of u number of photons and the SPD detection efficiency.

4.3.1.1 Transmission of Pulses with an Average Photon Number $u = 100$

For the transmission simulations in this section, the probability of having an addition error is $p_{\text{add}} = 0.05\%$, which is a direct consequence of the SPD detection efficiency. Tests are performed at simulated distances of $L = 0$ km and $L = 5$ km respectively. In both cases, the pulses are of size $u = 100$ photons and the detection efficiency is $\eta_{\text{eff}} = 10\%$. Under these conditions, a distance of $L = 0$ km gives a loss probability of $p_{\text{loss}} = 19.28\%$ and the results of the simulation can be seen in figure 4.27. In figure 4.28 and 4.29, the results of the simulated transmission and correction process are laid out in tables. At a simulated transmission distance of $L = 5$ km, the loss probability is $p_{\text{loss}} = 34.56\%$ and the results of the simulation can be seen in figure 4.30. In figure 4.31 and 4.32, the results of the simulated transmission and correction process are laid out in tables.

4.3. Results of Software Simulated Transmissions of Super-blocks: Experimentally Derived Values for p_{loss} and p_{add}

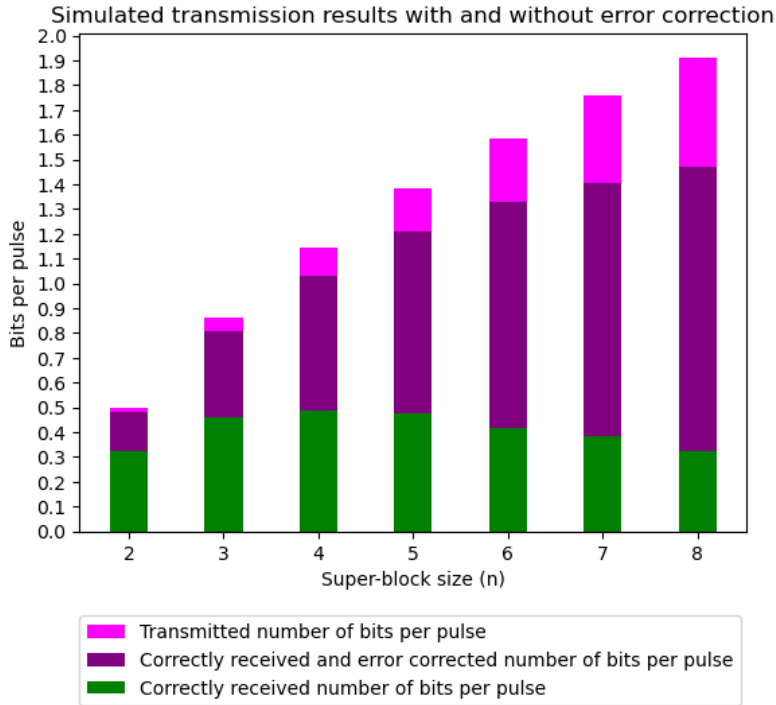


Figure 4.27: Error-corrected simulated transmission with $p_{\text{loss}} = 19.28\%$, $p_{\text{add}} = 0.05\%$ and 100 photons per pulse at a fiber distances of 0 km. The plot shows the average number of successfully received (green) vs transmitted (pink) vs successfully received and error-corrected (purple) bits per pulse for each super-block of size n .

n	Transmitted without errors (%)	Solved addition and loss errors (%)	Unsolved errors (%)
2	64.82	31.28	3.9
3	53.21	40.34	6.45
4	42.35	47.46	10.19
5	34.31	53.26	12.43
6	26.34	57.52	16.14
7	21.7	58.31	19.99
8	16.85	60.04	23.11

Figure 4.28: The table shows the size n of the transmitted super-blocks and the respective percentage of super-blocks that are not distorted during the transmission, vs the percentage of super-blocks that are successfully corrected, vs the percentage of super-blocks that can not be corrected using EC.

4.3. Results of Software Simulated Transmissions of Super-blocks: Experimentally Derived Values for p_{loss} and p_{add}

n	Transmitted (bits/pulse)	Correctly received and EC (bits/pulse)	Ratio (%)
2	0.5	0.48	96.1
3	0.86	0.81	93.55
4	1.15	1.03	89.81
5	1.38	1.21	87.57
6	1.58	1.33	83.86
7	1.76	1.41	80.01
8	1.91	1.47	76.89

Figure 4.29: The table shows the size n of the transmitted super-blocks and the respective average number of transmitted information bits per pulse, vs the average number of bits per pulse that are correctly received with and without EC, vs the ratio between the two.

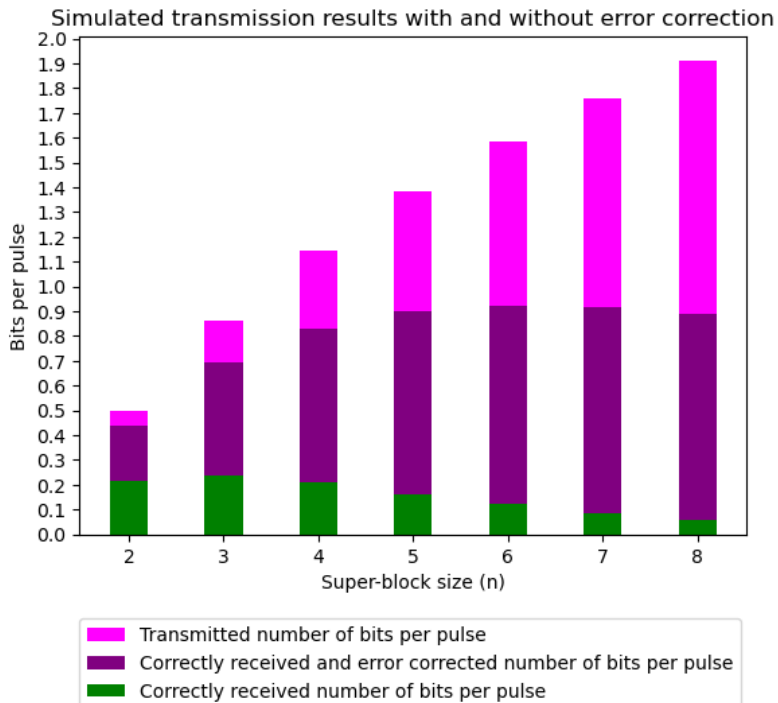


Figure 4.30: Error-corrected simulated transmission with $p_{\text{loss}} = 34.56\%$, $p_{\text{add}} = 0.05\%$ and 100 photons per pulse at a fiber distances of 5 km. The plot shows the average number of successfully received (green) vs transmitted (pink) vs successfully received and error-corrected (purple) bits per pulse for each super-block of size n .

4.3. Results of Software Simulated Transmissions of Super-blocks: Experimentally Derived Values for p_{loss} and p_{add}

n	Transmitted without errors (%)	Solved addition and loss errors (%)	Unsolved errors (%)
2	43.08	44.84	12.08
3	27.83	52.65	19.52
4	18.26	54.19	27.55
5	11.78	53.4	34.82
6	7.65	50.74	41.61
7	4.75	47.4	47.85
8	3.1	43.48	53.42

Figure 4.31: The table shows the size n of the transmitted super-blocks and the respective percentage of super-blocks that are not distorted during the transmission, vs the percentage of super-blocks that are successfully corrected, vs the percentage of super-blocks that can not be corrected using EC.

n	Transmitted (bits/pulse)	Correctly received and EC (bits/pulse)	Ratio (%)
2	0.5	0.44	87.92
3	0.86	0.69	80.48
4	1.15	0.83	72.45
5	1.38	0.9	65.18
6	1.58	0.92	58.39
7	1.76	0.92	52.15
8	1.91	0.89	46.58

Figure 4.32: The table shows the size n of the transmitted super-blocks and the respective average number of transmitted information bits per pulse, vs the average number of bits per pulse that are correctly received with and without EC, vs the ratio between the two.

4.3.1.2 Discussion

When comparing figures 4.27 (simulated distance 0 km) and 4.30 (simulated distance 5 km), it can be seen how the BPPM error correction capabilities change over a simulated distance of 5 km. At the average number of photons per pulse $u = 100$ and detection efficiency $\eta_{\text{eff}} = 10\%$, the protocol performs quite well. The relatively low detection efficiency will keep the addition probability p_{add} low and the high number of photons per pulse will keep the loss probability p_{loss} relatively low. This ultimately means that much of the lost information can be recovered for all super-block sizes of $n = 2, \dots, 8$. Though naturally, the results are affected by the simulated propagation distance between sender and receiver. For the simulation results presented in figure 4.27, the BPPM error correction protocol improves the results with 31.28-60.04% for super-block sizes between $n = 2, \dots, 8$, compared to using BPPM with no EC (see table in figure 4.28). This means that the successfully received and error corrected amount of super-blocks is between 76.89-96.10% (see table in figure 4.29) of what was originally transmitted.

For the simulation results presented in figure 4.30, the BPPM error correction protocol improves the results with between 43.48-54.19% (see table in figure 4.31) for super-block sizes between $n = 2, \dots, 8$. This means that the successfully received and error corrected amount of super-blocks is between 46.58-87.92% (see table in figure 4.32) of what was originally transmitted. The maximum improvement that is achieved with BPPM and EC (versus BPPM with no EC) is in this scenario found at super-block size of $n = 4$.

4.3.1.3 Transmission of Pulses with an Average Photon Number $u = 10$

For the transmission simulations in this section, the probability of having an addition error is $p_{\text{add}} = 0.05\%$, which is a direct consequence of the SPD detection efficiency. Tests are performed at simulated distances of $L = 0 \text{ km}$ and $L = 5 \text{ km}$ respectively. In both cases, the pulses are of size $u = 10$ photons and the detection efficiency is $\eta_{\text{neff}} = 10\%$. Under these conditions, a distance of $L = 0 \text{ km}$ gives a loss probability of $p_{\text{loss}} = 48.98\%$ and the results of the simulation can be seen in figure 4.33. In figure 4.34 and 4.35, the results of the simulated transmission and correction process are laid out in tables. At a simulated transmission distance of $L = 5 \text{ km}$, the loss probability is $p_{\text{loss}} = 58.63\%$ and the results of the simulation can be seen in figure 4.36. In figure 4.37 and 4.38, the results of the simulated transmission and correction process are laid out in tables.

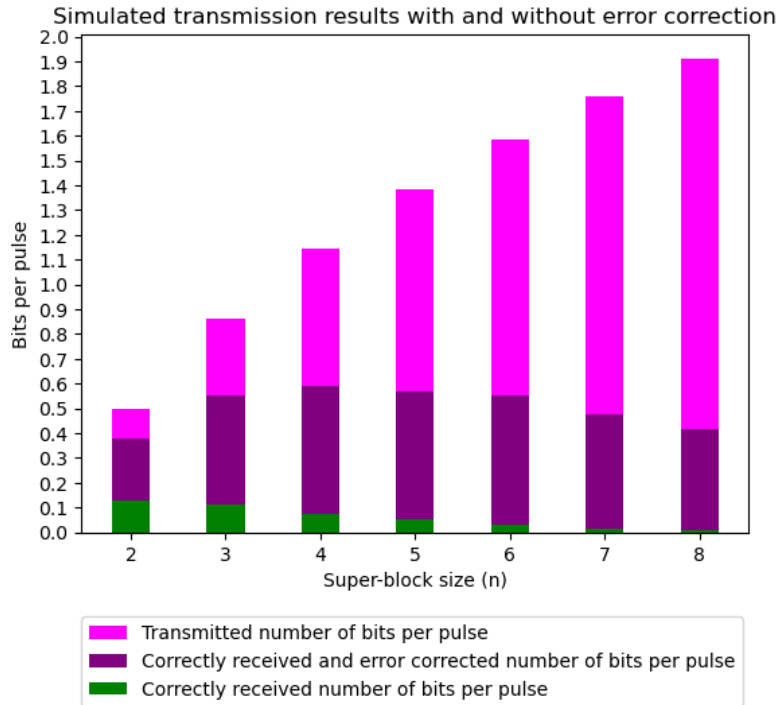


Figure 4.33: Error-corrected simulated transmission with $p_{\text{loss}} = 48.98\%$, $p_{\text{add}} = 0.05\%$ and 10 photons per pulse at a fiber distances of 0 km. The plot shows the average number of successfully received (green) vs transmitted (pink) vs successfully received and error-corrected (purple) bits per pulse for each super-block of size n .

4.3. Results of Software Simulated Transmissions of Super-blocks: Experimentally Derived Values for p_{loss} and p_{add}

n	Transmitted without errors (%)	Solved addition and loss errors (%)	Unsolved errors (%)
2	26.01	49.55	24.44
3	13.13	50.68	36.19
4	6.33	45.02	48.65
5	3.79	37.45	58.76
6	1.85	32.95	65.2
7	0.71	26.53	72.76
8	0.4	21.41	78.19

Figure 4.34: The table shows the size n of the transmitted super-blocks and the respective percentage of super-blocks that are not distorted during the transmission, vs the percentage of super-blocks that are successfully corrected, vs the percentage of super-blocks that can not be corrected using EC.

n	Transmitted (bits/pulse)	Correctly received and EC (bits/pulse)	Ratio (%)
2	0.5	0.38	75.56
3	0.86	0.55	63.81
4	1.15	0.59	51.35
5	1.38	0.57	41.24
6	1.58	0.55	34.8
7	1.76	0.48	27.24
8	1.91	0.42	21.81

Figure 4.35: The table shows the size n of the transmitted super-blocks and the respective average number of transmitted information bits per pulse, vs the average number of bits per pulse that are correctly received with and without EC, vs the ratio between the two.

4.3. Results of Software Simulated Transmissions of Super-blocks: Experimentally Derived Values for p_{loss} and p_{add}

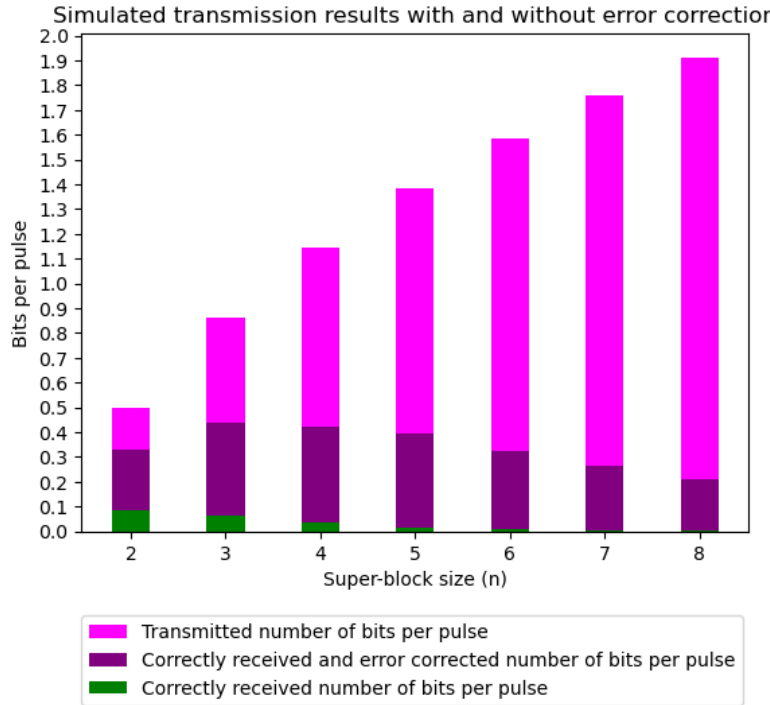


Figure 4.36: Error-corrected simulated transmission with $p_{\text{loss}} = 58.63\%$, $p_{\text{add}} = 0.05\%$ and 10 photons per pulse at a fiber distances of 5 km. The plot shows the average number of successfully received (green) vs transmitted (pink) vs successfully received **and** error-corrected (purple) bits per pulse for each super-block of size n .

n	Transmitted without errors (%)	Solved addition and loss errors (%)	Unsolved errors (%)
2	17.35	48.35	34.3
3	7.41	43.41	49.18
4	3.1	33.89	63.01
5	1.07	27.45	71.48
6	0.51	19.9	79.59
7	0.16	14.97	84.87
8	0.09	10.8	89.11

Figure 4.37: The table shows the size n of the transmitted super-blocks and the respective percentage of super-blocks that are not distorted during the transmission, vs the percentage of super-blocks that are successfully corrected, vs the percentage of super-blocks that can not be corrected using EC.

4.3. Results of Software Simulated Transmissions of Super-blocks: Experimentally Derived Values for p_{loss} and p_{add}

n	Transmitted (bits/pulse)	Correctly received and EC (bits/pulse)	Ratio (%)
2	0.5	0.33	65.7
3	0.86	0.44	50.82
4	1.15	0.42	36.99
5	1.38	0.39	28.52
6	1.58	0.32	20.41
7	1.76	0.27	15.13
8	1.91	0.21	10.89

Figure 4.38: The table shows the size n of the transmitted super-blocks and the respective average number of transmitted information bits per pulse, vs the average number of bits per pulse that are correctly received with and without EC, vs the ratio between the two.

4.3.1.4 Discussion

In figures 4.33 (simulated distance 0 km) and 4.36 (simulated distance 5 km), the average number of photons per pulse is $u = 10$. Naturally, this means that the probability for loss is larger than for pulses containing $u = 100$ photons. Even with the higher values for p_{loss} , some of the lost transmitted information can be recovered. For the simulation results presented in figure 4.33, the BPPM error correction protocol improves the results with between 21.41-50.68% (see table in figure 4.34) for super-blocks of sizes between $n = 2, \dots, 8$ (maximum improvement at $n = 3$). This means that the successfully received and error corrected amount of super-blocks is between 21.81-75.56% (see table in figure 4.35) of what was originally transmitted.

For the simulation results presented in figure 4.36, the BPPM error correction protocol improves the results with 10.80-48.35% (see table in figure 4.37) for super-block sizes between $n = 2, \dots, 8$. This means that the successfully received and error corrected amount of super-blocks is between 10.89-65.70% (see table in figure 4.38) of what was originally transmitted.

In conclusion, both the increased simulated transmission distance, as well as the lower average number of photons per pulse, affects the final results for the worse, which is to be expected. Even so, the BPPM protocol with error correction does improve the transmission results somewhat for all super-block sizes $n = 2 - 8$ under the proposed conditions (compared to BPPM without EC).

4.3.2 Super-block Transmission with Detection Efficiency $\eta_{\text{eff}} = 20\%$

During these software simulated transmissions, 10 000 super-blocks of size n number of sub-blocks from the sequence of allowed lengths $\{1, 2, 4, 7, 12, 20, \dots\}$ are used. All super-blocks are constructed with lengths in rising order: shortest → longest. The probabilities for addition and loss errors are derived from figures 4.22 and 4.24 respectively. The addition probability p_{add} is based on the SPD detection efficiency η_{eff} and the loss probability p_{loss} is based on a simulated propagation distance of L km, average pulse size of u number of photons and the SPD detection efficiency.

4.3.2.1 Transmission of Pulses with an Average Photon Number $u = 100$

For the transmission simulations in this section, the probability of having an addition error is $p_{\text{add}} = 6.48\%$, which is a direct consequence of the SPD detection efficiency. Tests are performed at simulated distances of $L = 0$ km and $L = 5$ km respectively. In both cases, the pulses are of size $u = 100$ photons and the detection efficiency is $\eta_{\text{eff}} = 20\%$. Under these conditions, a distance of $L = 0$ km gives a loss probability of $p_{\text{loss}} = 19.82\%$ and the results of the simulation can be seen in figure 4.39. In figure 4.40 and 4.41, the results of the simulated transmission and correction process are laid out in tables. At a simulated transmission distance of $L = 5$ km, the loss probability is $p_{\text{loss}} = 34.99\%$ and the results of the simulation can be seen in figure 4.42. In figure 4.43 and 4.44, the results of the simulated transmission and correction process are laid out in tables.

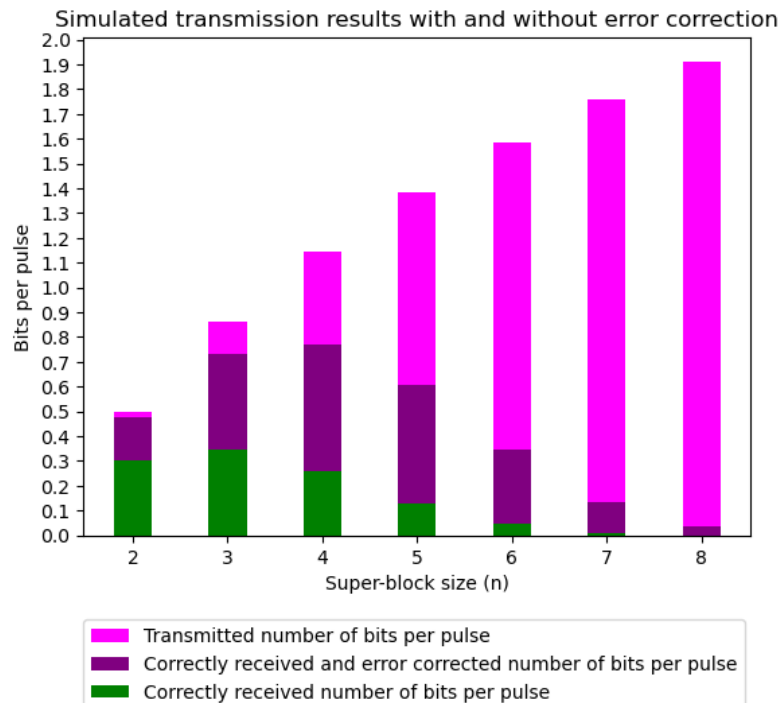


Figure 4.39: Error-corrected simulated transmission with $p_{\text{loss}} = 19.82\%$, $p_{\text{add}} = 6.48\%$ and 100 photons per pulse at a fiber distances of 0 km. The plots shows the average number of successfully received (green) vs transmitted (pink) vs successfully received and error-corrected (purple) bits per pulse for each super-block of size n .

4.3. Results of Software Simulated Transmissions of Super-blocks: Experimentally Derived Values for p_{loss} and p_{add}

n	Transmitted without errors (%)	Solved addition and loss errors (%)	Unsolved errors (%)
2	60.61	34.08	5.31
3	40.1	45.02	14.88
4	22.4	44.93	32.67
5	9.41	34.4	56.19
6	2.81	19.05	78.14
7	0.46	7.05	92.49
8	0.01	1.84	98.15

Figure 4.40: The table shows the size n of the transmitted super-blocks and the respective percentage of super-blocks that are not distorted during the transmission, vs the percentage of super-blocks that are successfully corrected, vs the percentage of super-blocks that can not be corrected using EC.

n	Transmitted (bits/pulse)	Correctly received and EC (bits/pulse)	Ratio (%)
2	0.5	0.47	94.69
3	0.86	0.73	85.12
4	1.15	0.77	67.33
5	1.38	0.61	43.81
6	1.58	0.35	21.86
7	1.76	0.13	7.51
8	1.91	0.04	1.85

Figure 4.41: The table shows the size n of the transmitted super-blocks and the respective average number of transmitted information bits per pulse, vs the average number of bits per pulse that are correctly received with and without EC, vs the ratio between the two.

4.3. Results of Software Simulated Transmissions of Super-blocks: Experimentally Derived Values for p_{loss} and p_{add}

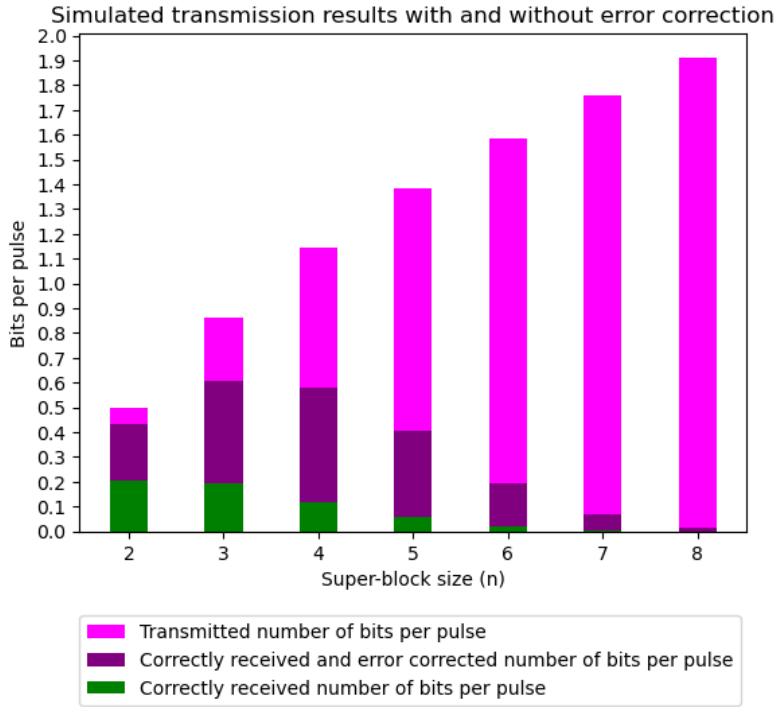


Figure 4.42: Error-corrected simulated transmission with $p_{\text{loss}} = 34.99\%$, $p_{\text{add}} = 6.48\%$ and 100 photons per pulse at a fiber distances of 5 km. The plots shows the average number of successfully received (green) vs transmitted (pink) vs successfully received **and** error-corrected (purple) bits per pulse for each super-block of size n .

n	Transmitted without errors (%)	Solved addition and loss errors (%)	Unsolved errors (%)
2	40.38	45.86	13.76
3	22.38	48.26	29.36
4	10.37	40.14	49.49
5	4.15	25.4	70.45
6	1.09	11.03	87.88
7	0.19	3.58	96.23
8	0	0.72	99.28

Figure 4.43: The table shows the size n of the transmitted super-blocks and the respective percentage of super-blocks that are not distorted during the transmission, vs the percentage of super-blocks that are successfully corrected, vs the percentage of super-blocks that can not be corrected using EC.

4.3. Results of Software Simulated Transmissions of Super-blocks: Experimentally Derived Values for p_{loss} and p_{add}

n	Transmitted (bits/pulse)	Correctly received and EC (bits/pulse)	Ratio (%)
2	0.5	0.43	86.24
3	0.86	0.61	70.64
4	1.15	0.58	50.51
5	1.38	0.41	29.55
6	1.58	0.19	12.12
7	1.76	0.07	3.77
8	1.91	0.01	0.72

Figure 4.44: The table shows the size n of the transmitted super-blocks and the respective average number of transmitted information bits per pulse, vs the average number of bits per pulse that are correctly received with and without EC, vs the ratio between the two.

4.3.2.2 Discussion

When comparing figures 4.39 (simulated distance 0 km) and 4.42 (simulated distance 5 km), it can be seen how the simulated error correction capabilities change over a simulated distance of 5 km. At the average number of photons per pulse $u = 100$ and detection efficiency $\eta_{\text{eff}} = 20\%$, the error correction performs quite well for super-blocks up to a certain size. Here, the detection efficiency is higher than in section 4.3.1. This gives a higher probability for addition errors p_{add} which contributes to higher complexity errors for super-blocks of larger sizes n . The large average number of photons per pulse will however keep p_{loss} relatively low. For the simulation results presented in figure 4.39, the BPPM EC protocol gives a maximum improvement of the transmission results for $n = 3$, at 45.02% (see the table in figure 4.40). At this point 85.12% of the transmitted information is received and error corrected properly (see the table in figure 4.41). The maximum amount of correctly received (no EC) and error corrected super-blocks combined, is found at super-block size of $n = 2$, where 94.69% of super-blocks are successfully obtained.

For the simulation results presented in figure 4.42, there is a maximum improvement of the transmission results with the BPPM EC protocol for $n = 3$, at 48.26% (see the table in figure 4.43). At this point 70.64% of the transmitted information is received and error corrected properly (see the table in figure 4.44). The maximum amount of correctly received (no EC) and error corrected super-blocks combined, is found at super-block size of $n = 2$, where 86.24% of super-blocks are successfully obtained.

In both figures 4.39 and 4.42, error correction with BPPM does not improve the results when the super-block size is larger than $n = 8$, most likely due to the relatively large probability for addition errors.

4.3.2.3 Transmission of Pulses with an Average Photon Number $u = 10$

For the transmission simulations in this section, the probability of having an addition error is $p_{\text{add}} = 6.48\%$, which is a direct consequence of the SPD detection efficiency. Tests are performed at simulated distances of $L = 0 \text{ km}$ and $L = 5 \text{ km}$ respectively. In both cases, the pulses are of size $u = 10$ photons and the detection efficiency is $\eta_{\text{neff}} = 20\%$. Under these conditions, a distance of $L = 0 \text{ km}$ gives a loss probability of $p_{\text{loss}} = 30.67\%$ and the results of the simulation can be seen in figure 4.45. In figure 4.46 and 4.47, the results of the simulated transmission and correction process are laid out in tables. At a simulated transmission distance of $L = 5 \text{ km}$, the loss probability is $p_{\text{loss}} = 43.79\%$ and the results of the simulation can be seen in figure 4.48. In figure 4.49 and 4.50, the results of the simulated transmission and correction process are laid out in tables.

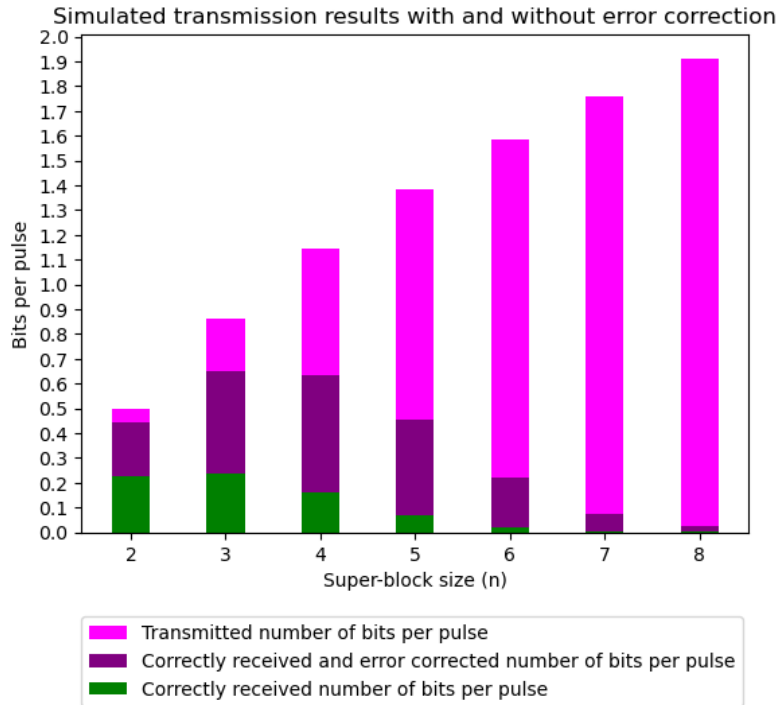


Figure 4.45: Error-corrected simulated transmission with $p_{\text{loss}} = 30.67\%$, $p_{\text{add}} = 6.48\%$ and 10 photons per pulse at a fiber distances of 0 km. The plots shows the average number of successfully received (green) vs transmitted (pink) vs successfully received and error-corrected (purple) bits per pulse for each super-block of size n .

4.3. Results of Software Simulated Transmissions of Super-blocks: Experimentally Derived Values for p_{loss} and p_{add}

n	Transmitted without errors (%)	Solved addition and loss errors (%)	Unsolved errors (%)
2	45.47	43.31	11.22
3	27.24	48.43	24.33
4	14.02	41.48	44.5
5	4.91	27.91	67.18
6	1.23	12.7	86.07
7	0.23	4.13	95.64
8	0.04	1.15	98.81

Figure 4.46: The table shows the size n of the transmitted super-blocks and the respective percentage of super-blocks that are not distorted during the transmission, vs the percentage of super-blocks that are successfully corrected, vs the percentage of super-blocks that can not be corrected using EC.

n	Transmitted (bits/pulse)	Correctly received and EC (bits/pulse)	Ratio (%)
2	0.5	0.44	88.78
3	0.86	0.65	75.67
4	1.15	0.64	55.5
5	1.38	0.45	32.82
6	1.58	0.22	13.93
7	1.76	0.08	4.36
8	1.91	0.02	1.19

Figure 4.47: The table shows the size n of the transmitted super-blocks and the respective average number of transmitted information bits per pulse, vs the average number of bits per pulse that are correctly received with and without EC, vs the ratio between the two.

4.3. Results of Software Simulated Transmissions of Super-blocks: Experimentally Derived Values for p_{loss} and p_{add}

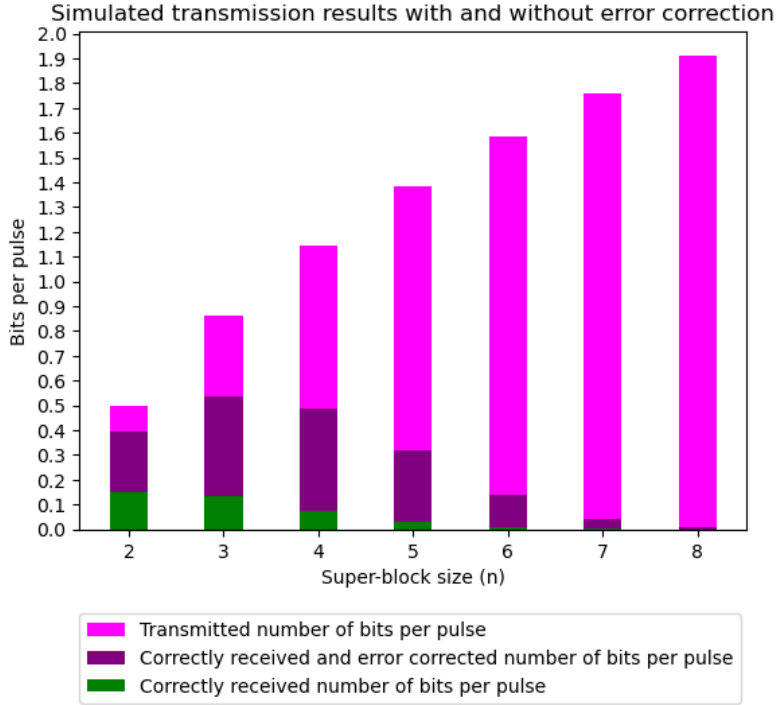


Figure 4.48: Error-corrected simulated transmission with $p_{\text{loss}} = 43.79\%$, $p_{\text{add}} = 6.48\%$ and 10 photons per pulse at a fiber distances of 5 km. The plots shows the average number of successfully received (green) vs transmitted (pink) vs successfully received and error-corrected (purple) bits per pulse for each super-block of size n .

n	Transmitted without errors (%)	Solved addition and loss errors (%)	Unsolved errors (%)
2	30.18	48.93	20.89
3	15.27	47.24	37.49
4	6.56	35.98	57.46
5	2.36	20.67	76.97
6	0.51	8.26	91.23
7	0.08	2.2	97.72
8	0	0.44	99.56

Figure 4.49: The table shows the size n of the transmitted super-blocks and the respective percentage of super-blocks that are not distorted during the transmission, vs the percentage of super-blocks that are successfully corrected, vs the percentage of super-blocks that can not be corrected using EC.

4.3. Results of Software Simulated Transmissions of Super-blocks: Experimentally Derived Values for p_{loss} and p_{add}

n	Transmitted (bits/pulse)	Correctly received and EC (bits/pulse)	Ratio (%)
2	0.5	0.4	79.11
3	0.86	0.54	62.51
4	1.15	0.49	42.54
5	1.38	0.32	23.03
6	1.58	0.14	8.77
7	1.76	0.04	2.28
8	1.91	0.01	0.44

Figure 4.50: The table shows the size n of the transmitted super-blocks and the respective average number of transmitted information bits per pulse, vs the average number of bits per pulse that are correctly received with and without EC, vs the ratio between the two.

4.3.2.4 Discussion

In figures 4.45 (simulated distance 0 km) and 4.48 (simulated distance 5 km), the average number of photons per pulse is $u = 10$. Naturally, this means that the probability for loss errors is larger than for $u = 100$. Even with the higher values for p_{loss} , some of the erroneous transmitted super-blocks can be recovered, at least up until a certain super-block size of n . For the simulation results presented in figure 4.45, a maximum improvement of the transmission results using BPPM error correction (versus BPPM with no EC) is found at super-block size of $n = 3$, with 48.43% (see table in figure 4.46). This means that the successfully received and EC amount of information at this point is 75.67% of what was originally transmitted (see table in figure 4.47). The maximum amount of correctly received (no EC) and error corrected super-blocks combined, is found at super-block size of $n = 2$, where 88.78% of super-blocks are successfully obtained.

For the simulation results presented in figure 4.48, the BPPM EC protocol gives a maximum improvement (compared to BPPM without EC) for the super-block size of $n = 2$, at 48.93% (see table in figure 4.49). This means that at this point, the combined successfully received and error corrected amount of information is 79.11% of what was originally transmitted (see table in figure 4.50). In both figures 4.45 and 4.48, error correcting with BPPM does not improve the result when the super-block size is larger than $n = 8$.

In conclusion, both the increased simulated transmission distance, as well as the lower average photon number per pulse, affects the final results for the worse, which is to be expected. Even so, the BPPM EC protocol does improve the transmission results under the proposed conditions.

4.4 Simulated Image Transmission

In this section, the results of simulated transmission using image data is presented, which corresponds to the tests described in section 3.6.3.3. During these simulations, the pixel data of the images is mapped to super-blocks of varying sizes n . In the reconstructed images, the pixels corresponding to successfully error-corrected super-blocks are highlighted using green pixels and the pixels corresponding to uncorrectable super-blocks are highlighted using red pixels.

4.4.1 Image Transmission Using Detection Efficiency $\eta_{\text{eff}} = 10\%$

During these simulations, the detection efficiency is $\eta_{\text{eff}} = 10\%$ and the average number of photons per pulse is $u = 100$.

4.4.1.1 Transmission of Image Using Super-block Size of $n = 2$

During these transmission simulations, super-blocks of size $n = 2$ are used for transmission, to which the pixel data is mapped. The simulations are performed at distances $L = 0 \text{ km}$ and $L = 5 \text{ km}$, with $u = 100$ photons/pulse. Since there are only two permutations of super-blocks of size $n = 2$, permutation (1,2) is mapped to white pixel data, and (2,1) is mapped to black pixel data. In figures 4.51 and 4.52 the original, erroneous and error corrected images can be seen and in figure 4.53 the error correction results are displayed using pie statistics. From left to right in figures 4.51 and 4.52, the four images display:

- The original image (700 pixels, dimensions 25x28).
- The received image without error correction.
- The received image showing successful error-corrections (green pixels) and uncorrectable errors (red pixels).
- The restored image after error correction.

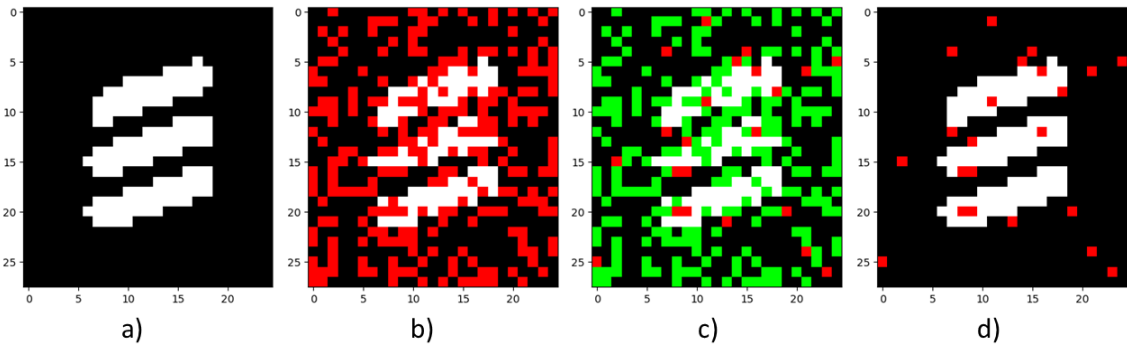


Figure 4.51: Error corrected simulated image transmission, at a transmission distance of $L = 0 \text{ km}$ (transmitter and receiver placed back-to-back), with $p_{\text{add}} = 0.05\%$ and $p_{\text{loss}} = 19.28\%$.

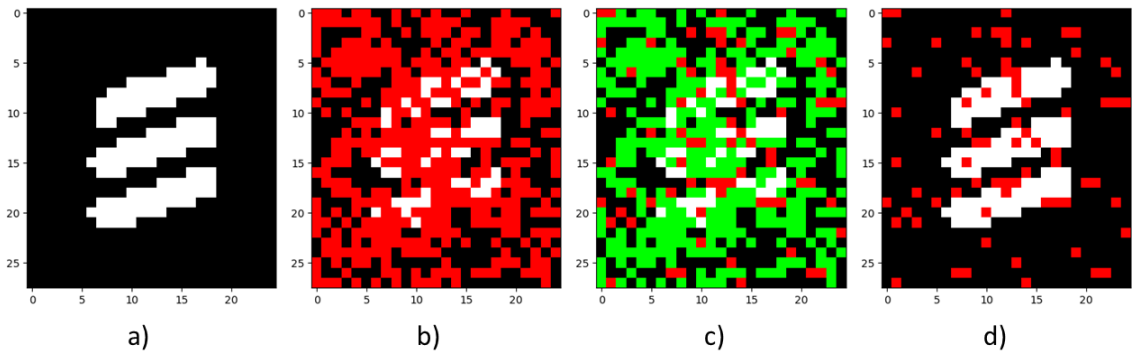


Figure 4.52: Error corrected simulated image transmission at a transmission distance of $L = 5$ km, with $p_{\text{add}} = 0.05\%$ and $p_{\text{loss}} = 34.56\%$.

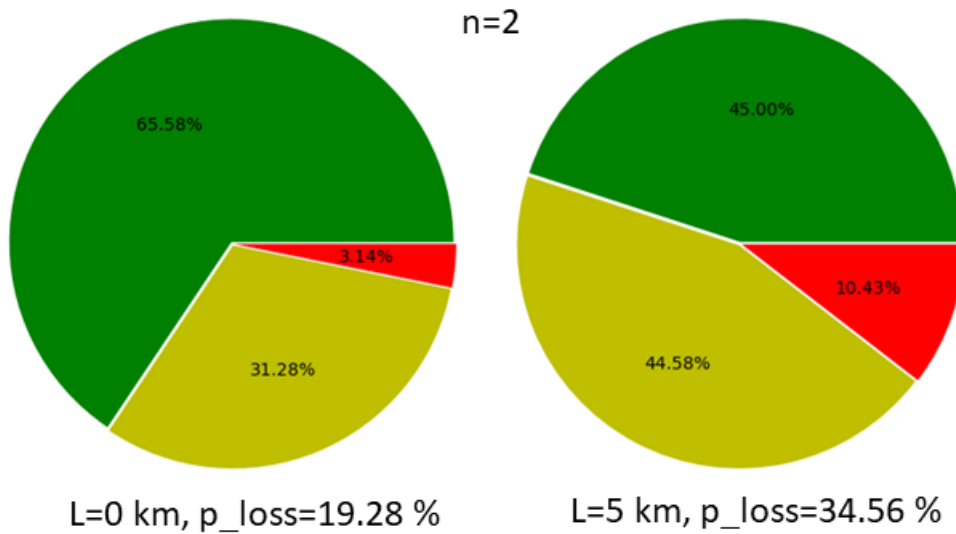


Figure 4.53: Ratios of super-blocks of size $n=2$ that are successfully received (green), successfully error corrected (yellow) and non-correctable (red).

4.4.1.2 Discussion

Let's study figures a), b), c), d) in 4.51 and 4.52, as well as the statistics presented in figure 4.53. At a distance of $L=0$ km of added distance between sender and receiver, 34.42% of the transmitted super-blocks would be lost without the error correction. However, because of the error correction, only 3.14% is ultimately lost. At an added distance of 5 km between sender and receiver, instead of losing 55.00% of the super-blocks, the error correction makes it so that only 10.43% are lost.

4.4.1.3 Transmission of Image Using Super-block Size of $n = 3$

During these transmission simulations, super-blocks of size $n = 3$ are used for transmission, to which the pixel data is mapped. The simulations are performed at distances $L = 0$ km and $L = 5$ km, with $u = 100$ photons/pulse. Since there are more than two permutations of super-blocks of size $n = 3$, the permutations (1,2,4) and (4,2,1) are chosen for pixel mapping. Permutation (1,2,4) is mapped to white pixel data and (4,2,1) is mapped to black pixel data. In figures 4.54 and 4.55 the original, erroneous and error corrected images can be seen and in figure 4.56 the error correction results are displayed using pie statistics. From left to right in figures 4.54 and 4.55, the four images display:

- a) The original image (700 pixels, dimensions 25x28).
- b) The received image without error correction.
- c) The received image showing successful error corrections (green pixels) and uncorrectable errors (red pixels).
- d) The restored image after error-correction.

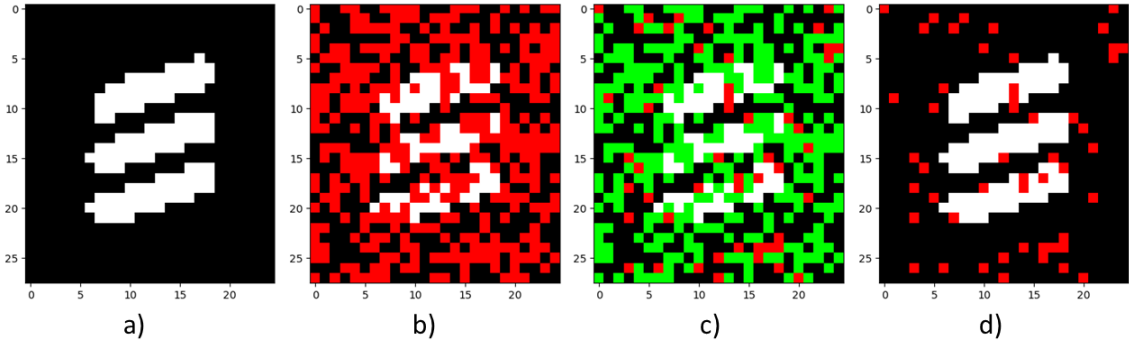


Figure 4.54: Error corrected simulated image transmission, at a transmission distance of $L = 0$ km, with $p_{\text{add}} = 0.05\%$ and $p_{\text{loss}} = 19.28\%$ and transmitter and receiver placed back-to-back.

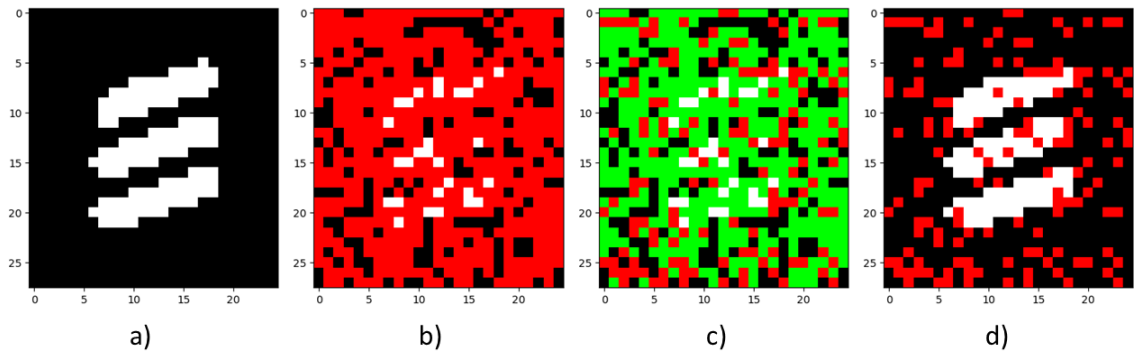


Figure 4.55: Error corrected simulated image transmission, at a transmission distance of $L = 5$ km, with $p_{\text{add}} = 0.05\%$ and $p_{\text{loss}} = 34.56\%$.

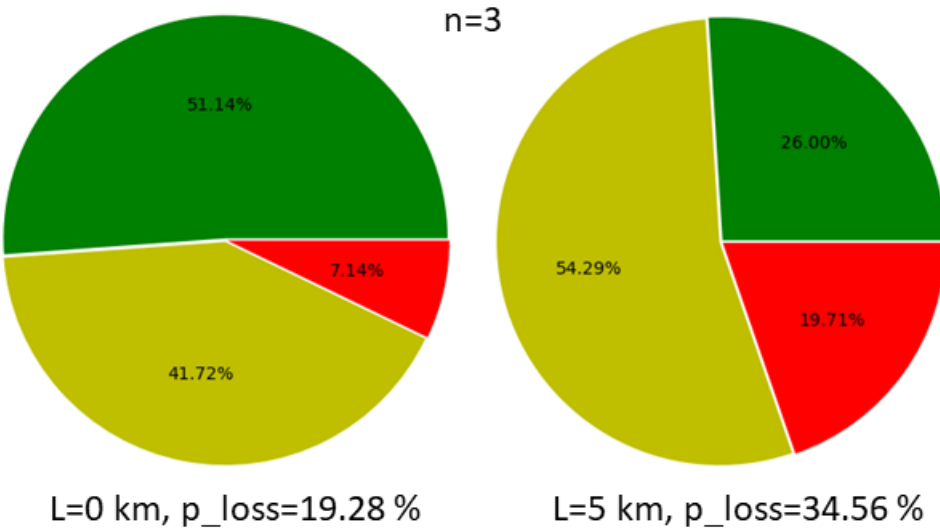


Figure 4.56: Ratios of super-blocks of size $n = 3$ that are successfully received (green), successfully error corrected (yellow) and non-correctable (red).

4.4.1.4 Discussion

Let's study figures a), b), c), d) in 4.54 and 4.55, as well as the statistics presented in figure 4.56. At a distance of $L=0 \text{ km}$ added distance between sender and receiver, 48.86% of the transmitted super-blocks would be lost without the error correction. However, because of the error correction, only 7.14% are ultimately lost. At an added distance of 5 km between sender and receiver, instead of losing 74% of the super-blocks, the error correction makes it so that only 19.71% are lost.

4.4.1.5 Transmission of Image Using Super-block Size of $n = 4$

During these transmission simulations, super-blocks of size $n = 4$ are used for transmission, to which the pixel data is mapped. The simulations are performed at distances $L = 0$ km and $L = 5$ km, with $u = 100$ photons/pulse. Since there are more than two permutations of super-blocks of size $n = 4$, the permutations (1,2,4,7) and (7,4,2,1) are chosen for pixel mapping. Permutation (1,2,4,7) is mapped to white pixel data and (7,4,2,1) is mapped to black pixel data. In figures 4.57 and 4.58 the original, erroneous and error corrected images can be seen and in figure 4.59 the error correction results are displayed using pie statistics. From left to right in figures 4.57 and 4.58, the four images display:

- The original image (700 pixels, dimensions 25x28).
- The received image without error correction.
- The received image showing successful error corrections (green pixels) and uncorrectable errors (red pixels).
- The restored image after error-correction.

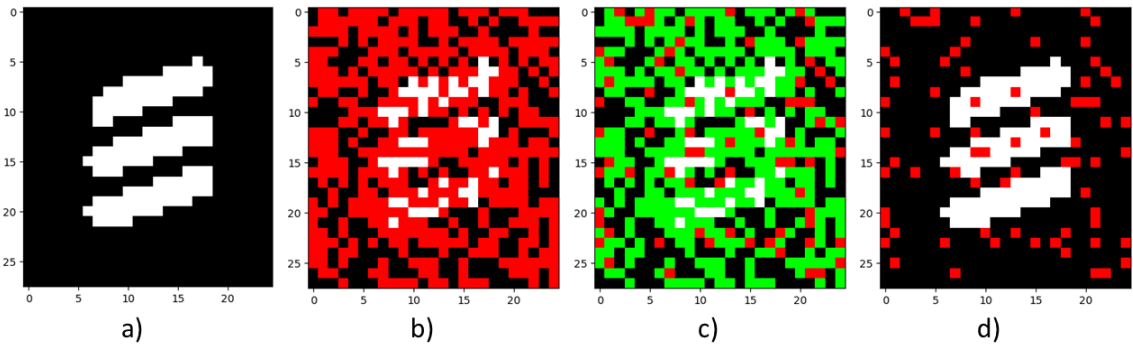


Figure 4.57: Error corrected simulated image transmission at a transmission distance of $L = 0$ km, with $p_{\text{add}} = 0.05\%$ and $p_{\text{loss}} = 19.28\%$. The image shows the successfully error corrected pixel data (green) and the non-correctable pixel data (red).

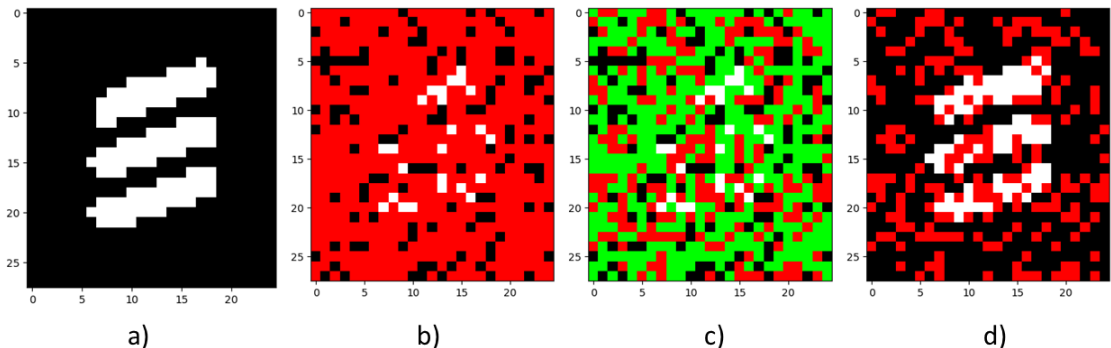


Figure 4.58: Error corrected simulated image transmission at a transmission distance of $L = 5$ km, with $p_{\text{add}} = 0.05\%$ and $p_{\text{loss}} = 34.56\%$. The image shows the successfully error corrected pixel data (green) and the non-correctable pixel data (red).

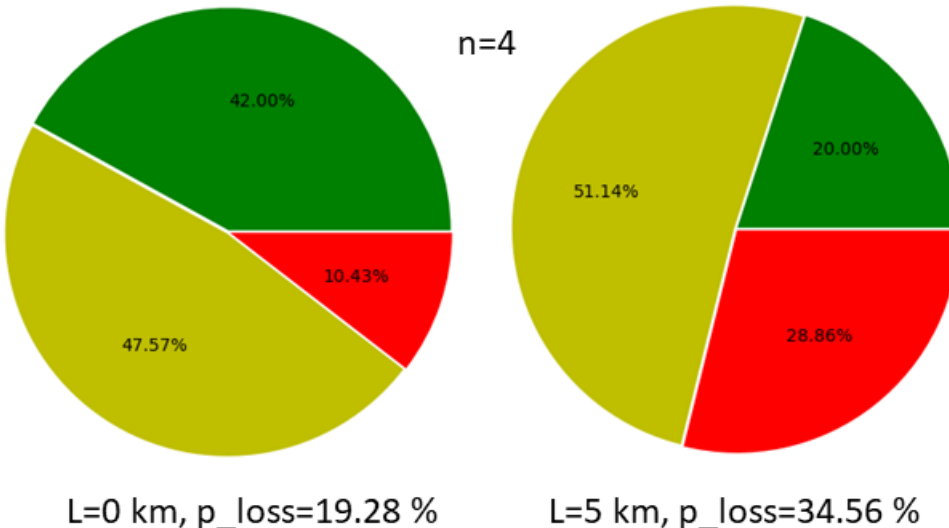


Figure 4.59: Ratios of super-blocks of size $n=4$ that are successfully received (green), successfully error corrected (yellow) and non-correctable (red).

4.4.1.6 Discussion

Let's study figures a), b), c), d) in 4.57 and 4.58, as well as the statistics presented in figure 4.59. At a distance of $L=0$ km added distance between sender and receiver, 58.00% of the transmitted super-blocks would be lost without the error correction. However, because of the error correction, only 10.43% are ultimately lost. At an added distance of 5 km between sender and receiver, instead of losing 80.00% of the super-blocks, the error correction makes it so that only 28.86% are lost.

4.4.1.7 Transmission of Image Using Super-block Size of $n = 5$

During these transmission simulations, super-blocks of size $n = 5$ are used for transmission, to which the pixel data is mapped. The simulations are performed at distances $L = 0$ km and $L = 5$ km, with $u = 100$ photons/pulse. Since there are more than two permutations of super-blocks of size $n = 5$, the permutations (1,2,4,7,12) and (12,7,4,2,1) are chosen for pixel mapping. Permutation (1,2,4,7,12) is mapped to white pixel data and (12,7,4,2,1) is mapped to black pixel data. In figures 4.60 and 4.61 the original, erroneous and error corrected images can be seen and in figure 4.62 the error correction results are displayed using pie statistics. From left to right in figures 4.60 and 4.61, the four images display:

- a) The original image (700 pixels, dimensions 25x28).
- b) The received image without error correction.
- c) The received image showing successful error corrections (green pixels) and uncorrectable errors (red pixels).
- d) The restored image after error-correction.

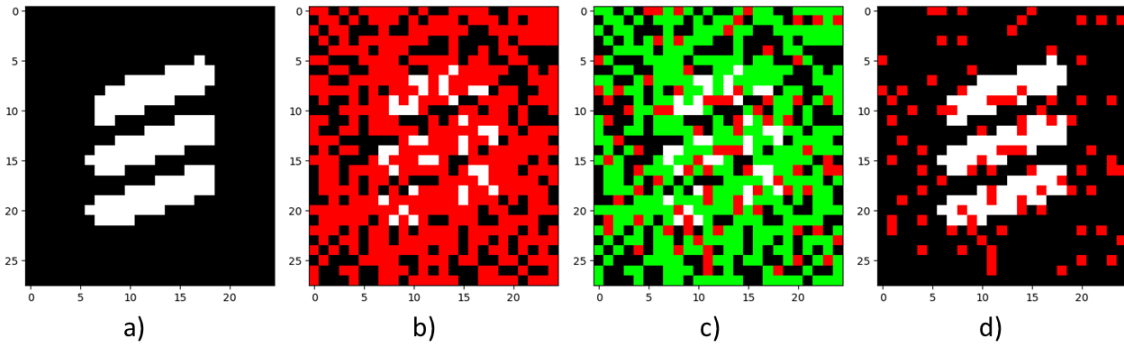


Figure 4.60: Error corrected simulated image transmission at a transmission distance of $L = 0$ km, with $p_{\text{add}} = 0.05\%$ and $p_{\text{loss}} = 19.28\%$. The image shows the successfully error corrected pixel data (green) and the non-correctable pixel data (red).

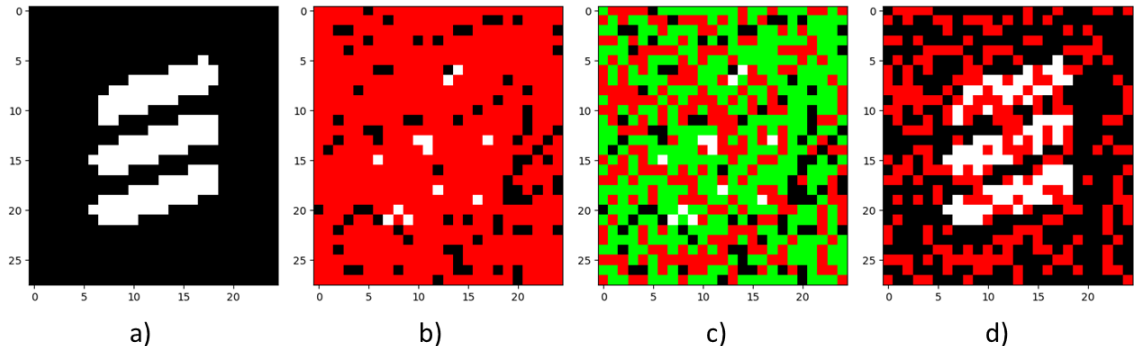


Figure 4.61: Error corrected simulated image transmission at a transmission distance of $L = 5$ km, with $p_{\text{add}} = 0.05\%$ and $p_{\text{loss}} = 34.56\%$. The image shows the successfully error corrected pixel data (green) and the non-correctable pixel data (red).

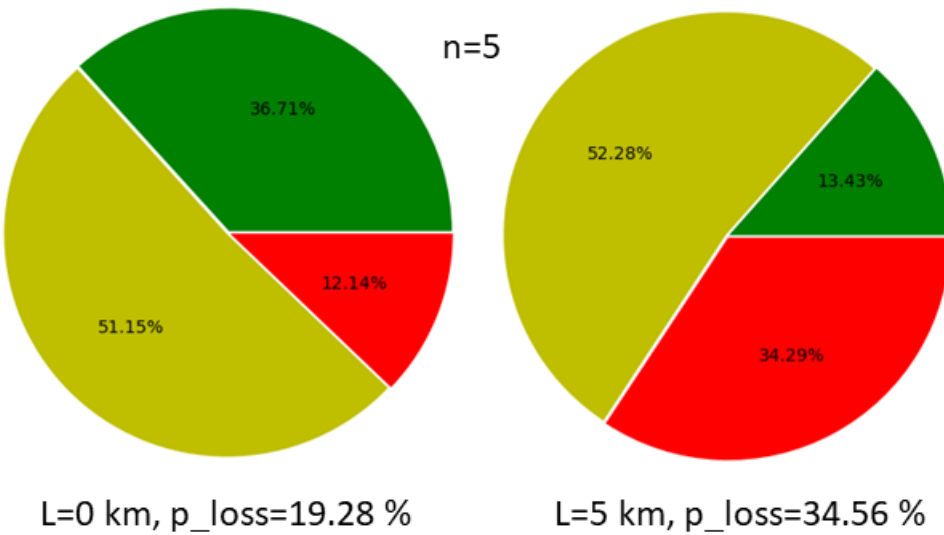


Figure 4.62: Ratios of super-blocks of size $n=5$ that are successfully received (green), successfully error corrected (yellow) and non-correctable (red).

4.4.1.8 Discussion

Let's study figures a), b), c), d) in 4.60 and 4.61, as well as the statistics presented in figure 4.62. At a distance of $L=0$ km added distance between sender and receiver, 63.29% of the transmitted super-blocks would be lost without the error correction. However, because of the error correction, only 12.14% are ultimately lost. At an added distance of 5 km between sender and receiver, instead of losing 86.57% of the super-blocks, the error correction make it so that 34.29% are lost.

4.4.2 Re-send Image

In this section, the results of re-sending non-correctable super-block pixel data can be seen. The results correspond to the simulations described in section 3.6.3.4

4.4.2.1 Re-send Image: Super-block size of $n=3$, photon number 100 and $\eta_{\text{eff}}=10\%$

This simulation is performed using a pulse size of 100 photons/pulse and detection efficiency of 10% at a transmission distance of 5 km. The amount of successfully received and error corrected super-blocks of size $n = 3$ should be around 80.48% of what is transmitted per iteration (see table in figure 4.32). In figure 4.63 the first seven iterations of simulated transmission and error correction are displayed.

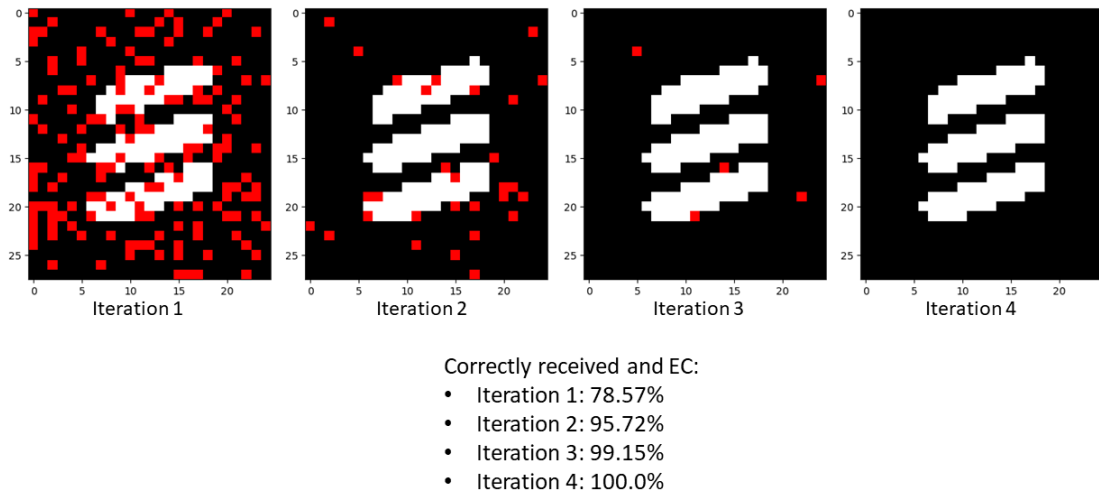


Figure 4.63: Repeated error corrected image transmission simulation with super-block size of $n = 3$ at a transmission distance of $L = 5$ km, with $p_{\text{add}} = 0.05\%$ and $p_{\text{loss}} = 34.56\%$. The image shows the percentage of properly received data (with and without error correction) for each iteration. Non-correctable pixel data is illustrated using red pixels for each iteration. The average photon number per pulse is $u = 100$.

4.4.2.2 Re-send Image: Super-block size of $n=3$, photon number 10 and $\eta_{\text{eff}}=20\%$

This simulation is performed using a pulse size of 10 photons/pulse and detection efficiency of 20% at a transmission distance of 5 km. The amount of successfully received and error corrected super-blocks of size $n = 3$ should be around 62.51% of what is transmitted per iteration (see table in figure 4.50). In figure 4.64 the first seven iterations of simulated transmission and error correction are displayed.

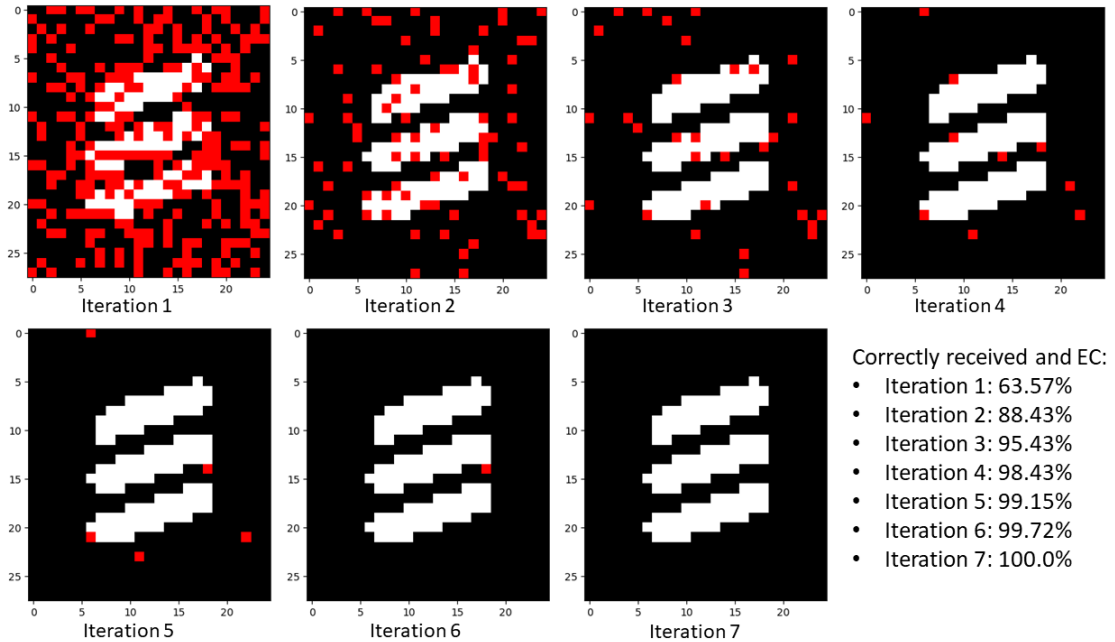


Figure 4.64: Repeated error corrected image transmission simulation with super-block size of $n = 3$ at a transmission distance of $L = 5$ km, with $p_{\text{add}} = 6.48\%$ and $p_{\text{loss}} = 43.79\%$. The image shows the percentage of properly received data (with and without error correction) for each iteration. Non-correctable pixel data is illustrated using red pixels for each iteration. The average photon number per pulse is $u = 10$.

4.4.2.3 Discussion

As can be seen in figures 4.63 and 4.64, for each simulated transmission and error correction iteration, more and more pixels are recovered. At the 4th iteration in figure 4.63 and the 7th iteration in 4.64, all pixel data has been recovered. Using a super-block size of $n = 3$, at a propagation distance of 5 km, the two sets of conditions in sections 4.4.2.1 ($\eta_{\text{eff}} = 10\%$ and $u = 100$) and 4.4.2.2 ($\eta_{\text{eff}} = 20\%$ and $u = 10$) perform about as well. The results displayed at iteration 4 in figure 4.63 are only marginally better than those in figure 4.64 for the same number of iterations, at 100% versus 98.43% successfully received and error corrected codewords. The process in figure 4.63 uses 10 times as much energy per transmitted pixel in comparison to the simulation in figure 4.64. For this particular super-block size, the higher detection efficiency (20%) in combination with the lesser number of photons per pixel (10 photons) is therefore more energy efficient than the lower detection efficiency (10%) in combination with the larger photon number per pulse (100 photons).

4.4.2.4 Re-send Image: Super-block size of $n=5$, photon number 100 and $\eta_{\text{eff}}=10$

This simulation is performed using a pulse size of 100 photons/pulse and detection efficiency of 10% at a transmission distance of 5 km. The amount of successfully received and error corrected super-blocks of size $n = 5$ should be around 65.18% of what is transmitted per iteration (see table in figure 4.32). In figure 4.65 the first seven iterations of simulated transmission and error correction are displayed.

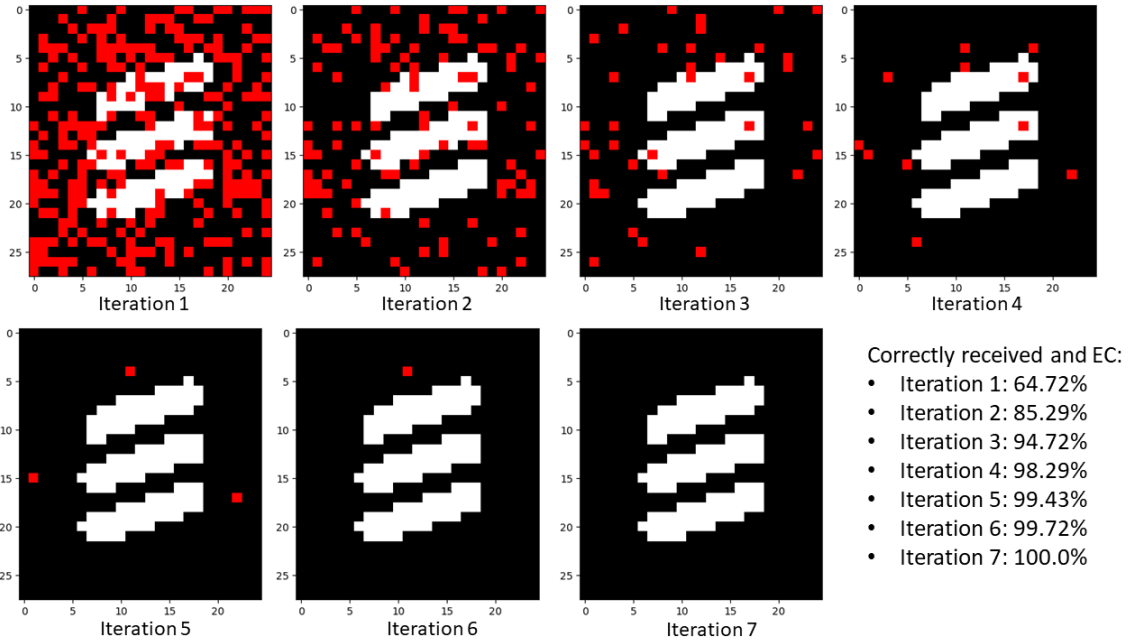


Figure 4.65: Repeated error corrected image transmission simulation with super-block size of $n = 5$ at a transmission distance of $L = 5$ km, with $p_{\text{add}} = 0.05\%$ and $p_{\text{loss}} = 34.56\%$. The image shows the percentage of properly received data (with and without error correction) for each iteration. Non-correctable pixel data is illustrated using red pixels for each iteration. The average photon number per pulse is $u = 100$.

4.4.2.5 Re-send Image: Super-block size of $n=5$, photon number 10 and $\eta_{\text{eff}}=20\%$

This simulation is performed using a pulse size of 10 photons/pulse and detection efficiency of 20% at a transmission distance of 5 km. The amount of successfully received and error corrected super-blocks of size $n = 5$ should be around 23.03% of what is transmitted per iteration (see table in figure 4.50). In figure 4.66 the first seven iterations of simulated transmission and error correction are displayed.

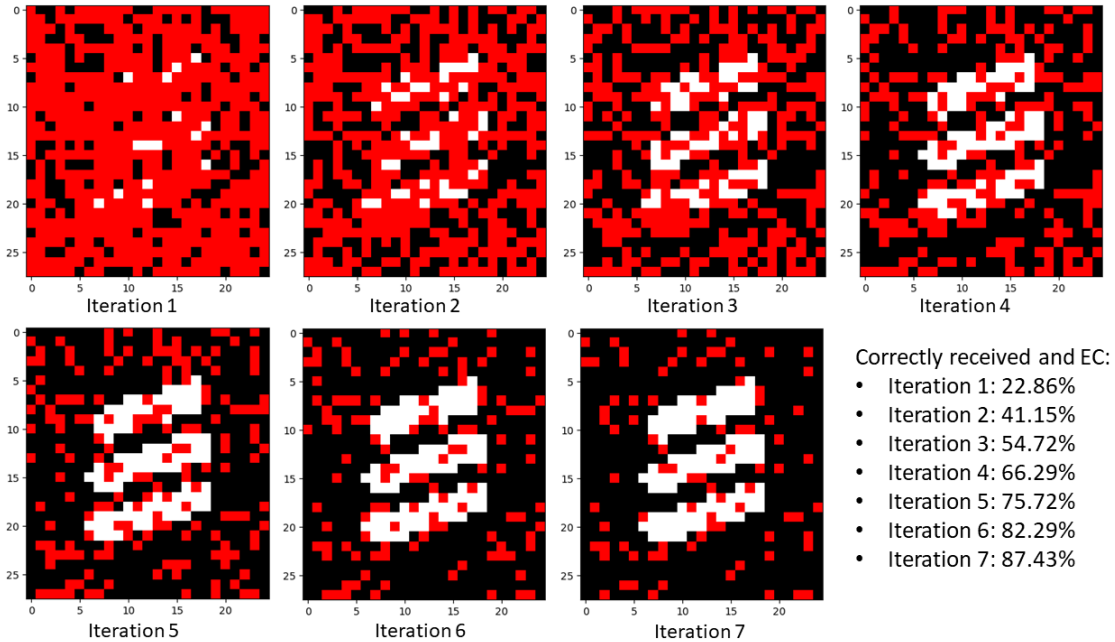


Figure 4.66: Repeated error corrected image transmission simulation with super-block size of $n = 5$ at a transmission distance of $L = 5$ km, with $p_{\text{add}} = 6.48\%$ and $p_{\text{loss}} = 43.79\%$. The image shows the percentage of properly received data (with and without error correction) for each iteration. Non-correctable pixel data is illustrated using red pixels for each iteration. The average photon number per pulse is $u = 10$.

4.4.2.6 Discussion

As can be seen in figures 4.65 and 4.66, for each transmission and error correction iteration, more and more pixels are recovered. At the 7th iteration in figure 4.65, all pixel data has been recovered. At iteration 7 in figure 4.66, 12.57% of the pixels are still missing. Using a super-block size of $n = 5$, at a propagation distance of 5 km, the simulation using 100 photons per pulse and detection efficiency 10% performs much better in regards to the number of iterations needed to transmit all pixel data properly. However, this set of conditions also requires 10 times more energy per transmitted pixel. It is very possible that the required energy for each additional iteration using 10 photons/pixel is more energy efficient than using 100 photons/pixel for fewer iterations. Although realistically, the process of continuously re-sending erroneous super-blocks is more time consuming.

It takes 4 transmission iterations for the BPPM protocol to recover all pixels when using detection efficiency 10% and 100 photons/pulse with super-blocks of size $n = 3$. For super-blocks of size $n = 5$ it instead takes 7 transmission iterations with detection efficiency

10% and 100 photons/pulse. For $n = 5$, only 1.71% of pixels are still missing on iteration 4.

It seems that the increase in super-block size has a much larger impact on the results when using detection efficiency 20% and 10 photons/pulse. Namely, at the 7th iteration, $n = 3$ gives 100% correctly transmitted pixels and $n = 5$ gives only 87.43%. Once again, it is proven that a higher rate of addition errors will create more error complexity for larger super-blocks.

4.5 Results and Discussion Summary

In this section, the conclusions drawn regarding the results of the thesis work are summarized.

4.5.1 Results and Discussion Summary: Simulation with Arbitrary Values

In section 4.1 the error generation and EC simulations with arbitrary values for losses and additions are presented and discussed. In summary, when simulating only loss errors (at 10% probability), EC with the BPPM protocol is useful for all super-block sizes of $n = 2 - 8$. Meaning, that the BPPM protocol with EC does improve the results in all cases, compared to using BPPM when there is no EC.

Regarding simulation of only addition errors (at 10% probability), the error correction protocol does not recover any lost information when the super-blocks are of size $n > 8$. For the simulations where the loss- and addition probabilities are of the same magnitude, the results show that the addition errors dominate the loss errors although $p_{\text{loss}} = p_{\text{add}}$. In other words, the BPPM protocol is in general much more capable of correcting for loss errors than addition errors. This is reasonable since there are more potential additions than losses in every sub-block length > 2 . For every sub-block in a super-block, no matter the length, only one photon can be lost. However, as the sub-block lengths increase, so does the probability of having several additions per sub-block. For each sub-block of length x , there is the potential of gaining up to $x - 1$ addition errors. For these reasons, it is preferable to keep $p_{\text{loss}} \gg p_{\text{add}}$.

4.5.2 Results and Discussion Summary: Experiments

In section 4.2, the results of the experiments performed in the lab are presented. The addition probability is calculated based on the measured dark-counts at different detection efficiency settings on the SPD. At a detection efficiency of $> 12.5\%$, the addition probability goes up drastically.

The loss probability is modeled for detection efficiencies 10 and 20%, for a fiber propagation distance of 0-75 km and for different photon numbers per pulse (minimum 1 photon/pulse and maximum 100 photons/pulse). For 1 photon/pulse, the loss probability is between 85-93% for detection efficiencies between 10-20%, when transmitter and receiver are back-to-back. Because of these very high probabilities of photon loss, an average photon number of 10 and 100 photons/pulse are used in the simulations presented in sections 4.3 and 4.4, which implement experimentally derived values for loss- and addition probability. Although optical transmission using pulses containing several photons require more energy than using only 1 photon/pulse, 10 and 100 photons/pulse is still much less than the billions of photons that are utilized during classical optical communication. According to the produced models for loss probability (for detection efficiency 10 and 20%), there is no point in using much larger pulses of light than 100 photons, since this does not lower the loss probability any further.

The loss probability minimum is $p_{\text{loss}} = 19.28\%$ for an average 100 photons/pulse at 10% detection efficiency and 0 km propagation distance. For pulses containing an average of 10 photons, the loss probability minimum is $p_{\text{loss}} = 48.98\%$ for the same detection efficiency and fiber distance. Detection efficiency 10% provides an addition probability of 0.05%.

For a detection efficiency of 20%, the addition probability is 6.48% and the loss probability minimum is $p_{\text{loss}} = 19.82\%$ for an average 100 photons/pulse at a propagation distance of 0 km. At the same detection efficiency and fiber distance $p_{\text{loss}} = 30.67\%$, with 10 photons/pulse.

4.5.3 Results and Discussion Summary: Simulation with Experimentally Derived Values

For the results presented in section 4.3, using simulated SPD detection efficiency 10%, the simulated loss probability at 5 km propagated distance and using 100 photons/pulse, is 34.56%. The addition probability is 0.05% (see figure 4.30). For this simulation, the BPPM protocol with EC improves the results with 43.48-54.19% for super-block sizes between $n = 2 - 8$, compared to using BPPM with no EC. This means that the successfully received and EC amount of information is between 46.58-87.92% of what was originally transmitted. Using the same detection efficiency and propagation distance, with an average of 10 photons/pulse, the BPPM protocol with EC improves the results with 10.8-48.35% for super-block sizes between $n = 2 - 8$, compared to using BPPM without EC. This means that the successfully received and EC amount of information is between 10.89-65.70% of what was originally transmitted (see figure 4.36).

For a simulated SPD detection efficiency of 20%, propagation distance 5 km and an average of 100 photons/pulse, the simulation results presented in figure 4.42 show that there is a maximum improvement of 48.26% with EC for $n = 3$. At this point 70.64% of the transmitted information is received and error corrected properly. In this simulation, error correcting with BPPM does not improve the result when the super-block size is larger than $n = 8$. Using the same detection efficiency and propagation distance, but instead an average of 10 photons/pulse, the simulation results presented in figure 4.48 show that the BPPM EC protocol provides a maximum improvement in EC of 48.93% for $n = 2$. This means that the successfully received and EC amount of information is 79.11% of what was originally transmitted. In this scenario, error correcting with BPPM does not improve the result when the super-block size is larger than $n = 8$.

In conclusion, both the increased simulated transmission distance, as well as the lower average number of photons per pulse, affects the final results for the worse, which is to be expected. Even so, the BPPM EC protocol does improve the transmission results under the proposed conditions, both for simulations using detection efficiency of 10 and 20%.

It is worthy to note a couple of things regarding the chosen values for n_{eff} and u . Using a low value for n_{eff} (at 10%) will require more photons per pulse u to acquire sufficient detection. However, the lower detection efficiency n_{eff} will also decrease the probability for p_{add} (see figure 4.22), which is preferable since the error correction protocol over all is much better at correcting for loss errors than addition errors for super-block sizes of $n > 2$. In general, for larger super-blocks (i.e. when transmitting data with more variation) it is better to use larger pulses in the available experimental setup (ca 100 photons/pulse) to decrease the amount of transmission iterations needed to recover all lost data. When transmitting shorter super-blocks (data with less variation) it is better to use smaller pulses in the available setup (ca 10 photons) and a higher detection efficiency, which results in more energy efficient transmission.

4.6 Future Work

This section contains recommendations for any future experimental work regarding the BPPM error correction protocol.

4.6.1 Experimental Setup

During the thesis project it is proven that the BPPM protocol can to some extent be used for successful experimentation using the available setup, provided some compromise is made regarding the rules of the protocol. For example, the average number of photons per pulse u must be larger than 1. In order to test the protocol as it was originally intended (using single photons), it is instead recommended to use a superconducting nanowire single-photon detector (SNSPD). Namely, these types of single photon detectors can reach a detection efficiency of 80-95% and still acquire dark-count rates of mHz, meaning that the addition probability would be small even for high detection efficiencies[Gourguès2019SuperconductingK]. Being able to use detection efficiencies of this magnitude would in turn decrease the loss probabilities during single photon transmissions.

For future experimental implementations of the BPPM protocol, there is also a recommendation for some type of active polarization stabilization. This requires the usage of either polarization maintaining fiber, or electrical polarization controllers (EPC:s) which continuously stabilizes the polarization of the propagated photons using a reference laser source.

4.6.2 Hardware Implementation

In addition to the upgrades of the experimental setup that are proposed in section 4.6.1 (using an SNSPD for detecting pulse sizes of $u = 1$ photons), also the control system would need to be fully implemented. This includes a control system for both the transmitter and receiver. On the transmitter side, this means controlling the intensity modulators which polarizes the light and chops it into smaller pulses containing one single photon. Implementing the receiver side includes making it possible to save data properly in the FPGA memory. For both transmitter and receiver, the temporal BPPM encoding must be implemented and proper synchronization must be achieved.



5 Conclusion

During the thesis project, a feasibility study is performed of the BPPM error correction protocol, invented at Ericsson AB. In general, the BPPM protocol is better at correcting for loss errors than addition errors, since the complexity of the respective error types increase much more drastically for additions in comparison to losses as the codewords become longer. Throughout the project, an experimental setup is designed and used to measure polarization drift and probability of photon loss during transmission. The loss probability is modeled over a propagation distance of 0-75 km. The experimentally derived probabilities for additions are established using an SPD. Ultimately, the photon addition probabilities at detection efficiencies 10 and 20% are used for software simulation processes of error generation and correction with the BPPM protocol. In these simulations, photon losses for 0 and 5 km of propagated distance are utilized. The simulated light pulses are of sizes 10 and 100 photons. The simulation results provide adequate EC ratios with the BPPM protocol for the utilized codeword lengths. At a simulated transmission distance of 5 km, a maximum amount of result improvement of 54.19% can be achieved using the BPPM protocol with EC (compared to using the BPPM protocol without EC) at a pulse size of 100 photons (detection efficiency 10%). At the same distance, and using 10 photons/pulse (detection efficiency 20%), a maximum improvement in the recovered data amount of 48.93% can be achieved using the BPPM protocol with EC versus when there is no EC.



A

System Design for Single Photons

This chapter describes an experimental setup design suitable for transmitting and detecting single photons. This is in contrast to the system described in section 3.3, which instead utilizes classical pulses of light. Therefore, the system described in 3.3 utilizes two photodetectors for signal detection, while the system described here instead uses two single photon detectors (SPD:s). It is the sensitivity difference between the SPD:s and photodiodes that make it so that the setup in section 3.3 requires classical light pulses, while this setup instead uses single photons. The system design described in 3.3 is chosen for the experimental process because of its feasibility in regards to the availability of components. The system utilizing single photon detection is left as a suggestive design for possible future work with single photon error correction using the BPPM protocol.

A.1 System Design for Single Photons

The experimental setup design for transmission of single photons consists of the experimental setup illustrated in figure A.1 as well as the control system in the form of FPGA and software described in sections 3.4 and 3.5.1.

A.1.1 Experimental Setup Design for Single Photons

The experimental setup consists of a transmitter and a receiver side, with a single-mode optical fiber channel connecting them. How these two parts of the setup are composed can be seen in figure A.1. The process of transmitting light through the setup is described in section A.1.1.1 and A.1.1.2. Note that knowledge of the original polarization of an incoming photon is important for the error correction process (see chapter 2), therefore it is crucial that this information is preserved during transmission. I.e. bit-flips are assumed to be highly unlikely.

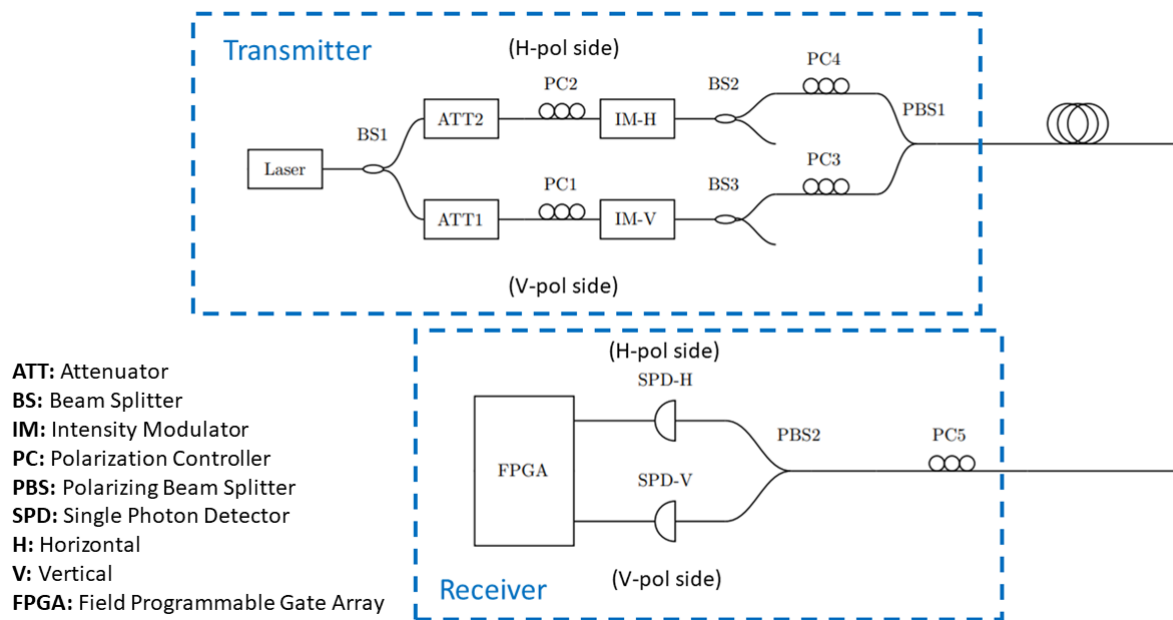


Figure A.1: Scheme describing the experimental setup for single photon transmission.

A.1.1.1 Transmitter

The transmitter side of the experimental setup includes the following components:

- 1 Telecom continuous wave DFB laser source (1550 nm) (*Laser*)
- 2 variable attenuators (*ATT1, ATT2*)
- 1 50:50 non-polarizing beamsplitter (*BS1*)
- 2 90:10 beamsplitters (*BS2, BS3*)
- 4 manual fiber polarization controllers (*PC1, PC2, PC3, PC4*)
- 2 intensity modulators (*IM-V, IM-H*), type: lithium niobate (LiNbO_3)
- 1 polarizing beamsplitter (*PBS1*), model: PBC1550SM-APC

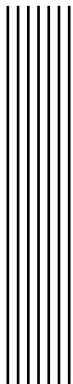
The transmitter can be seen in the upper part of figure A.1. The transmission process starts with an 1550 nm telecom cw-DFB laser emitting light. The continuous wave is split into two fiber paths by a non-polarizing 50:50 beamsplitter (*BS1*). The light passing through each fiber path is manually attenuated to single-photon levels using the variable attenuators *ATT1* and *ATT2* respectively. The light then passes through the manual polarization controllers *PC1* and *PC2*, for which the paddles are set into the angles that allow for maximum power. The three paddles in each PC function as wave plates that change the polarization of the passing light, dependant on the angle in which they are placed, which causes stress-induced birefringence. Thereafter, the intensity modulators *IM-H* and *IM-V* are used to section of the continuous wave of light into 0.1 ms long pulses, each containing a single photon. The IM-components are also used to polarize the incoming photons, as they have built in polarizers. The intensity modulators are each followed by a non-polarizing 90:10 beamsplitter (*BS2* and *BS3*), to make it possible to examine a small portion of the signal (10 %) during transmission, if there is a need for it. The polarized photons then pass through the manual polarization controllers (MPC) *PC3* and *PC4*, where their polarization is rotated into the respective horizontal/vertical states. Subsequently, the photons from both respective fiber paths are combined into the single-mode transmission fiber channel (model: SMF-28), via the polarizing beamsplitter (*PBS1*).

A.1.1.2 Receiver

The receiver side of the experimental setup includes the following components:

- 1 manual fiber polarization controller (*PC5*)
- 1 polarization beam splitter (*PBS2*), model: PBC1550SM-APC
- 2 Single Photon Detectors (*SPD-H, SPD-V*), (model: id210A)

The receiver can be seen in the lower part of figure A.1. At the receiver side of the setup, the incoming photons will pass the *PC5* component, which corrects any potential rotation of the linear polarization states, before they are separated by a polarizing beamsplitter (*PBS2*), based on their respective polarization (H/V). Finally, the vertically polarized and horizontally polarized photons are detected by the single photon detectors *SPD-V* and *SPD-H* respectively.



Bibliography

1. Czegledi, C. B. *Modeling and Compensation of Polarization Effects in Fiber-Optic Communication Systems* PhD thesis (Gothenburg, Sweden, 2018). ISBN: 9789175977027.